Sun, Songcheng

SURFACE ENHANCED RAMAN SPECTROSCOPY FROM ELECTRODE/SOLUTION INTERFACE

City University of New York PH.D. 1987

PLEASE NOTE:

In all cases this material has been filmed in the best possible way from the available copy. Problems encountered with this document have been identified here with a check mark __✓__.

1. Glossy photographs or pages _____
2. Colored illustrations, paper or print _____
3. Photographs with dark background _____
4. Illustrations are poor copy _____
5. Pages with black marks, not original copy _____
6. Print shows through as there is text on both sides of page _____
7. Indistinct, broken or small print on several pages ✓
8. Print exceeds margin requirements _____
9. Tightly bound copy with print lost in spine _____
10. Computer printout pages with indistinct print _____
11. Page(s) _____ lacking when material received, and not available from school or author.
12. Page(s) _____ seem to be missing in numbering only as text follows.
13. Two pages numbered _____. Text follows.
14. Curling and wrinkled pages _____
15. Dissertation contains pages with print at a slant, filmed as received ✓
16. Other _____

_____

_____

University
Microfilms
International

SURFACE ENHANCED RAMAN SPECTROSCOPY FROM ELECTRODE/SOLUTION INTERFACE

by

Songcheng Sun

A dissertation submitted to the Graduate Faculty in Chemistry in partial fulfillment of the requirements for the degree of Doctor of Philosophy, The City University of New York.

1987

This manuscript has been read and accepted for the Graduate Faculty in Chemistry in satisfaction of the dissertation requirement for the degree of Doctor of Philosophy.

Sept 26, 1986
Date

Ronald D Archer
Chair of Examining Committee

October 2, 1986
Date

J. M.
Executive Officer

William E. L. Grossman

Supervisory Committee

The City University of New York

Abstract

SURFACE ENHANCED RAMAN SPECTROSCOPY
FROM ELECTRODE/SOLUTION INTERFACE

by

Songcheng Sun

Advisers: Professor Ronald L. Birke

Professor John R. Lombardi

The application of the technique of surface enhanced Raman spectroscopy (SERS) to the study of electrode/solution interfaces is described. We have observed that pyridinium is not directly adsorbed on a Ag electrode surface, rather, it forms an ion pair with a specifically adsorbed chloride anion. We have measured the pH at the outer-Helmholtz plane based on the relative SERS intensity of pyridinium and pyridine, and found that the surface pH is much different from the bulk solution pH. It is a function of chloride concentration and electrode potential.

The interaction of a Ag electrode surface with different types of surfactants has been determined with the SERS technique. The strength of the interaction is found to be different depending on the charge types of the head group. A head-on orientation is found for all types of surfactants when the

potential is on the positive side of -0.8 V vs. SCE, but a reversed orientation is formed when the potential is on the negative side of -0.8 V. The change of the hydrophilic properties of the Ag electrode and an additional enhancement at negative potentials is considered due to the formation of a layer of hydrogen film.

The adsorption behavior of methyl viologen has been studied on a Ag surface by both SERS and cyclic voltammetry. The adsorption peak can be well separated from diffusion peaks in cyclic voltammetry by choosing proper conditions. The surface coverage is measured and the SERS enhancement factor is calculated based on the adsorption current of methyl viologen.

Finally, a surface induced photochemical reduction of p-nitrobenzoate is observed on both Ag island films and electrode/solution interfaces by SERS measurements. Our observations indicate that the chemical reactions which occur on the SERS activated surface is not due to a laser heating effect. The photolysis rate is studied as a function of the photon flux of excitation, the excitation frequency of the laser light and the electrode potential. A charge transfer mechanism, similar to the same mechanism for SERS, can be employed to interpret the enhancement of the photochemistry on roughened metal surfaces.

CONTENTS

CHAPTER (I)

AN INTRODUCTION TO SURFACE ENHANCED RAMAN SPECTROSCOPY FROM ELECTRODE SURFACES

Section 1.1 Introduction

The study of the nature of the chemical and physical processes that occur on metal surfaces is one of the most rapidly expanding fields in modern science.

Now there is a variety of spectroscopic techniques which have been used to characterize the chemical and physical processes on metal surfaces. These techniques include Auger Electron Spectroscopy [1], Secondary Ion Mass Spectroscopy [2], Ultra-violet (X-ray) Photoelectron Spectroscopy [3,4] and High Resolution Electron Energy Loss Spectroscopy [5], which are able to characterize the molecular identity of the surface species. Also widely employed are the techniques of low Energy Electron Diffraction [6] and Scanning Electron Microscopy [7], which are used to detect structural and morphological variations, as well as the FTIR [8] technique, which offers vibrational information about the species adsorbed on surfaces. Besides these techniques, surface enhanced Raman scattering (SERS) spectroscopy is a newly developed technique which has many advantages over the techniques listed above: (i) There is no limitation by the requirement of ultra high vacuum (UHV) conditions. SERS can be studied at almost all types of interfaces: solid/vacuum, solid/gas, solid/liquid as well as solid/solid interfaces; (ii) it offers an in-situ measurement which gives a great convenience to electrochemists in the study of electrode/electrolyte interfaces; (iii) it is probably the most sensitive vibrational spectroscopic technique available as a surface analytical probe; (iv) it can be used to follow in

real time electrochemical or photochemical processes.

In this chapter we will briefly discuss the properties of SERS on an electrode/solution interface, and we will give a brief view of the enhancement mechanisms. Based on many studies of enhancement mechanisms it has been postulated that two main mechanisms are operating: (i) an electromagnetic enhancement related to the enhancement of the oscillating electric field of the exciting light by large scale metal surface structures and (ii) a charge transfer resonance Raman type enhancement. These two mechanisms are complementary to each other and have been used to interpret most of the surface enhanced phenomena quite satisfactorily.

Section 1.2 The Raman Effect And Raman Spectroscopy

Predicted by Smekal in 1923 [9] and experimentally confirmed by Raman in 1928 [10], the Raman effect originates from the interaction between a molecule and the oscillating electric field associated with light. A small dipole moment is induced by this interaction through the polarizability of the molecule. This can be presented as

$$\mu = \alpha E \qquad (1.1)$$

where μ is an induced dipole moment, E is the electric field strength that the molecule sees, and α is the polarizability. However, most collisions of the incident photons with the sample molecules are elastic, i.e., the electric field produced by a polarized molecule oscillates at the same frequency as the pass-

ing electromagnetic wave, so that, the molecule acts as a source sending out radiation of that frequency in all direction (known as Rayleigh scattering).

An additional type of scattering is obtained due to the fact that molecules themselves are vibrating at frequencies corresponding to various normal modes of motion. These characteristic vibrational frequencies can mix with the exciting light to form sum and difference frequencies in the scattered radiation (known as anti-Stokes and Stokes scattering). These frequencies may be detected as shifts from the Rayleigh frequency, and are called normal Raman spectra. The measurement of these shifts reflects the characteristic vibrations of the molecules, and may be utilized as a complement to infrared spectroscopy. If the excitation light is chosen to coincide with an electronic absorption, the Raman spectra are greatly intensified. This phenomenon is termed resonance Raman spectroscopy (RRS).

Section 1.3 The Properties of the Surface Enhanced Raman Scattering

(a) The observation of anomalously intense surface spectra

Since the first observation of an anomalously intense Raman signal from pyridine adsorbed on a silver electrode [11,12], known as the surface enhanced Raman scattering effect, a variety of ions and molecules adsorbed on or placed near rough metal surface have been shown to exhibit unusually intense SERS spectra. This anomalous effect has been observed in many configurations of metal surfaces (mechanically, chemically or photochemically roughened crystal

or polycrystal surfaces, evaporated films, island films, colloids, gratings and tunnel junctions), but only on limited number of materials (Ag, Cu and Au). Other metals such as the alkali metals [13,14] and possibly Ni, Ti, Pd [15] and Al [16] show SERS but these substrates have not been demonstrated to give SERS in the electrochemical environment.

It has been well established that the relative increase in Raman scattering cross-section, the so-called 'Enhancement Factor' is as much as 10^4-10^6 [11,12,17]. These results offer the encouraging prospect that the SERS effect may provide a valuable in-situ method for exploring the optical properties of rough metal surfaces and their adsorbates.

(b) The effect of surface roughness

A typical oxidation reduction cycle (ORC) pretreatment with a double potential step or triangular sweep is widely used for roughening an electrode surfaces. In this work an optimum condition was obtained with an anodic potential limit of +0.3 V vs. SCE in the presence of chloride and +0.6 V in the absence of halides. The anodic charge passed is around 50-60 mC/cm^2. Scanning electron microscopy has been used to examine the roughness of the metal substrate. A dendritic growth with nodule heights and lateral spacing of several hundred [18] or several thousand [19] angstroms has been reported. It has long been a controversy to estimate the enhancement factor attributed to the surface roughness. A large Raman scattering enhancement has been seen

from the surface with roughness due to nodules of ca. 1000 Å in diameter for a Ag surface in ultra high vacuum (UHV) system, whereas for smooth surface the scattering is not detectable [20]. However, some investigations indicate that an oxidation reduction cycle is not a prerequisite to observe SERS. Van Duyne and coworkers [21] found that a polished silver or copper electrode, without electrochemical pretreatment, gives an enhancement factor 10^4, so that the roughness only contributes a factor of 100 to the enhancement mechanism.

In this work we are only interested in the total enhancement of Raman scattering cross section compared with the normal Raman intensity in the solution phase. We have not attempted to separate the enhancement due to the roughness from that due to other effects. But the roughness does affect the enhancement factor. In latter chapters, where we calculate a enhancement factor, the data are always related to the pretreatment conditions.

(c) Spectral dependence

The dependence of surface enhanced Raman intensity on wavelength does not follow the ν^4 behavior of spontaneous Raman scattering for free molecules, but instead follows the resonance profile of the particular surface on which enhanced scattering is observed [22]. The frequency dependence is a strong function of the surface state and the vibrational mode observed [23]. It has been considered that the frequency dependence of SERS intensity is related to the excitation of localized plasmon resonances on surface protrusions. A

complete electrodynamic calculation gives a resonance wavelength of 400 nm for a spherical particle of 400 Å diameter and as the sphere becomes larger (1000 Å) the primary resonance shifts to 410 nm but a secondary resonance appears near 500 nm [24]. If a spheroid shape and the interaction of the particles with the surface are considered, a resonance frequency of 510 nm is calculated [25]. This frequency is quite close to the resonance wavelength observed experimentally in Raman enhancement. Another consideration for frequency dependence is the excitation of delocalized surface plasmon modes via surface roughness, which should produce a maximum enhancement where the density of surface plasmon states is greatest. A full calculation for the rough surface resonance frequency, indicating the effects of roughness on the surface plasmon dispersion relation, place the maximum Raman enhancement at 390 nm [26]. This value is more than 100 nm lower than that observed experimentally in SERS spectrum.

(d) The interaction between surface and molecules

The interaction of the rough metal surface with molecules adsorbed on or placed near a surface plays an important role in the surface enhancement. A major part of this research is related to the study of the interaction on electrode/solution interfaces. The interaction between molecules and surface can be classified in three types (a) directly bonded, (b) adsorbed through an ion pair and (c) physisorbed.

In the first type a weak chemical bond between molecule and metal may be involved. This is usually more likely if the molecule has a lone pair of electrons such as in a nitrogen heterocycle (pyridine) or cyanide, carboxylate etc. In this case we call the molecule chemisorbed. In a recent report Roy and Furtak [27] suggest that a pyramidal Ag_4^+ cluster may be responsible for some of what has been called the short range or chemical component of SERS from co-adsorbed molecules. This aggregated clusters are formed on an electrochemically roughened electrode and stabilized on the surface by chemisorbed Cl^- ions (or other anions/molecules when present). According to the calculations of Baetzold [28], the Ag_4^+ species is reasonably stable by itself. The chemisorption of the molecules may occur between the positively charged Ag_4^+ cluster, which acts as a Lewis acid, and the lone pair of electrons of a molecule, which acts as Lewis base. It is likely that this interaction is enhanced in comparison with the interaction between adsorbate and bulk metal surface, and this interaction is necessary for the chemical enhancement.

A π bond interaction between molecule and surface may also be involved in the first type. The SERS spectra of ethylene, propylene [29], butene and its isomers [30] have been observed on Ag island films. But there is no observable SERS signal of methane, ethane or propane at similar conditions. In the SERS spectra of an alkene the most highly shifted band around 1650 cm^{-1} compared to normal Raman is the C=C bond, indicating that the molecules are π bonded to the silver surface through the double bond. A similar result has been re-

ported for acetylene HC≡CH. A strong SERS spectrum of acetylene has been obtained on colloidal silver, but there is no observation of SERS from ethane at the same conditions [31]. The SERS spectra of benzene and many monosubstituted benzenes have been reported and it is obvious that they absorb via π adsorbate-surface interaction [32].

The second type of interaction may involve the ions which have no lone pair of electrons but can interact with specifically adsorbed anions (or cations) to form an ion pair, such cations are pyridinium, methyl pyridinium, etc. These ions have no lone pair of electrons and they are positively charged. As will be discussed in chapter (II), the adsorption of pyridinium is closely related to the specific adsorption of halides. The pyridinium ion is unlikely to adsorb on a Ag surface directly, rather, it forms an ion pair with adsorbed halide anions. Again we may assume that the Raman active sites involve the Ag_4^+ cluster. The positively charged pyridinium cation seems to be electrically repelled by the positively charged Ag_4^+ cluster. However, halide anion has been known to be chemisorbed on Ag_4^+ cluster. Pyridinium cation may interact with the adsorbed halide through an electrostatic attraction or through a conjugated π orbital. A charge transfer enhancement may still be possible even though the molecule does not directly interact with Ag_4^+ cluster. We can consider the molecule (or ion)- halides-metal cluster as a whole. The halide ion can act as a bridge for the electron transfer between the metal and molecules.

The third type of interaction involves those molecules which do not have

chemical interactions with metal surfaces. This kind of molecule is said to be physisorbed. The interaction of physisorption may involve an electrostatic attraction or a dipole-dipole interaction. As the molecule approaches the surface, the surface may act as a mirror where the molecular dipole moment induces an image dipole on the opposite side of the surface of opposite polarity. These two dipoles tend to attract each other by means of dipole-dipole interaction. In this kind of interaction, only an electromagnetic enhancement effect may be involved. For example, the pentaammineosmium (III) or pentaammineruthenium (II) complex with pyridine ligand, $Os(NH_3)_5py$, $Rh(NH_3)_5py$ may be physisorbed on metal surfaces [33]. This is indicated by the fact that the complexes with a ligand of pyridine show much lower intensity than that of the complexes with a ligand of pyrazine or 4',4'-bipyridinium which contains a remote N lone pair of electrons with which the complex seems to bond to the metal surface.

(e) Polarization

The polarization of a molecule has definite direction components and as such, is a tensor quantity. The direction of the induced dipole moment will depend upon the value of the components of α. For a spherically symmetric molecule such as CCl_4, $\alpha_x=\alpha_y=\alpha_z$. Thus the direction of the induced dipole will always be the same as the direction of the plane of the incident radiation. It can be seen that a vibration which preserves the molecular symmetry will

give rise to a modulated induced dipole moment in a direction parallel to the plane of polarization of the incident radiation. Modes which distort the molecular symmetry will give rise to a modulated induced dipole moment which will have components in directions other than parallel to the place of polarization of the incident radiation. Extending this, it may be seen that the ratio of intensities of the light scattered with plane polarization perpendicular to, and parallel to, that of the incident radiation will be a measure of the non-totally symmetric character of the mode. This ratio is known as the depolarization ratio, and is given by the symbol ρ. For totally symmetric modes ρ is found to be zero. For non-totally symmetric modes, ρ lies between zero and 0.75 if plane polarized incident radiation is used, and zero and 0.86 if natural radiation is used [34].

However, for an adsorbed molecule the situation is different from that of the free molecule. The polarization properties for reflection spectroscopy of adsorbates on planar metal surface are well understood [35,36]. For an adsorbed molecule whose principle axis of molecular polarizability lies along the surface normal and which has a vibrational mode which transforms as α_{zz}, for example, there will be substantial excitation of the vibrational mode using p-polarized light at a high angle of incidence and very little excitation using s-polarized light.

A considerable difference of the polarization properties for the molecule adsorbed on rough surface from that on smooth surface and free species is ob-

served in all of the SERS studies. The value of ρ=0.60 to 0.75 is found for all SERS bands, either totally symmetric or non-totally symmetric modes. This behavior is attributed to the decrease of the symmetry for the molecules adsorbed on a roughened surface. When a molecule is chemisorbed on a surface, the point group no longer corresponds to a free molecule, rather to the molecule-metal system. On a rough surface the active site in which the molecule sits is not likely to have any symmetry because of the irregular geometry of the protrusion, and the random direction to the surface plane of the symmetry axis of the molecule. It is more than likely that no symmetry element will exist in the molecule-metal system. Therefore, according to the-trict symmetry requirement of transitions, all vibrations will be allowed, and no particular variation in the depolarization ratio among the various normal modes. We can use this property to distinguish the spectra from the molecules adsorbed on a surface (surface enhanced Raman or surface enhanced resonance Raman), from that of the molecules in a solution phase (normal Raman or resonance Raman).

Section 1.4 A Brief View of The Mechanisms of Surface Enhancement

(a) Electromagnetic enhancement

One source of the electromagnetic enhancement comes from the interaction of the incident electric field with the metallic particle. The metallic particle has a high conductivity which is expressed by its internal dielectric function

ϵ_i. The incident field polarizes the metal particle so that there develops surface charges of opposite sign on either side of the particle which alternate with the frequency of incident radiation. This mode is called a localized dipolar surface plasmon (DPS). Such a localized plasmon mode is distinct from a surface plasmon which propagates along a dielectric surface when excited by an electromagnetic wave. For a spherical particle, the average field in the radial direction, E_n, at position r can be derived as in the following equation

$$E_n = (1/3)^{1/2} E_0 [1 + 2g (a/r)^3] \quad (1.2)$$

where E_0 is incident field, E_n is the total field outside the particle, a is the radius of the particle and r is the distance to the center of the particle with

$$g = (\epsilon_i (\omega_L) - \epsilon_0) / (\epsilon_i (\omega_L) + 2\epsilon_0) \quad (1.3)$$

where ϵ_i is the dielectric function of metal, which is a function of the frequency of the oscillating radiation ω_L, and ϵ_0 is the dielectric function of medium which surrounding the metal particle. From equation (1.2) we can see that there are two terms, the first is from the incident field, and the second term is from the field of an electric dipole located at the center of the sphere, that is, the total field is enhanced by the second additional term, the reflected field produced by the metal sphere.

A calculation shows that the electromagnetic enhancement decays fairly slowly with distance from the metal sphere. So this enhancement is also called the long range effect.

The calculation also shows that the DSP enhancement with a spherical me-

tal particle does not give a large enhancement (only 50 in the conditions we are interested in) and can not explain the enhancement factor experimentally obtained (10^5-10^6). However, an improved treatment, in which the particle is considered as a prolate metal spheroid gives much higher enhancement. In this treatment the resonance maximum depend on the shape of the spheroid, for example, the resonance maximum is 480 nm at a/b=2, 580 nm at a/b=3 and 690 nm at a/b=4, where a/b is the ratio of a semi-major axis of length to a semi-minor axis of length.

There is also a further electromagnetic enhancement effect which is caused by the oscillating molecular dipole inducing a dipole in the metal particle. Thus the metal particle acts as an antenna for the near field of the oscillating molecular dipole and the emitted Raman radiation from the molecule is then enhanced by the presence of the metal particle. The antenna effect has the same form of average field as equation (1.2), but the frequency of light is the Raman frequency ω_S. This frequency is manifested in the dielectric function which becomes

$$g_0 = (\epsilon_i(\omega_S) - \epsilon_o) / (\epsilon_i(\omega_S) + 2\epsilon_o) \qquad (1.4)$$

Considering these two effects, for a molecule adsorbed on the surface of a metal sphere (r=a) with its vibrational mode oriented normal to the sphere, the total average DPS enhancement can be represented as

$$G_n = (1/9)(1+2g)^2(1+2g_0)^2 \qquad (1.5)$$

There are also some other mechanisms for the electromagnetic enhance-

ment, for example, the image effect, which involves that the electric field E of the electromagnetic wave induces an oscillating dipole μ_{ind} in the adsorbate, which in turn induces an image dipole μ_{image} in the metal. μ_{image} has a field E_{image} associated with it, which adds constructively to E, and enhances the overall field experienced by the molecule. This makes μ_{ind} larger and since the apparent adsorbate polarizability α is proportional to μ_{ind}, this is also larger. However, this effect requires very short distance between the adsorbate and the surface, and practically is not important in the electromagnetic enhancement.

(b) The Chemical enhancement

When molecules are chemisorbed on a metal surface, we can consider the molecule and the metal system as a whole, and we can assume that the Fermi level of the metal lies between the molecular ground state and one of the excited states of the molecule. The charge transfer model involves transitions from the Fermi level to the excited state or from the ground state to the Fermi level. Based on the potential dependence, we have shown [37] that molecules could be divided into two classes, those for which the voltage at maximum intensity, V_{max}, had a positive slope with excitation frequency (case I) and those for which the slope was negative (case II). This effect could be correlated with the electron withdrawing ability of the ground or excited electronic states of the molecules involved. We found that the voltage maxima

of substituted pyridines (case I) can be correlated with the Hammett sigma function, and the voltage maxima of saturated nitrogen heterocycles (case II) can be correlated with pKa. In case (I) an electron is transferred from the Fermi level of the metal to the lowest unoccupied orbital in the molecule. Conversely, in case (II) an electron is transferred from the highest occupied molecular orbital to the Fermi level of the metal.

The theoretical treatment of the charge transfer mechanism has been given [38] and can be used to interpret many SERS phenomena quite satisfactory. Based on the classic expression for the dipole moment polarizability the intensity of Raman scattering for a transition from the initial state I to the final state F is given by the expression

$$I = [8\pi (\omega + \omega_{FI})^4 I_L / 9c^4] \Sigma | \alpha_{\rho\sigma} |^2 \qquad (1.6)$$

where I_L is the incident laser intensity at frequency ω, while ω_{FI} is a molecular transition frequency between states I and F. In terms of the quantum mechanical wave functions associated with the molecular states we may use second order perturbation theory to obtain the polarizability

$$\alpha_{\sigma\rho} = \sum_{K \neq I,F} \left\{ \frac{\langle I|\mu_\sigma|K\rangle \langle K|\mu_\rho|F\rangle}{E_K - E_I - \hbar\omega} + \frac{\langle I|\mu_\rho|K\rangle \langle K|\mu_\sigma|F\rangle}{E_K - E_F + \hbar\omega} \right\}. \qquad (1.7)$$

In this equation μ is the dipole moment operators for the polarization directions σ and ρ. E_I and E_F are the energys of the initial and final states, $< I | \mu_\rho | K >$ represents the dipole moment matrix element.

For most molecules of interest to us we may make the zero order Born-Oppenheimer approximation to separate the nuclear from the electronic motions. But in the treatment of Raman intensities it is necessary to consider the small deviations in the electronic wave functions with nuclear motion. In the Herzberg-Teller theory [39,40] it is assumed that the corrected electronic wave functions may be obtained by the use of a first order perturbation expansion as a linear combination of the complete set of zero-order Born-Oppenheimer functions, and this expansion allow states to 'borrow' intensity from one another. A transition from M to K, which may be forbidden in the zero-order theory may obtain intensity from a nearby state I from which a transition (I--K) is allowed. The degree to which a particular vibration can mix state M with state I is represented by a coupling matrix element $h_{IM}(Q)$

$$h_{IM}(Q) = \langle I_e,0 \mid \partial H'/\partial Q \mid M_e,0 \rangle \qquad (1.8)$$

This term is normally neglected in the Born-Oppenheimer approximation. This intensity borrowing is not important for the transition between molecular states because of the large energy gap between ground and electronic excited states. However, if we consider the metal state as an intermediate state which may lie close to the molecular ground state, this intensity borrowing may be possible.

In a metal (Ag) to molecule charge transfer (case I), the process can be described [41] as (i) a metallic electron in a conduction band absorbs a photon, the electron being promoted to vacant band above the Fermi level leaving a

hole below the Fermi level in the filled band; (ii) the electron either tunnels to a temporary negative molecular complex or crosses over to an excited state of the molecule metal system which is the charge transfer acceptor level of the chemisorbed molecule; (iii) the electron returns to the metal, recombines with the hole and in the process reradiates a Raman shifted photon; (iv) and the molecule is left in the exited vibrational state. The charge transfer resonance energy is the difference between adatom surface state level and charge transfer acceptor level.

A similar set of steps can be described for the case of the molecule to metal charge transfer (case II).

This charge transfer mechanism well explains the resonance excitation and resonance potential dependence. The resonance maximum occurs at $E_K - [E_{F(0)} + eV] = h\omega$ for case (I) and $[E_{F(0)} + eV] - E_I = h\omega$ for case (II). The electrode potential can tune the Fermi level to match the resonance excitation. A negative shift of the potential will raise the Fermi level, and therefore reduce the energy difference between the Fermi level and the excited state of the molecule in case (I), then a shift to the lower energy for the resonance frequency will be observed. Conversely, in case (II), the negative shift of the potential will increase the energy difference between the Fermi level and the ground state of the molecule, then a shift to a higher energy for resonance frequency will be observed. A theoretical calculation shows that the predicted intensity resonance vs. voltage fits the experimental curves quite well [38].

In chapter (V) we will discuss surface enhanced photochemistry. A similar charge transfer process will be described (i) the electron in metal absorbs a photon then the electron is promoted to vacant band; (ii) the electron either tunnels or crosses over to an excited state of molecule-metal system; (iii) instead of returning back to the metal, a subsequent chemical process may occur in this excited state. In this case a surface enhanced chemical reduction may take place. In the other case, the charge transfer is from molecule to metal, after the electron transfers to the metal, the molecule is temporary positively charged, so a subsequent chemical reaction may occur and cause an oxidation.

The enhancement of the photochemistry of adsorbed molecules is reflected in the shift of the excitation radiation to lower energy (from UV to visible) in comparison with the free molecules since the energy between the Fermi level and molecular-metal complex may much smaller than the energy between the ground state and the excited state of free molecules. Based on the charge transfer mechanism a resonance excitation and a potential dependence for photochemistry will be discussed in chapter (V).

Section 1.5 An over view of this thesis

This thesis is concerned with the SERS study of the physical and chemical properties of some molecules at the electrode/solution interfaces.

In chapter (II), the study is concentrated on the equilibrium between pyridine and its protonated form, pyridinium. Based on the dependence of the in-

tensity of pyridinium on chloride concentration and the concentration of background electrolyte, pyridinium is considered not to be directly adsorbed on the electrode surface, but rather located in the diffuse double layer and associated with specifically adsorbed chloride to form an ion pair. The in-situ measurement of pH and the SERS of pyridine and pyridinium during a pH titration reveal a linear relation between surface pH and bulk pH. Specifically adsorbed chloride causes a decrease in the surface pH. This decrease is explained by a shift of the electrostatic potential at the outer Helmholtz plane caused by specific adsorption of chloride.

In chapter (III), the interaction between different types of surfactants and the electrode surface is discussed. This is the first systematic study of the surfactants using SERS technique. A head-on orientation is determinend for the surfactants with all types of head groups. But a reversed orientation is observed when the potential is shifted to more negative than -0.8 V vs. SCE. The SERS spectrum in a C-C stretching region is consistent with a trans conformation of the alkane chain on a Ag surface, indicating that the surfactant is packed as a 'solid like' layer. An additional enhancement at a very negative potential is attributed to the change of the dielectric constant at the interface due to the formation of a hydrogen layer.

In chapter (IV), the surface concentration of methyl viologen is measured by cyclic voltammetry and the enhancement factor of SERS is calculated based on the measurement of the surface concentration. A linear relation is found

between SERS intensity and surface concentration in a certain concentration range. The determination of the surface coverage is based on the separation of the adsorption current from the diffusion current by choosing proper conditions. The surface concentration is also detected at different ORC pretreatment conditions. This study indicates that only two fold increase of the surface concentration is obtained after a moderate ORC pretreatment in the absence of adsorbate, and a four fold increase of the surface concentration is obtained when the pretreatment is carried in presence of adsorbate. The latter case indicates that a large amount of adsorbate is trapped in the silver layer during the ORC treatment.

In chapter (V), a surface enhanced photochemical reduction of p-nitrobenzoic acid (PNBA) is studied on Ag island films and roughened Ag electrode surfaces. A change in the SERS spectrum as the irradiation of laser light is attributed to a photo induced electrochemical reduction of PNBA. The reduction product is identified as p-aminobenzoic acid (PABA) however azodibenzoate, as a reduction product, may also be possible. It is found that the reduction necessitates both laser excitation and roughened metal surface. This reduction is more likely a photo induced process rather then a thermal induced reaction. The photolysis is determined as the function of photo flux, excitation radiation, electrode potential and the nature of solvent. A charge transfer mechanism is described for the surface enhanced photochemical reduction.

REFERENCES

[1] W. G. Johnson and L. A. Heldt, J. Electrochem. Soc. 121 (1974) 34

[2] G. J. Slusser and N. Winograd, Surface science 95 (1980) 53

[3] M. Bowker and R. J. Madix, Surface Science 95 (1980) 190

[4] R. Ducros, M. Alnot, J. J. Ehrhardt, M. Housely, C. Piguard and A. Cassuto, Surface Science 94 (1980) 154

[5] H. Frotzheim, in 'Topics in Current physics' Vol. 4, p205 Springer-Verlag New york (1977)

[6] S. Shibata, Electrochim. Acta., 17 (1972) 395

[7] H. J. Read and R. Weil, J. Appl. Phys. 21 (1950) 1068

[8] F. Kimura, J. Umemura and T. Takenaka, Langmuir 2 (1936) 96

[9] A. Smekal, Naturwiss, 11 (1923) 873

[10] C. V. Raman and K. S. Krishnan, Nature 121 (1928) 501

[11] M. G. Albrecht and J. A. Creighton, J. Am. Chem. Soc., 99 (1977) 5215

[12] D. J. Jeanmaire and R. P. Van Duyne, J. Electroanal. Chem. 84 (1977) 1

[13] M. Moskovits and D. P. DiLella in 'Surface Enhanced Raman Scattering' (R. K. Chang and T. E. Furtak, eds) pp 243-273 Plenum Press. New York (1982)

[14] P. A. Lund R. R. Smardzewki, I. E. Tevault, Chem. Phys. Lett. 89 (1982) 508

[15] W. Krasser, Int. Conf. of Raman Spectroscopy, Ottawa, Canada (1980) p420

[16] T. Lopeez-Rios, C. Petternkoffer, I. Pockrand and A. Otto, Surf. Sci. 121 (1982) L541

[17] T. E. Furtak and J. Reyes, Surface Science 93 (1980) 351

[18] B. Pettinger, U. Wenning and H. Wetzel, Chem. Phys. Lett. 67 (1979) 192

[19] J. P. Evans, M. G. Albrecht, D. E. Ullevig, and R. M. Hexter, J. Electroanal. Chem. 106 (1980) 209

[20] J. E. Rowe, C. V. Shank, D. A. Zwemer and C. A. Murray, Phys. Rev. Lett. 44 (1980) 1770

[21] C. S. Allen, G. C. Schatz and R. P. Van Duyne, Chem. Phys. Lett. 75 (1980) 201

[22] J. A. Creighton in 'Vibrational Spectroscopy of Adsorbates' ed. R. F. Willis, (Springer-Verlag, New York, 1980) p145

[23] I. Pockrand and A. Otto, Solid State Commun. 35 (1980) 861

[24] B. J. Messinger, K. W. von Raben, R. K. Chang and P. W. Barber, Phys. Rev. B 24 (1981) 649

[25] P. W. Barber, R. K. Chang and H. Massoudi, Phys. Rev. B27 (1983) 7251

[26] K. Arya, R. Zeyher and A. A. Maradudin, Solid State Commun. 42 (1982) 461

[27] D. Roy and T. E. Furtak, Chem. Phys. Lett. 124 (4) (1986) 299

[28] R. C. Baetzold, J. Chem. Phys. 55 (1971) 4363

[29] M. Moskovits and D. P. DiLella, Chem. Phys. Lett. 73 (1980) 500

[30] D. P. DiLella and M. Moskovits, J. Phys. Chem. 85 (1981) 2042

[31] K. Manzel, W. Schutze and M. Moskovits, Chem. Phys. Lett. 85(2) (1982) 183

[32] Ping Gao and M. J. Weaver, J. Phys. Chem. 89 (1985) 5040

[33] S. Farquharson, K. L. Guyer, P. A. Lay and R. H. Maynuson, Gov. Rep. Announce., Index (U.S.) 84(20) (1984) 64

[34] H. A. Syzmanski in 'Raman Spectroscopy, Theory and Practice' Vol. 1, Penum Press, (1967) p130

[35] R. G. Greenler, J. Chem. Phys. 44 (1966) 310

[36] D. R. Mullins and A. Campion, J. Chem. Phys. 88 (1984) 8

[37] J. R. Lombardi, R. L. Birke, L. A. Sanchez, I. Bernard, S. C. Sun, Chem. Phys. Lett. 104 (1984) 240

[38] J. R. Lombardi, R. L. Birke, Tianhong Lu and Jia Xu, J. Chem. Phys. 84(8) (1986) 4174

[39] A. C. Albrecht, J. Chem. Phys. 34 (1961) 1436

[40] J. Tang and A. C. Albrecht in 'Raman Spectroscopy, Theory and Practice' (H. A. Szymanski, ed) Vol. 2 p35-68 Plenum, New York (1970)

[41] R. K. Chang and B. L. Laube in 'CRC Critical Reviews in Solid State and Materials Science' pp 1-73 vol. 12 CRC Press. Inc. 1984

CHAPTER (II)

THE EFFECT OF pH, CHLORIDE ION AND BACKGROUND ELECTROLYTE CONCENTRATION ON THE SERS OF PYRIDINIUM SOLUTION

Section 2.1 Introduction

Following the initial discovery of surface enhanced Raman scattering (SERS) [1], a large number of experimental investigations were carried out with pyridine as a SER scatterer. Less consideration has been given to its protonated form, the pyridinium ion [2-6]. Van Duyne [2] was the first to study the effect of pH on the SERS of pyridine solution; however, the electrode potential in this investigation was negative to -0.5 V vs. SCE and the spectrum of pyridinium could not be obtained. The SERS of pyridinium, however, can be found at potentials positive to ca. -0.5V vs. SCE as discussed by Regis and Corset [3], Atkinson et al. [4], Birke et al. [5], and Rogers et al. [6]. The spectrum in the region of 1000-1050 cm^{-1} and the low frequency band around 235 cm^{-1} have recently been discussed as a function of pH [6]. Comparing the profile of the broad 235 cm^{-1} band in 1.0 M KCl, 1.0 M KBr and 0.1 M KBr/0.05 M pyridine, Rogers et al. [6] concluded that this surface band is due to a combination of Ag-Cl vibrations from different surface sites and not to a Ag-N vibration. Results of a spectral band shape analysis to be presented in this paper suggest that there is a significant change of the 235 cm^{-1} band in the presence of pyridinium. Since the pyridinium ion is positively charged and does not have a lone pair of electrons at the nitrogen, the pyridinium ion is unlikely to be directly adsorbed on a Ag surface. Thus an ion-pair interaction of the pyridinium with specifically adsorbed chloride has been suggested by several workers [3-6] as a model of the surface species.

Early results from this laboratory have briefly discussed the SERS of pyridinium ion at a Ag electrode [5], and the present investigation is a more detailed study in this system of the effects of pH, solution chloride ion concentration, and background electrolyte concentration on the SERS of pyridinium. We have found that when solution conditions are varied, the use of a flow-cell and optical multichannel analyzer (OMA) detection give results which are independent of time and alignment. We report for the first time the SERS bands of pyridinium over the full spectral region of 100-4000 cm^{-1}. These bands are assigned and also compared with the normal Raman bands of aqueous pyridinium and the SERS of pyridine. Comparison of the effects of chloride ion and electrolyte concentration on the SERS of both pyridinium and pyridine gives additional evidence that pyridine is directly adsorbed on the surface while pyridinium is separated from the surface by specifically adsorbed chloride and located in the diffuse double layer. A similar mechanism for other positively charged species which are unable to bind directly to a positively charged metal surface has been given recently [7] based on the attraction of the positively charged species into the diffuse double layer by specific anion adsorption. Results presented in this paper indicate that SERS can be directly used to probe both changes in the potential at the outer Helmholtz plane and changes in surface pH as the amount of specifically adsorbed chloride is changed.

Section 2.2 Experimental

All the spectra were excited with the 488 nm line of an Ar^+ laser (Spectra Physics 64) with a power of 50mw. The spectra were recorded with a Spex 1401 double spectrometer (bandpass 2 cm^{-1}). In some experiments a Spex 1877 triplemate spectrometer with an intensified Tracor Northern photodiode linear array (TN-1223-2I) and a model TN-1710 Tracor Northern optical multichannel analyzer (OMA) was used. For the later case, a grating of 1800 grooves per mm gave a spectral coverage of about 870 cm^{-1}, with a bandpass of 0.046 nm (1.7 cm^{-1} at 19436 cm^{-1}).

The electrode potential at a 99.99% pure polycrystalline Ag electrode was controlled with a Princeton Applied Research (EG & G PARC) Model 173 Potentiostat, together with a PARC Model 175 Universal Programmer. All potentials are quoted versus a saturated calomel electrode (SCE).

A double potential step (DPS) -0.2 V to +0.6 V to -0.2 V was used for the oxidation reduction cycle (ORC) when the pretreatment was carried out in the absence of chloride, and a DPS -0.2 V to +0.3 V to -0.2 V was used for the ORC pretreatment in the presence of chloride. The potential was held at +0.6 V or +0.3 V for 2 seconds. All pretreatments were performed in the dark. Two types of preteatment methods were used. In one method the pretreatment was made with the same solution used to obtain the SERS spectrum. A second method was used when the chloride and/or background electrolyte concentrations for the SERS measurement were different from the pretreatment solu-

tion. In this case a flow-cell (20 ml in volume) was used, in which a 15 ml pretreatment solution was washed out by a 250 ml test solution, which was deoxygenated in advance. The large amount of solution ensured a complete replacement of the original solution in the flow-cell. During the replacement, the electrode potential was held constant and the electrode was immersed in the solution throughout, so that there was less risk of losing active sites. This method has an advantage over an out-of-cell pretreatment process, where after pretreatment the electrode has to be disconnected and then washed. Since the active sites are sensitive to the potential change, the active sites may be lost during the transfer of the electrode from one cell to another. In the flow-cell pretreatment method each change of chloride and/or background electrolyte concentration constituted a new experiment, that is, the electrode was taken out and repolished using 0.1 μ alumina powder, then washed and cleaned in Ultrasonic cleaner for 3 minutes. The cell was washed first and then filled with the solution for pretreatment (0.05 M pyridine and 0.1 M KNO_3). After pretreatment and before replacement, the 1008 cm^{-1} line was taken as a standard line. All of the intensities were calibrated by this standard.

Section 2.3 Results and Discussion

(a) The assignment of the pyridinium spectrum

The band position and assignments of the surface enhanced Raman spectrum of pyridinium (0.05 M in 0.1 M KCl at pH=2, -0.3V) are listed in Table

1. The normal Raman bands of aqueous pyridinium (about 4.5 M) and the SERS of pyridine are also listed for comparison. Considering the high concentration of pyridinium necessary to obtain a normal Raman spectrum, there is no doubt the in-situ measurements are surface enhanced. The vibrational mode assignments of the SERS of pyridinium is based on the assignment of aqueous pyridinium [8], and solid state pyridinium chloride [9]. A rather close agreement between the SERS and aqueous Raman can be seen; the frequency shifts are less than 6 cm^{-1} between the SERS of pyridinium and its normal Raman (NR) spectrum . The relative intensities are also similar, except for the N-H vibrational modes, which are hardly seen in SERS. The 1252 cm^{-1} in-plane N-H deformation is quite strong in normal Raman but very weak in SERS. Another N-H in-plane deformation band at 1242 cm^{-1} is absent in SERS. This might indicate an interaction of pyridinium with specifically adsorbed chloride.

A five to ten-fold decrease in intensity in the ring breathing mode region of pyridinium (at pH=1.9) in comparison with pyridine (at pH=8.5) has been reported [6]. The same extent of decrease was observed in our experiment when pretreatment was carried out in acidic solution (pH=2). But only a one third decrease in intensity was observed when the pretreatment was first carried out at pH=8 (0.1 M chloride and 0.05 M pyridine) and the spectrum was then measured after in-situ adjustment of the pH to 2.0.

Table 1 Raman shift and assignment of pyridinium

SERS of pyridinium [a]				normal Raman [b] of pyridinium		SERS of [c] pyridine
Wilson's number	Approximate description of vibration	freq. /cm^{-1}	rel. int.	freq. /cm^{-1}	rel. int.	freq. /cm^{-1}
		238	71			238
16 a	out-of-plane ring deformation	394	4	393	4	412
				580	1	
6 a	in-plane ring deformation	610	4	608	10	623
6 b	in-plane ring deformation	636	9	637	18	651
						750
				806	2	
10 a	out-of-plane C-H deformation	878	3	872	1	884
						945
1	total symmetric ring "breathing"	1008	100	1009	100	1008
12	trigonal ring "breathing"	1026	31	1026	40	1036
18 a	in-plane C-H deformation	1056	6	1057	10	1068
15	in-plane C-H deformation	1160	1	1160	4	1153
9 a	in-plane C-H deformation	1196	13	1198	15	1214
	in-plane N-H deformation			1242	1	
	in-plane N-H deformation	1252	1	1252	9	
				1339	2	
				1383	2	
				1487	2	1498
19 b	ring stretch	1598	5			
8 b	ring stretch	1610	10	1612	10	1570
8 a	ring stretch	1630	21	1634	16	1595
		2958	1			2960
7 b, 20 a	C-H stretch	3032	3			2997
2, 13, 20 b	C-H stretch	3090	14			3067
						3142
						3186

a: SERS spectrum of pyridinium at -0.3V, in 0.05 M pyridinium (pH=2) and 0.1 M KCl, double-potential step pretreatment -0.2V to +0.3V to -0.2V; 2 sec. pulse.

b: Normal Raman spectrum of aqueous pyridinium (pyridine hydrochloride in H_2O 60%) [8].

c: SERS spectrum of pyridine at -0.3V, in 0.05 M pyridine (pH=8) and 0.1 M KCl.

(b) The 1000-1050 cm^{-1} region

Fig.1 shows a portion of the spectrum obtained with an OMA in the region 950-1050 cm^{-1}, as a function of pH and applied voltage. At pH=2.2 the ratio of pyridinium to pyridine in solution is about 1000:1, and only the spectrum of pyridinium is observed. The two strongest lines are at 1008 cm^{-1} and at 1026 cm^{-1}. The intensity maxima are at about -0.25V. The accepted assignments (Wilson numbering) are ν_1 and ν_{12} respectively [8,9]. Both lines are of a_1 symmetry. Upon deuteration a low frequency shift from 1026 cm^{-1} for PyH^+ to 1022 cm^{-1} for PyD^+ indicates that this vibration includes a motion of the N-H part of the molecule, so we assign this band to ν_{12} (trigonal breathing), instead of ν_{18} (in-plane C-H deformation). This is in agreement with the assignment by Spinner [8], but disagrees with the assignment by Cook [10]. At pH=8.2 the ratio of pyridinium to pyridine in solution is about 1:1000, and only the spectrum of pyridine is observed. The two strongest lines are at 1008 cm^{-1} and 1036 cm^{-1}. At about -0.6V the intensities reach a maximum. It should be noted that there is another line at 1025 cm^{-1} for pyridine (pH=8), which has been assigned to strongly bound Lewis acid coordinated (chemisorbed) pyridine [11]. This line only occurs for pretreatment conditions where a large amount of charge is passed, such as a long step time in the DPS or a slow triangular sweep for an ORC, or where several sequential DPS pulses are used for pretreatment. The exposure of the electrode to an Ar^+ laser beam during the ORC also increases the intensity of the chemisorbed species. In our work the pretreatment conditions were always carefully controlled to avoid

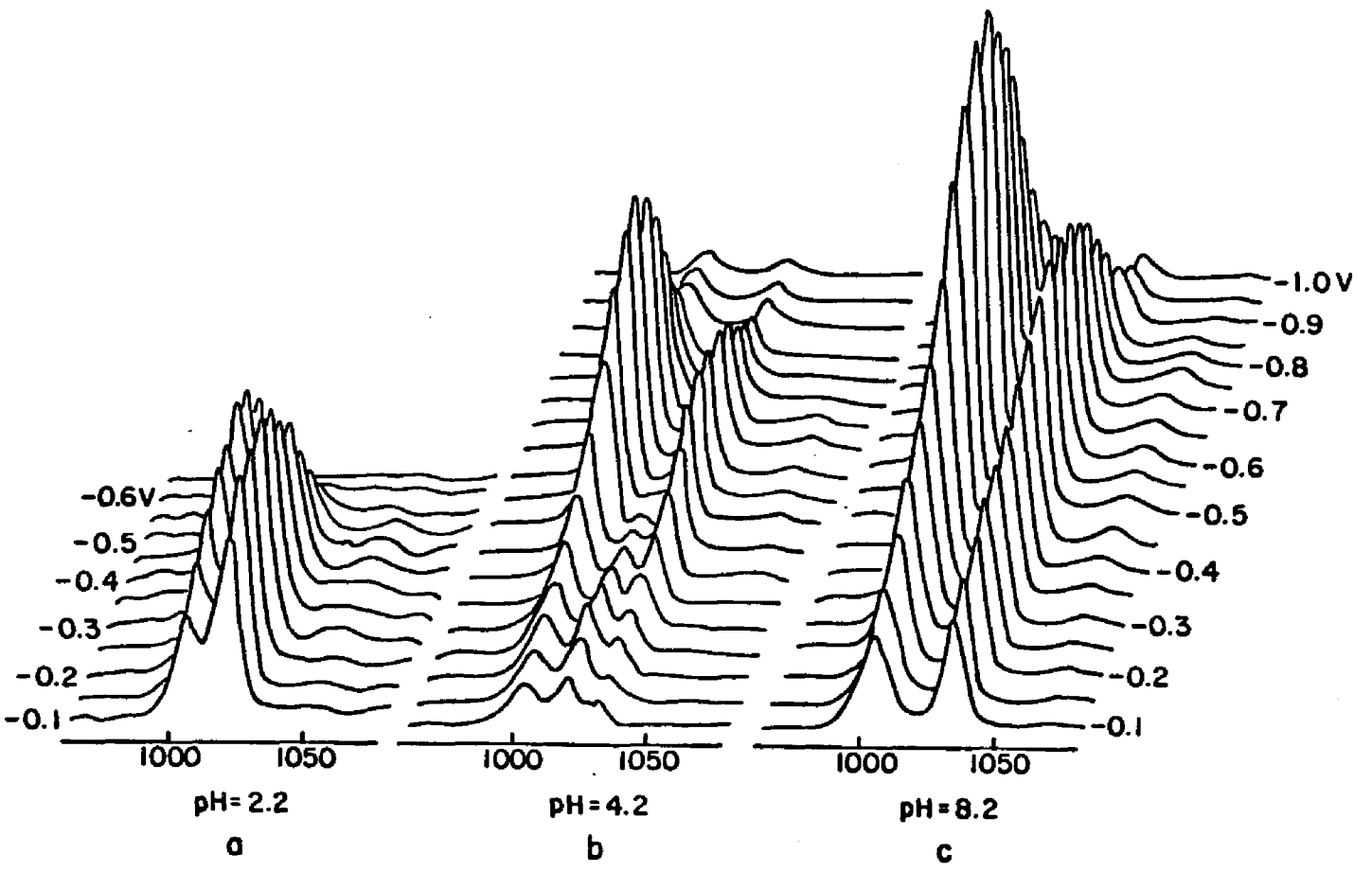

Fig.1: SERS spectrum of pyridine in the 950-1050 cm^{-1} region at various potentials. (a) pH=2.2; (b) pH=4.2; (c) pH=8.2 in 0.05 M pyridine and 0.1 M KCl. The pH was adjusted with HNO_3. Double potential step pretreatment -0.2 to +0.3 to -0.2V with a 2 sec. pulse duration was used.

the formation of the chemisorbed pyridine. Thus in this study the 1025 cm^{-1} line can be used to characterize the pyridinium species. At a pH=4.2 the ratio of pyridinium to pyridine in solution is about 10:1, and the spectrum is a mixture of both species. The SERS of pyridinium disappears almost completely at -0.6V. The potential dependence of our pyridinium spectrum which shows a maximum is different from that reported by Rogers [6], who indicated a simple decay of the intensity of the 1008 cm^{-1} and 1025 cm^{-1} bands (pH=1.9) from -0.05V through -0.6V. The difference between the experiments is that in their work [6] the intensity measurements were made following about 30 minutes at each new potential, while in our study the spectrum was recorded by an OMA system, and each 50 mV voltage increment was stepped in 30 seconds.

(c) The surface band

The low lying SERS vibration at about 235 cm^{-1} in the silver-pyridine-chloride system was studied as a function of pH and voltage [Fig.2]. The 235 cm^{-1} band in the pyridinium solution (pH=2.2) peaks around -0.2V, similar to the 1008 and 1026 cm^{-1} bands, and disappears at -0.6V. As the potential changes to more negative values, the low frequency line in either pyridinium or pyridine solution shifts to lower frequency. There has been some controversy as to whether the band around 235 cm^{-1} is to be attributed to a Ag-N vibration [12-14] or to Ag-halide vibrations [6,15-20]. For pyridine in basic medium, it has been suggested that both vibrations occur, with the Ag-Cl stretch-

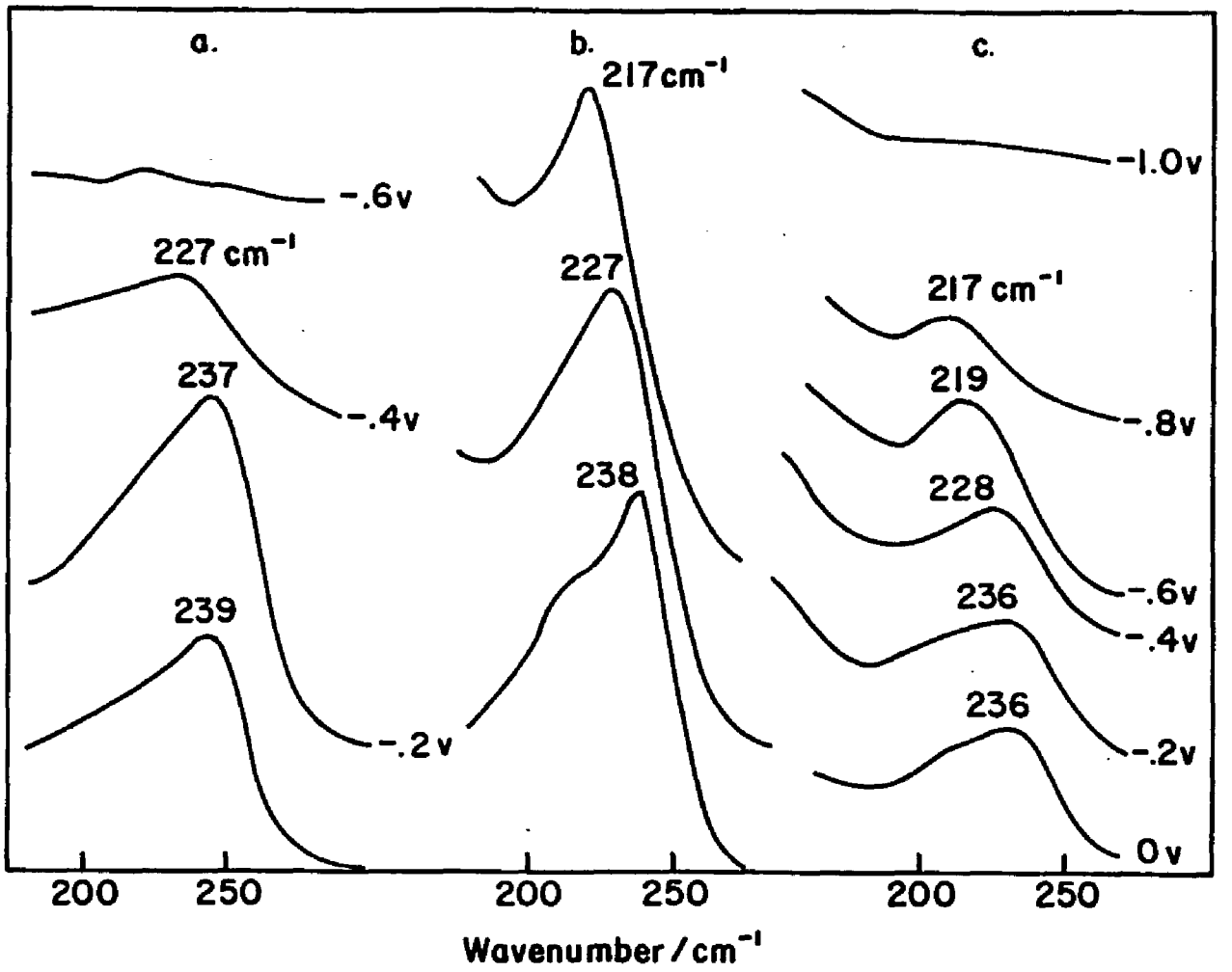

Fig.2: SERS spectrum of pyridine in the 150-300 cm^{-1} region at various potentials. (a) pH=2.2; (b) pH=4.2; (c) pH=8.2 in 0.05M pyridine and 0.1 M KCl. pH was adjusted with HNO_3 and pretreatment conditions are the same as Fig.1.

ing vibration corresponding to the 236 cm^{-1} band at potentials positive to -0.4 V and the Ag-N stretching vibration corresponding to 217 cm^{-1} band at potentials negative to -0.6 V [15]. In acidic medium [Fig.2a] the 217 cm^{-1} band does not appear which is consistent with this assignment; however, in basic medium [Fig.2c] there is a shift in the band position with potential which makes the assignment of the band to two different vibrations less convincing.

From a comparison of the profile of the 235 cm^{-1} band with solutions containing 1.0 M KCl, 1.0 M KBr, and 0.1 M KBr/0.05 M pyridine, it was concluded that only Ag-Cl vibrations are involved [6]. Using an empirical extrapolation of the background, we have compared the band shape at about 235 cm^{-1} in 1.0 M KCl/0.05M pyridine at different pH with the band shape of the 235 cm^{-1} band in pure 1.0 M KCl, both spectra being recorded at -0.2V. We analyzed these two bands using the method of moments [21,22]

$$M_n \approx \Sigma (\omega_i - \bar{\omega})^n S_i \Delta\omega / (2L+1) \Delta\omega$$

where ω is frequency, $\bar{\omega}$ is chosen so that the first moment $M_1 = 0$, L is chosen as limits beyond which the spectral intensity is negligible, and S_i are the digitized intensities. The square root of the second moment is related to the half-width of the spectral line. The cube root of the third moment may be taken to be a measurement of the skewness of the line. In the case of pure 1.0 M KCl, $M_2^{1/2}$ =18.0, 17.9 and 18.2 cm^{-1} for pH=2, 5 and 8 respectively. And for

1.0 M KCl/0.05M pyridine, $M_2^{1/2}$ =17.8, 17.9 and 17.9 cm^{-1} for pH=2, 5 and 8 respectively. These values are quite close to each other, and also coincide with the previous work in an isoquinoline-chloride system [22], where $M_2^{1/2}$ =18.0 cm^{-1}. However, the third moment measurement of the surface band in the presence of pyridinium is found to be more skewed than the band in the pure chloride. A momental skewness $\alpha_3/2 = M_3/M_2^{3/2}$ = 0.07, 0.04 and 0.03 was calculated for pure chloride solutions at pH=2, 5 and 8 respectively showing a quite symmetric band shape. On the other hand in the presence of pyridine, $\alpha_3/2$ =-0.22, -0.17 and -0.17 for pH=2, 5 and 8 respectively, which shows a negative momental skewness indicating a low frequency distortion.

From the facts that the 235 cm^{-1} band is observed in pure chloride either at pH=8, pH=2 or the pH in between and the band width of pure chloride is almost the same as that in the presence of pyridine or pyridinium, we conclude that the 235 cm^{-1} line must mainly involve a Ag-Cl vibration. However, the distortion of this line in the presence of pyridine or pyridinium indicates that some interaction between pyridinium and chloride lowers the vibration frequency of the Ag-Cl, giving the observed distortion. This is also consistent with the weak or absent N-H deformation bands in the SERS of pyridinium. Also as will be discussed further on, the 235 cm^{-1} band grows in intensity with an increase in pyridinium concentration at fixed chloride concentration. This again indicates that the presence of pyridinium in the interface influences the low frequency line.

A comparison of the SERS of pyridine and pyridinium was also made in a deuterium oxide medium. The experiments were carried out under dried nitrogen to avoid the interference of moisture. Well-defined spectra of both pyridine and pyridinium were obtained. The spectrum of pyridine (pH=8) in D_2O medium is identical with that in H_2O, because pyridine has no exchangeable hydrogen. The 1008 cm^{-1} band of pyridinium in H_2O shifts to 994 cm^{-1} in D_2O, whereas the 1026 cm^{-1} band only shifts to 1022 cm^{-1} (Fig.3). The low frequency band does not change peak position in D_2O on going from pyridine to pyridinium, both peaks are at 229 cm^{-1} (Fig.3). This supports the hypothesis that this low frequency band mainly involves the Ag-Cl vibration; however, the shift of the surface band from between 236-239 cm^{-1} in H_2O to 229cm^{-1} in D_2O does indicate that a weak interaction involving Ag-Cl and the solvent.

(d) The effect of chloride

In order to further elucidate the nature of the halide-pyridinium species, the effect of chloride concentration on the SERS intensity of pyridinium was studied. The pyridinium ion concentration was kept constant at 0.05 M (pH=2.2, at -0.2 V) and the chloride concentration was varied. The pretreatment was carried out in the absence of chloride (a solution containing 0.05 M pyridine and 0.1 M KNO_3). A flow-cell was used, and the pretreatment solution was replaced by a solution containing the same amount of pyridine and KNO_3 (pH=2) and different amounts of chloride. Each change of chloride concentration indicates a new experiment.

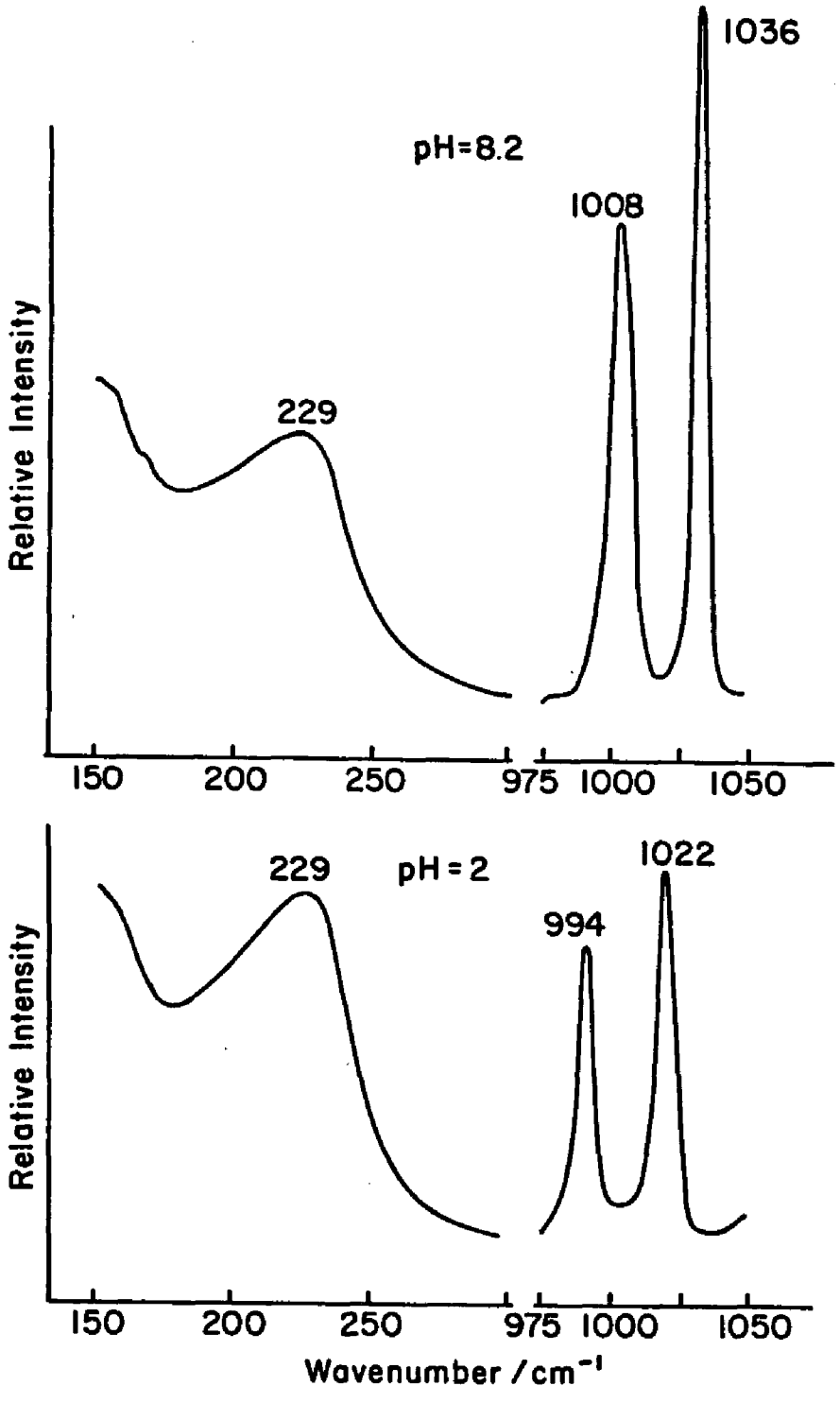

Fig.3: SERS spectrum of pyridine in D_2O at pH=8.2 and pH=2, in 0.05M pyridine and 0.1M KCl, at -0.2V. Conditions are the same as in Fig.1.

A peaked curve was observed for the plot of the intensity of the 1008, 1025 and 235 cm^{-1} lines vs. the logarithm of the chloride concentration (Fig. 4). As the chloride concentration is increased the intensity of all the three lines (1008, 1025, 235 cm^{-1}) increases until it reaches a maximum (at about 1:4 chloride to pyridinium). As the chloride concentration is further increased, the intensity of the three lines drops off. They are nearly parallel in the rise and fall of their intensities. The shape of these curves is similar to the result in the pyridine-chloride solution at pH=8 [2], where the curve of the intensity of the 1006 cm^{-1} band vs. the logarithm of chloride concentration peaks at a ratio of 2:1, chloride : pyridine. It has been suggested that the pyridine is bound to a silver atom through the lone pair of electrons on the nitrogen and that the halide stabilizes the active sites [2]. However, the model of the surface structure of the pyridinium-halide system would be different from that of the pyridine-halide system. First of all, an important observation is that in the absence of chloride there is no detectable intensity of the SERS signal of pyridinium at low pH, either when the preteatment is carried out at pH=2 or when the electrode is first pretreated at pH=8 (in this case, after pretreatment a high intensity of pyridine spectrum was observed) and then adjusted to pH=2. This indicates that the appearance of the pyridinium spectrum necessitates the presence of specifically adsorbed anions. As more chloride is added more chloride is adsorbed, and so more ion pairs can be formed on the surface. It seems probable that both an electromagnetic field enhancement and

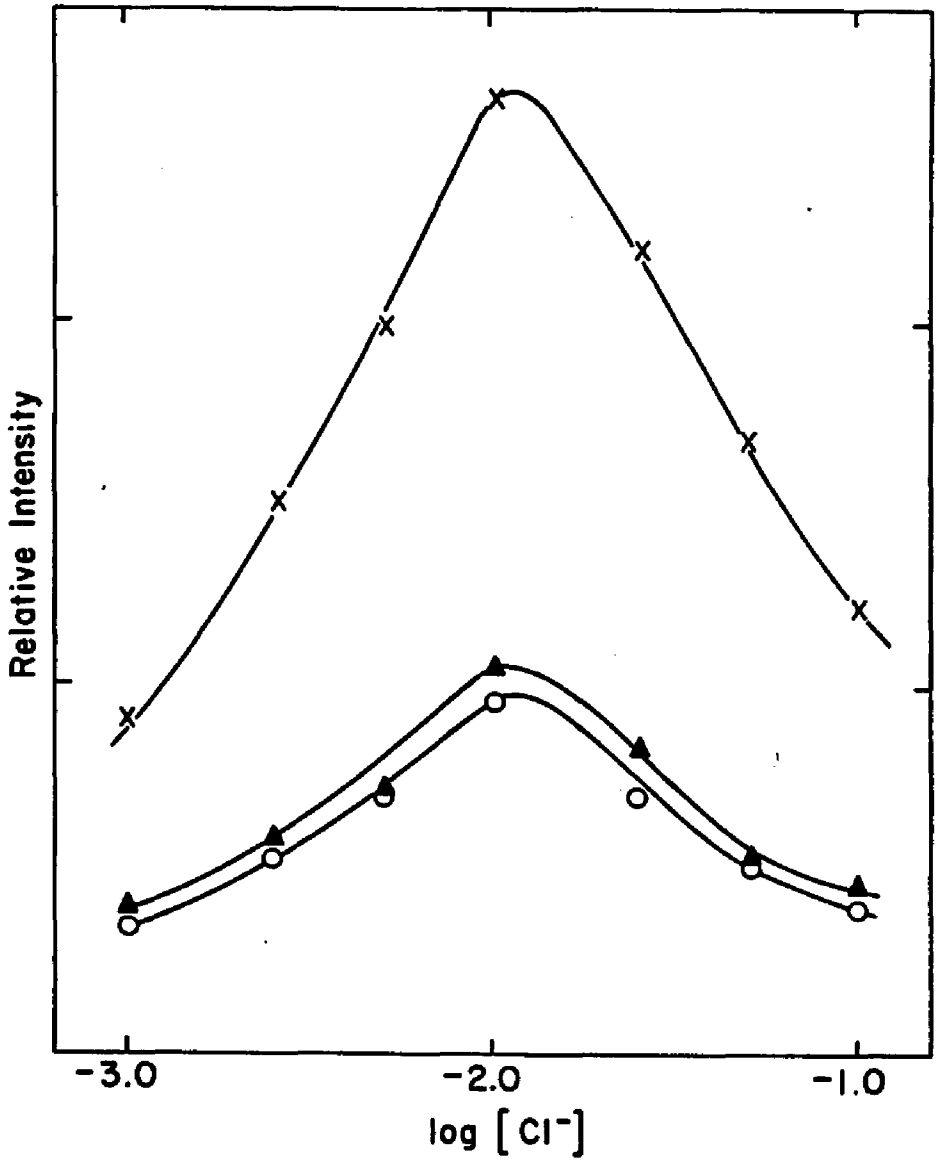

Fig.4: Relative SERS intensity of pyridinium vs. log[Cl^-] in solution containing 0.05 M pyridinium, 0.1 M KNO_3 and variable [Cl^-], at pH=2.2, -0.2V, (x) 1008 cm^{-1}; (Δ) 235 cm^{-1}; (o) 1025 cm^{-1}. Pretreatment was carried out in the absence of chloride, that is, in a solution containing 0.1 M KNO_3 and 0.05 M pyridine (pH=8.2). The pH of the test solution was adjusted with HNO_3. A double potential step -0.2 to +0.6 to -0.2V with a 2 sec. duration was used. Each change of chloride concentration constituted a new experiment.

a chemical enhancement may exist even though the pyridinium is separated from the Ag surface by chloride. It has been suggested that any electromagnetic field enhancement will not greatly diminish over the distance of a chloride ion diameter [6,23]. It is also possible that the chloride acts as a bridge for electron transfer between the Ag surface and pyridinium in a charge transfer type enhancement mechanism. At higher concentrations of chloride the intensities of the pyridinium bands and the surface band decrease as the chloride concentration is increased (Fig.4). This phenomenon may be explained by the formation of a water soluble Ag^+ chloro-complex from active Ag^+ adion sites, which would be lost due to the diffusion of the complex away from the surface. This intensity decrease is not reversible, since increasing the chloride concentration results in a decrease in the intensity but subsequently decreasing the chloride concentration does not reestablish the lost intensity. This quenching of SERS by high chloride concentration is analogous to the quenching by $S_2O_3^{2-}$ and SO_3^{2-} which was recently observed by Watanabe et al. [24].

The potential dependence of the curve of intensity vs. log[Cl^-] was also studied. A peak shift to higher chloride concentration was observed when the electrode potential was changed to more negative values. This indicates that at less positive potential less chloride will be adsorbed, and so less ion pairs can be formed. In order to keep the optimum ratio of chloride to pyridinium on the surface, the bulk chloride concentration must be increased.

It should be mentioned that it is meaningless to estimate the optimum ratio

of chloride to pyridinium on the surface from the solution concentration ratio in order to obtain a stoichiometric structure for the species on the surface. The surface ratio of $[Cl^-]/[PyH^+]$ is not only related to the bulk concentrations of chloride and pyridinium but is also affected by electrode potential and pretreatment. When the pretreatment is carried out in the absence of chloride, the intensity peaks at the ratio about 1:4 $[Cl^-]/[PyH^+]$ in solution. When the electrode is pretreated in the presence of chloride (0.005 M), the intensity maximum is at a ratio of 1:1.

(e) pH titration

The effect of chloride on pyridine and pyridinium was further studied in the following two experiments. In one experiment, the solution pH was held constant, and the concentration of chloride was changed gradually [Fig.5]. In another experiment, the concentration of chloride was kept constant, but the solution pH was gradually adjusted from basic to acidic [Fig.6]. In the first experiment, the pH was adjusted to 4.2. At this pH, the ratio of pyridinium to pyridine in the bulk is 10:1. At a low concentration of chloride only the spectrum of pyridine can be observed. On increasing the concentration of chloride, the intensities of pyridine bands decrease and the intensities of pyridinium bands increase. In the second experiment, the intensity ratio of pyridinium to pyridine as a function of bulk solution pH and chloride concentration was studied. A linear relation between the logarithm of the intensity ratio of pyridinium to pyridine, I_{PyH^+}/I_{Py}, and solution pH was found in the pH region

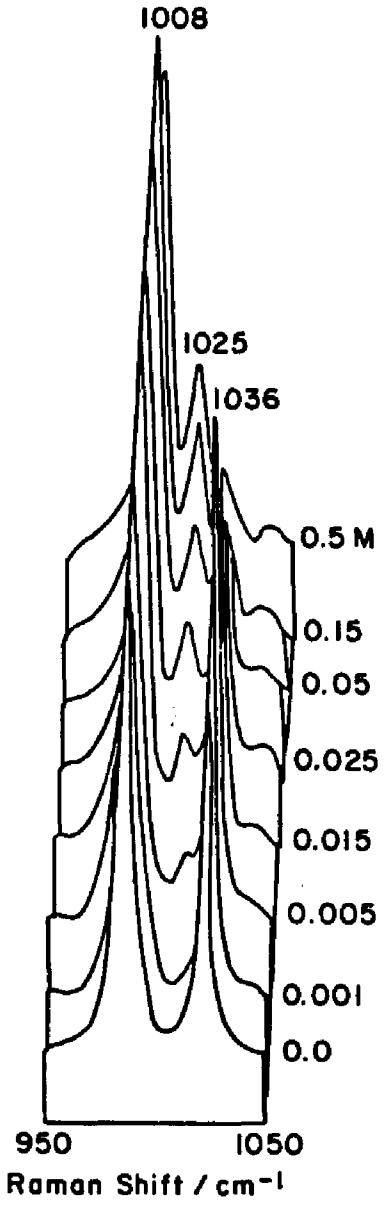

Fig.5 SERS spectrum of pyridine and pyridinium in the 950-1050 cm^{-1} region at pH=4.2 and various concentrations of chloride (from 0 to 0.5 M). Pretreatment was carried out in the absence of chloride (0.05 M pyridine, 0.1 M KNO_3, pH=4.2 adjusted with HNO_3).

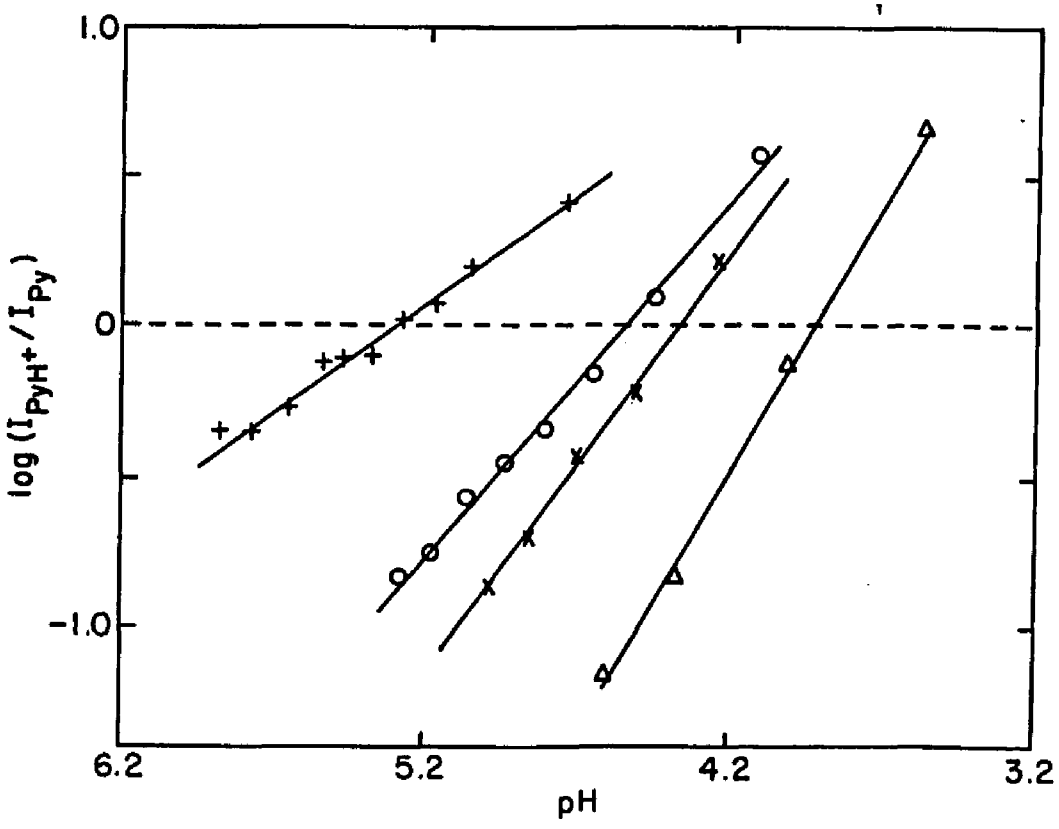

Fig.6: Logarithm of intensity ratio of I_{1025}/I_{1035} vs. pH in solution at different chloride concentrations. The concentrations of chloride are (Δ) 0.005 M; (x) 0.05 M; (o) 0.1 M; (+) 0.5 M. Solution pH and SERS spectrum were measured in-situ. Pretreatment was in the absence of chloride (0.1 M KNO_3 and 0.05 M pyridine, pH=8). After ORC the 1008 cm^{-1} line was measured as an intensity standard. The chloride was then added and the solution was titrated by 0.2 M HNO_3. Each change of chloride concentration constituted a new experiment.

where both pyridinium and pyridine intensities are comparable. This is shown in Fig.6. The pH titration was carried out in a flow-cell in order not to change the alignment. Both spectra and pH were measured in-situ. The pretreatment was carried out in the absence of chloride, then the chloride was added. Each change of chloride concentration constituted a new experiment.

In Fig.6 we chose the 1025 cm^{-1} and 1035 cm^{-1} bands to represent the intensity of pyridinium and pyridine. This seems reasonable, since for our experimental conditions the 1025 cm^{-1} band does not occur at pH=8. As previously discussed the chemisorbed pyridine was avoided by choosing appropriate preteatment conditions. A diode array detector and a multichannel analyzer were used for recording the spectra in the region of 800-1700 cm^{-1}. With a quick injection of HNO_3 into the cell, it was found that the spectrum changed from pyridine to pyridinium immediately. This indicates that this change is due to an acid-base reaction near the surface. Some other pairs of lines, such as 1196 cm^{-1} and 1212 cm^{-1} bands or 1630 cm^{-1} and 1595 cm^{-1} bands for pyridinium and pyridine were also analyzed. A similar linear relation was also obtained.

Considering the Boltzmann distribution in the diffuse double layer, the concentration of H^+ at the outer Helmholtz plane (OHP) can be represented by the following equation

$$[H^+]^o = [H^+]^* \exp (- F\phi_0/RT) \qquad (1)$$

where $[H^+]^o$ is the concentration of H^+ at the OHP, $[H^+]^*$ is the bulk con-

centration of H^+, and ϕ_0 is the electrostatic potential at the OHP with respect to bulk solution. We assume that the concentration of H^+ at the OHP is related to an "apparent" surface pH, since the thickness of whole diffuse layer for 0.1 M KNO_3 background electrolyte concentration is comparable with the size of pyridinium or pyridine (a few Å). Then from equation (1), the surface pH can be represented as

$$pH^o = pH^* + F\phi_0/2.3RT \qquad (2)$$

If we assume that the cross-section of Raman scattering does not change as the pH or chloride concentration is changed, then we have

$$I_{PyH^+}/I_{Py} = \alpha_{PyH^+} [PyH^+]^o / \alpha_{Py} [Py]^o \qquad (3)$$

where α_{PyH^+}, α_{Py} are the cross-sections of pyridinium and pyridine, respectively, and $[PyH^+]^o$, $[Py]^o$ are the concentration of pyridinium and pyridine on the surface (i. e., at the OHP). Considering the acid-base equilibrium at the OHP, we can write

$$pH^o = pK_a^o - \log ([PyH^+]^o / [Py]^o) \qquad (4)$$

where pK_a^o is the acidic ionization constant at the OHP. This pK_a^o might be different from that in bulk solution, because neither pyridine nor pyridinium are free species, and some interaction between pyridine or pyridinium with the Ag surface or the specifically adsorbed anion may change the ionization constant. Combing equations (2), (3) and (4) gives

$$\log (I_{PyH^+}/I_{Py}) = - pH^* - F\phi_0/2.3RT + pK_a^o + \log (\alpha_{PyH^+} / \alpha_{Py}) \qquad (5)$$

This equation can be compared to the empirical result from the linear relation

of Fig.6

$$\log (I_{PyH^+}/I_{Py}) = a\ pH^* + b \qquad (6)$$

where a is the slope and b is the intercept. From Fig.6 we can see that the slope a is close to -1 when the concentration of chloride is not too high, which is consistent with the theoretical relationship (5). If equation (5) were obeyed, the experimental intercept would be

$$b = - F\phi_o/2.3RT + pK_a^o + \log (\alpha_{PyH^+} / \alpha_{Py}) \qquad (7)$$

The intercept b links chloride concentration and ϕ_o. When the log (I_{PyH^+}/I_{Py}) variable is zero, the intercept value of the solution pH, pH^*_o, is directly related to ϕ_o from equation (5). If we assume that the pK_a^o and the SERS cross sections α_{PyH^+} and α_{Py} are not substantially changed by a change in adsorbed chloride ion, then $\Delta\phi_o = -0.059\ \Delta pH^*_o$. Thus the change in the intercept pH^*_o in Fig.6 should reflect a change in ϕ_o as the amount of specifically adsorbed chloride changes. When the bulk chloride ion concentration change is 0.005 M to 0.10 M, the ΔpH^*_o is 0.62 pH units indicating a -37 mV change in ϕ_o. This result is qualitatively consistent with the effect of specifically adsorbed chloride on the potential at the OHP.

Equation (2) shows that the surface pH will be lowered as ϕ_o is lowered by an increase in the amount of specifically adsorbed chloride. Substitution of equation (3) into (4) provides a means of estimating the change in surface pH^o, when the bulk chloride concentration is changed. Thus

$$pH^o = pK_a^o + \log (\alpha_{PyH^+} / \alpha_{Py}) - \log (I_{PyH^+}/I_{Py})$$

$$pH^{o} = pK_a^{ox} - \log (I_{PyH^+}/I_{Py}) \quad (8)$$

From Fig.6 it is seen that the ordinate value changes 1.0 log unit at bulk pH=4.2 when the chloride concentration is changed from 0.005 M to 0.10 M. This result shows that at the surface, the pH^{o} value is lowered by one unit on making these changes in the bulk chloride concentration, (again assuming that pK_a^{ox} is a constant).

(f) Effect of background electrolyte

The effect of background electrolyte on SERS intensity of pyridine and pyridinium was studied both in KNO_3 and $NaClO_4$ solution. We found that there was a similar effect for either KNO_3 or $NaClO_4$, which is reasonable, since both KNO_3 and $NaClO_4$ are relatively non-specifically adsorbed electrolytes. However, the effect on pyridine was very different from that on pyridinium. The pyridine spectrum is not affected much by the background electrolyte over a wide range of electrolyte concentrations from 0 to 1.5 M [Fig.7a]. However, an obvious decrease of the intensity of pyridinium was observed as the concentration of the background electrolyte was increased [Fig.7b]. It is clear that this decrease is not due to the impurities in the electrolyte, because this does not happen in the case of pyridine under the same experimental conditions. This large decrease in intensity can also not be attributed to an activity effect. The change of activity due to the change of ionic strength, which can be approximately calculated, is not as large as the change that was observed in SERS intensities. This effect seems to be attributable to a competition of Na^+ or K^+ and

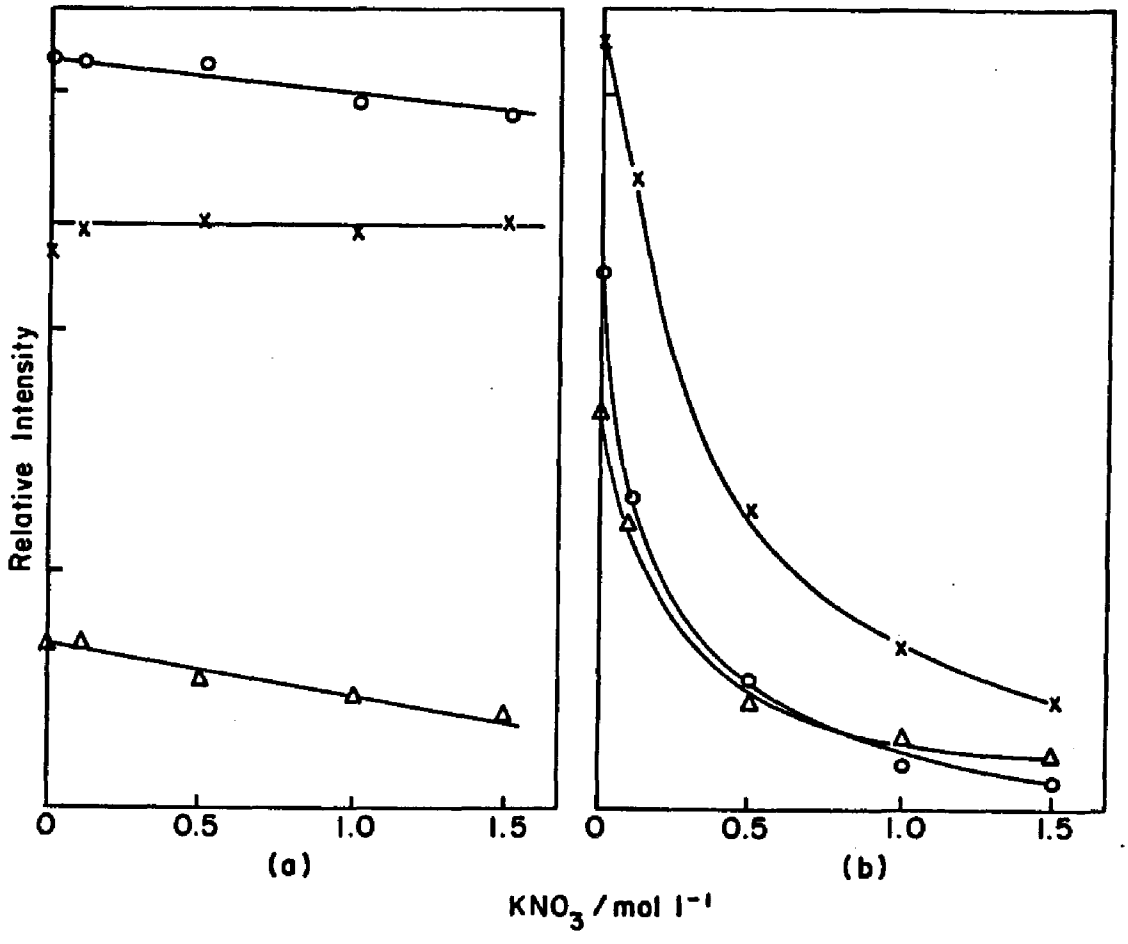

Fig.7: Relative intensity of (a) pyridine and (b) pyridinium vs. concentration of KNO_3: (×) 1008 cm^{-1}; (Δ) 235 cm^{-1}; (o) 1025 cm^{-1}. Pretreatment was carried in a solution containing 0.025 M chloride and 0.05 M pyridine at pH=8 for both (a) and (b). After ORC the 1008cm^{-1} band was recorded as an intensity standard. Then this solution was replaced by a solution containing 0.05 M pyridine, 0.025 M potassium chloride, variable concentrations of KNO_3, pH=8 for (a) and pH=2 (adjusted with HNO_3) for (b). Each change of nitrate concentration constituted a new experiment.

pyridinium in the diffuse layer. As we previously indicated, pyridinium can not be bound to the Ag surface directly, and the formation of an ion pair was suggested. The interaction between pyridinium and chloride seems to be of an electrostatic nature. As the concentration of electrolyte increases, there is more competition of K^+ or Na^+ with pyridinium at the outer Helmholtz plane. In the case of pyridine, which is a neutral molecule, the activity will not be changed by ionic strength and it can not be replaced by non-specifically adsorbed ions. Thus the spectrum of pyridine is not effected by non-specifically adsorbed electrolyte. A slight decrease in intensity of the 235 cm^{-1} line was observed in Fig.7a. This indicates that the intensity of 235 cm^{-1} band which is mainly attributed to Ag-Cl vibration decreases because of a decrease of activity of chloride on increasing the ionic strength.

A parallel change of the intensity of the 235 cm^{-1} band with other lines in the pyridinium spectrum (pH=2) can be seen in many different cases. When the chloride and pyridinium concentrations are kept constant, a parallel decrease of the intensity of the 235 cm^{-1} band with the 1025 cm^{-1} and 1008 cm^{-1} bands is observed in Fig.7b as the background electrolyte concentration is increased. When the pyridinium concentration is kept constant and the chloride concentration is changed, the peak-shaped curve of the relative intensity of the 235 cm^{-1} line vs. chloride concentration is almost parallel with the curve of the 1008 cm^{-1} and 1025 cm^{-1} lines [Fig.4]. In addition, the potential dependence of the 235 cm^{-1} line is very similar to the 1008 cm^{-1} and 1025 cm^{-1}

lines [Fig.1 and Fig.2]. Finally in Fig.8, it can be seen that when the chloride concentration is kept constant at 0.1 M, and the pyridinium concentration is increased, the relative intensity of the 235 cm^{-1} band also increases in parallel with the lines of pyridinium. All these observations show a strong dependence of the intensity of the 235 cm^{-1} surface line on the pyridinium. It is remakable that the intensity of this line changes with chloride concentration, background electrolyte concentration as well as pyridinium concentration in an identical manner to the pyridinium lines. This evidence along with others [13, 15] indicates clearly that this low frequency line involves a coadsorbed species.

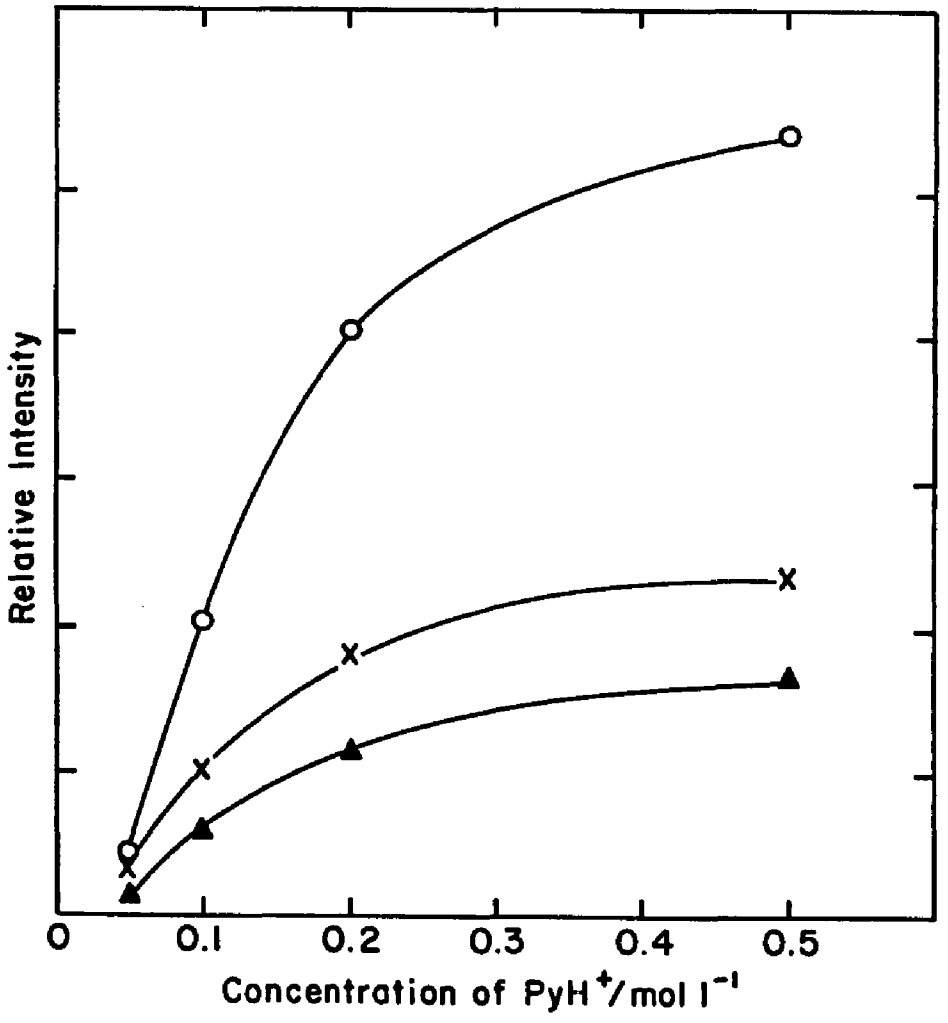

Fig.8 Relative SERS intensity vs. pyridinium concentration at -0.2V and pH=2: (o) 1008 cm^{-1}; (x) 235 cm^{-1}; (▲) 1025 cm^{-1}. Chloride concentration was kept constant at 0.1 M and pretreatment conditions are the same as in Fig.1.

REFERENCES

[1] M. Fleischmann, P. J. Hendra and A. J. McQuillan, Chem. Phys. Lett., 26 (1974) 163.

[2] D. L. Jeanmaire, R. P. Van Duyne, J. Electroanal. Chem., 84 (1977) 1-20.

[3] A. Regis, J. Corset, Chem. Phys. Lett., 70 (1980) 305.

[4] G. F. Atkinson, D. A. Guzonas and Irish, Chem. Phys. Lett., 75 (1980) 557.

[5] R. L. Birke, I. Bernard, L. A. Sanchez, and J. R. Lombardi, J. Electroanal. Chem., 150 (1983) 447.

[6] D. J. Rogers, S. D. Luck, D. E. Irish, D. A. Guzonas and G. F. Atkinson, J. Electroanal. Chem., 167 (1984) 237.

[7] M. A. Tadayyoni, S. Farquharson and M. J. Weaver, J. Chem. Phys., 80 (1984) 1363.

[8] E. Spinner, J. Chem. Soc., (1963) 3870.

[9] R. Foglizzo and A. Novak, J. Chem. Phys., 66 (1969) 1539.

[10] D. Cook, Canad. J. Chem., 39 (1961) 2009.

[11] M. Fleischmann and I. R. Hill, J. Electroanal. Chem., 146 (1983) 353

[12] B. H. Loo, J.Electroanal. Chem., 131 (1982) 381.

[13] J. R. Lombardi, E. A. Shields Knight and R. L. Birke, Chem. Phys. Lett., 79 (1981) 214.

[14] J. A. Creighton, M. G. Albrecht, R. E. Hester and J. A. D. Matthew, Chem. Phys. Lett., 55 (1978) 55.

[15] R. P. Van Duyne in C. B. Moore (Ed), Chemical and Biochemical Application of Laser, Vol. 4, Academic Press, New York, 1979

[16] H. Wetzel and Gerischer, Chem. Phys. Lett., 76 (1980) 460.

[17] R. Dornhaus and R. K. Chang, Solid State Commun., 34 (1980) 811

[18] H. Wetzel, H. Gerischer and B. Pettinger, Chem. Phys. Lett., 78 (1981) 392.

[19] J. F. Owen and K. Chang, Chem. Phys. Lett., 104 (1984) 59.

[20] B. Pettinger, J. Phys. Chem., 85 (1981) 2746.

[21] Handbook of Chemistry and Physics, Ed. C.D. Hodgman (Chemical Rubber Publ. Co., Cleveland, OH) p 307.

[22] J. R. Lombardi, R. L. Birke, Surface Science 95 (1980) L259

[23] M. Neviere and R. Reinisch, Phys. Rev. B., 26 (1982) 5403.

[24] T. Watanabe, O. Kawanami, K. Honda and B. Pettinger, Chem. Phys. Lett., 102 (1983) 565.

CHAPTER (III)

SURFACE ENHANCED RAMAN SPECTROSCOPY OF SURFACTANTS

Section 3.1 Introduction

The investigation of surfactants adsorbed on metal surfaces is extremely important in a variety of fields such as adhesion, lubrication, detergency and corrosion inhibition. Research advances in all these fields are closely related to an understanding of the interaction between the surfactant and the metal surface as well as the structure of the adsorbed species. Surface enhanced Raman spectroscopy (SERS) is an ideally suited in-situ method for studying surfactant molecules adsorbed on metal surfaces. However, SERS studies of long chain surfactant molecules has been rather spars and concentrated on metal island films and sols [1-7]. Even though some studies have dealt with a surfactant adsorbed on an electrode surface [8], these investigations were limited to a cationic surfactant and the potential dependence was not studied.

The purpose of this work is to utilize the SERS technique for a comparative study of the in-situ adsorption characteristics of the various types of surfactants: cationic, anionic and non-ionic, on a Ag electrode surface. We have found that the hydrophilic property of the metal surface is changed as the electrode potential changes based on the observation of the potential dependence of the SERS intensity.

Section 3.2 Experimental

Cetyltrimethylammonium bromide(CTAB) ($CH_3(CH_2)_{15}N^+(CH_3)_3Br^-$), Cetyl pyridinium chloride(CPC) ($CH_{16}H_{33}N^+C_5H_4Cl^-$), Sodium dodecyl

sulfate(SDS) ($CH_3(CH_2)_{11}OSO_3^-Na^+$), Polyoxyethylene(23)dodecanol (Brij-35) ($CH_3(CH_2)_{11}(OCH_2CH_2)_{23}OH$) and Triton X100 (CH_3-$(CH_2)_7$-  -$(OCH_2CH_2)_{9.5}$-OH) are reagent grade (Fisher Scientific) and were used without further purification. It was determined that there was no observable difference in the SERS spectrum with a purified surfactant as compared with a surfactant which was used without further purification.

The equipment for spectroscopic and electrochemical measurements has been described elsewhere [9]. All of the potentials are referenced to saturated calomel electrode (SCE).

For simplicity, in the measurement of depolarization ratios, we changed the direction of polarization of the analyzer which was located between the sample and the entrance slit of the monochrometer instead of changing the polarization direction of the incident light. In this case the polarization ratio is defined as the ratio of $I_\perp / I_\parallel$, where $I_\perp$ is the intensity of the scattered radiation polarized perpendicular to the scattering plane, and $I_\parallel$ is the intensity of scattered radiation polarized parallel to the scattering plane.

Section 3.3 Results and Discussion

(a) Spectrum origin

There are several criteria which have been used to verify that an observed Raman spectrum from an electrochemical interface originates from the molecules adsorbed on the metal surface, instead of from the free molecules in

the solution phase. These criteria include an observable potential dependence, laser excitation frequency dependence, and a dependence on the roughness of the metal surface. In addition, the depolarization property of the Raman scattering offers possibly the most obvious evidence for distinguishing between surface enhanced Raman scattering and the normal Raman scattering for a solution phase. For the normal Raman spectrum of the molecules in the solution phase, the depolarization ratio of non-totally symmetric modes is close to 0.75, but for highly symmetric modes it is close to zero. Whereas, in SERS spectrum both symmetric and non-symmetric modes for adsorbed molecules have similar values of the depolarization ratio (0.6-0.75). Fig. 1 shows the normal Raman spectrum (A) and SERS spectrum (B) of CTAB in the C-H stretching region. The upper spectrum is parallel polarized and the lower spectrum is perpendicular polarized. For the SERS spectrum the depolarization ratio differs only slightly from one mode to another, but for the normal Raman spectrum different modes have very different depolarization ratios. Tab. 1 shows the depolarization ratios of CTAB and CPC in the C-H stretching region. Almost all of the modes in the SERS spectrum have similar depolarization ratios (between 0.4-0.6). However, in the normal Raman spectrum the highly symmetric modes, such as the symmetric C-H stretching around 2845 cm^{-1} have very low depolarization ratio (close to zero) for both CTAB and CPC. The trigonal breathing for CPC at 1026 cm^{-1} is also listed in Tab. 1. It is a totally symmetric breathing mode and has the depolarization ratio of 0.04 in

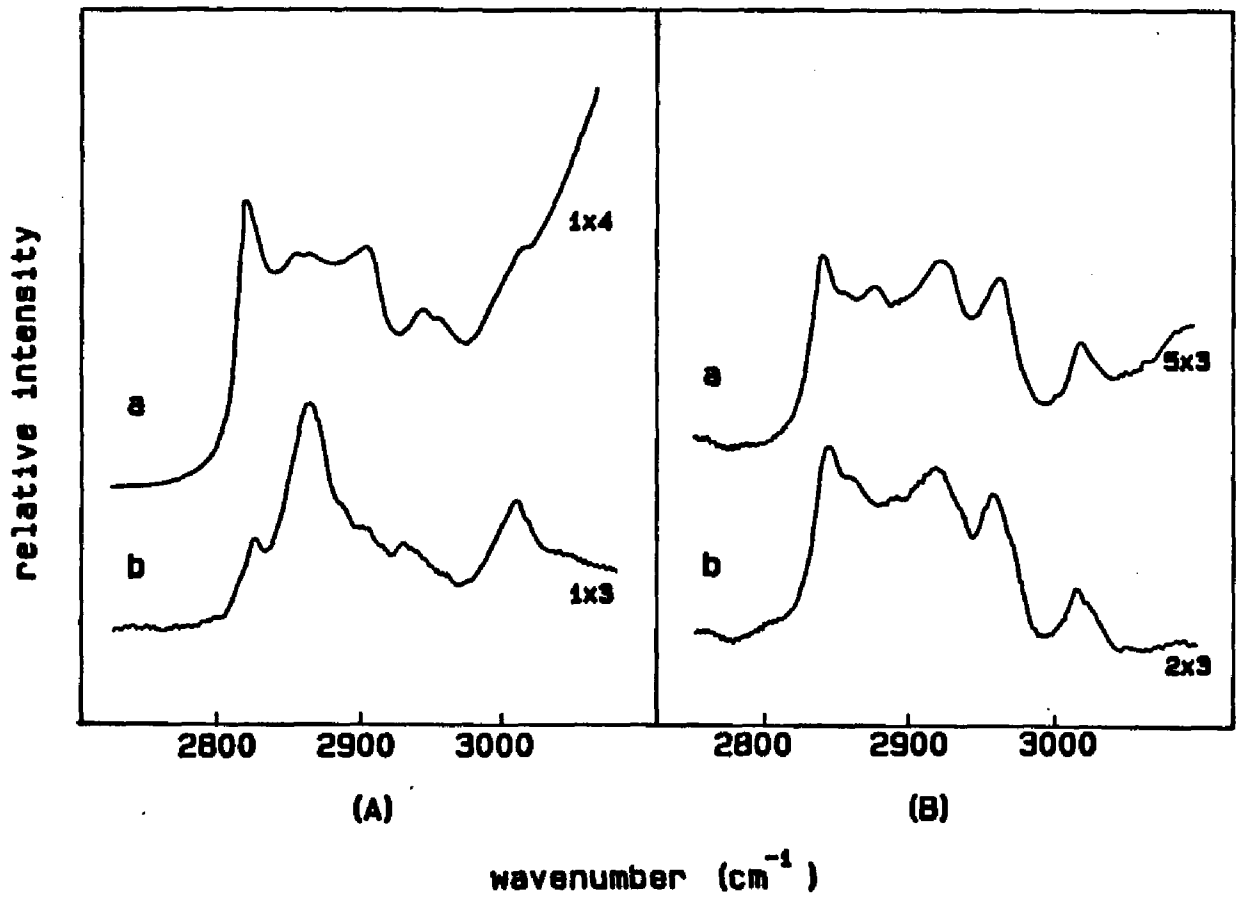

Fig.1 Depolarization property of CTAB around 2900 cm^{-1} region. (A) normal Raman of 0.1 M CTAB aqueous solution; (B) SERS spectrum of 10 mM CTAB on a roughened Ag electrode. The upper spectra (a) are parallel polarized and the lower spectra (b) are perpendicular polarized.

Table 1 Depolarization ratio of CTAB and CPC

	freq./cm^{-1}	assignments	$I_\perp/I_\parallel$	
			Normal	SERS
CTAB	2846	CH_2 symmetric stretch	0.08	0.40
	2885	CH_2 asymmetric stretch	0.30	0.40
	2925	CH_2 symmetric stretch and	0.12	0.38
	2960	overtone of CH_2 scissoring	0.20	0.38
CPC	2844	CH_2 symmetric stretch	0.07	0.51
	2884	CH_2 asymmetric stretch	0.18	0.43
	2922	CH_2 symmetric stretch and	0.12	0.46
	2956	overtone of CH_2 scissoring	0.31	0.41
	1026	symmetric and trigonal ring breathing	0.04	0.60
	3076	ring CH stretch	0.13	0.43

normal Raman, but of about 0.6 in the SERS spectrum.

Chemical quenching of active sites is another method for distinguishing SERS from a normal Raman spectrum. It has been found that [9,10] surface enhancement is related to the formation of Ag^+-adcluster complexes with halides or Raman scatterers. If an additional complexing reagent is added to form a new surface complex, which is readily soluble in water, the original Ag^+ center will be lost from the surface. For example, by adding $S_2O_3^{2-}$ or SO_3^{2-}, which has a strong tendency to form water soluble complexes with Ag^+, the active sites on the silver surface will be lost. This property has been discussed in our halide concentration dependence investigation [9]. We found that at high concentration of chloride, the intensity of pyridinium decreases as the chloride concentration increases and this decrease is irreversible. This decrease can be attributed to the formation of Ag^+ cluster-halides complexes at high concentrations of halides. Fig. 2 shows the C-H stretching range around 2900 cm^{-1} of the SERS spectrum of 10 mM Brij-35. The upper curve is the spectrum before adding $Na_2S_2O_3$. The lower spectrum is after injection of $Na_2S_2O_3$. The spectrum disappeared immediately after the injection. This quenching by $S_2O_3^{2-}$ gives further evidence of SERS. It is, therefore, safe to conclude that the observed spectrum is indeed a surface enhanced spectrum.

(b) Comparison of surfactants of different charge types

On comparing the SERS spectrum of various surfactants, we found that the

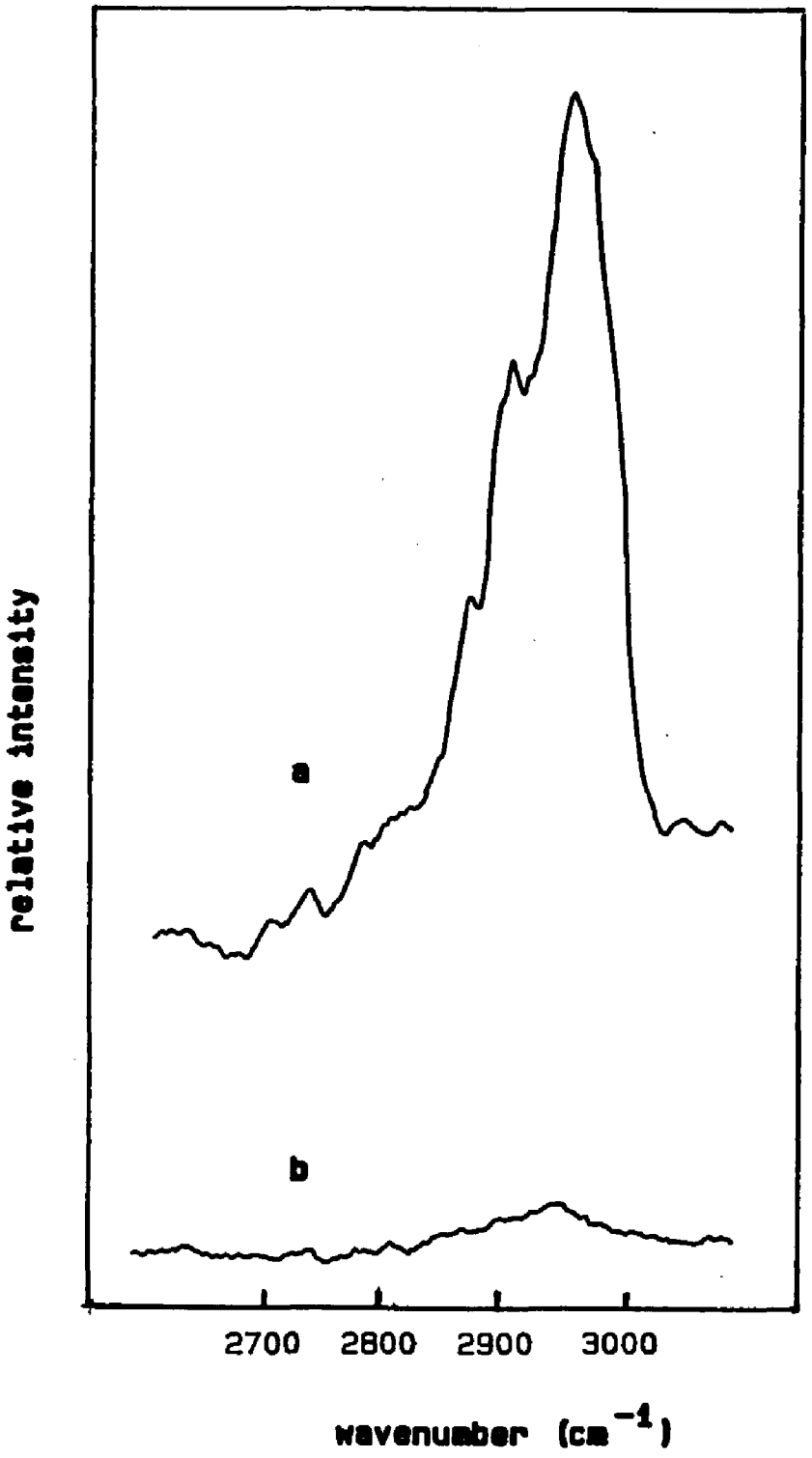

Fig.2 The SERS spectra of 10 mM Brij-35 in 0.01 M KBr solution around 2900 cm^{-1} region, (a) before and (b) after an injection of $Na_2S_2O_3$.

surfactant which has a nitrogen containing heterocyclic head (CPC) gave the strongest SERS intensity in comparison with other kinds of surfactants. The SERS spectrum of other cationic surfactants (CTAB) and non-ionic surfactants (Brij-35 or Triton X-100) were also obtained, but the intensities are much weaker than that of nitrogen containing heterocyclic surfactants. All of these spectra can be shown to be the surface enhanced Raman spectra and not the normal Raman spectra from solution phase with the methods previously discussed. Only a very weak signal was observed for anionic surfactants, such as SDS under the same conditions as other surfactants. These differences indicate, as would be expected, that different kinds of surfactants have different interactions with the metal surface. The CPC has a nitrogen containing heterocyclic head, however, it is different from pyridine, since the nitrogen atom is linked to an alkane chain. Also there is no lone pair of electrons which is able to directly bond to silver adatoms. One possible interaction between CPC and Ag active sites is the interaction through the conjugate π orbital of pyridine ring. Another possible interaction is through specifically adsorbed halide ions. The positively charged head is able to form an ion pair with adsorbed halide anions. This kind of interaction has been observed and discussed in detail for pyridinium [9] and methyl pyridinium [11].

In the case of CTAB a head group on orientation has been suggested [8]. The weaker intensity of CTAB in comparison with CPC is probably due to the weaker interaction between the cationic surfactant and the specifically ad-

sorbed halides. The interaction between halide and CPC molecules can not only be attributed to the electrostatic attraction but also to the overlap of the electron density between the halide anions and the π orbital of the pyridine ring. The weaker interaction between the halide and the CTAB molecules is probably due to the stereo-effect of three methyl groups on the head of CTAB.

For non-ionic surfactants, such as Brij-35 or Triton X100, a SERS intensity weaker than CPC but similar to CTAB was observed, again indicating a weaker interaction between the Ag surface and the non-ionic surfactant than with CPC. The non-ionic surfactant has a polyethyleneglycol moiety ($-OCH_2CH_2)_nOH$, which, as a Lewis base, interacts with the metal surface by the lone pairs of electrons on the oxygen atoms. The evidence for this interaction is the pronounced shift of the SERS bands of the polyethyleneglycol moieties upon adsorption [12]. It has also been suggested that the benzene ring moiety in Triton X100 may be adsorbed via a π-electron interaction with the surface based on the observation of relatively higher enhancement of the benzene ring modes than other modes [12]. It is also instructive to consider the alkane chain moiety in these surfactants. The alkane chains should be oriented away from the surface due to the hydrophilic property of the Ag surface. This can be seen from the SERS spectra of Brij-35 in C-H stretching range (2700-3000 cm^{-1}) in Fig. 2. The predominant bands around 2840, 2875, 2920 and 2950 cm^{-1} correspond to the C-H stretching modes of polyethyleneglycol moieties. The relative intensity of these modes are very different from that of

the alkane chain. For polyethyleneglycol moieties the relative intensities of 2920 and 2950 cm^{-1} are much higher than 2840 and 2875 cm^{-1} bands. But for the alkane chain the 2845 cm^{-1} band has the highest intensity compared with other C-H stretching bands.

The very weak signal for anionic surfactants, such as SDS is probably due to the weak interaction between the negatively charged head group and the surface. The spectrum is very weak not only in the absence of halides but also in the presence of halides. The latter case is presumably due to the competition between halides and surfactant. This kind of competition has been observed in the SERS measurement of p-nitrobenzoate anions. The halide ions were found to quench the SERS intensity of p-nitrobenzoate [13]. The SERS spectra of mono- and bicarboxylic acid adsorbed on silver surface has also been reported [7] and it has been found that the SERS spectra of mono-carboxylic acids became undetectable when chain lengths beyond dodecanoic acid were used. This is presumably due to the competition between micelles and the solid-liquid interface. The surfactant molecules with a longer hydrophobic chain prefer to stay in micelles rather than on the solid-liquid interface. Hence, the SERS spectrum for long chain anionic surfactant is hardly observed.

(c) Assignment of SERS spectrum of CPC

In order to utilize the SERS spectrum to study a surfactant, it is necessary to have a reasonable assignment. The SERS spectrum of 10 mM CPC on a Ag

electrode and the normal Raman spectrum of 0.5 M CPC in aqueous solution in the 100-1700 cm^{-1} region and in the 2800-3100 cm^{-1} region are shown in Fig. 3 and Fig. 4 respectively. The assignment of CPC spectrum is listed in Tab. 2. This assignment is based on a comparative analysis of the normal Raman spectra and the SERS spectra of a series of surfactants with different head groups [4,7,8] and on the early assignments of SERS spectrum for N-methyl pyridinium ion on a Ag electrode [11].

Comparing the relative intensities of SERS spectrum and the normal Raman spectrum in Tab.2, we can clearly see that the enhancement of the head group (pyridinium ring) and the tail group (alkane chain) is quite different. Comparing with the normal Raman spectrum, the average intensity of the modes from the tail group is about 5 times less enhanced than that from the head group. Based on many of the theoretical SERS models which have predicted stronger enhancement for bands associated with molecules that are close to the surface [14], we can conclude that the pyridinium head group is attached on to the surface, leaving the long tail away from the surface. Similarly, for CTAB molecules adsorbed on a Cu electrode surface a preferential enhancement of the vibration bands associated with the $(CH_3)_3N^+$ group has been observed [8].

There are five main bands in the 2500-3100 cm^{-1} region. The band at 3076 cm^{-1} has been assigned to the C-H stretching of the pyridine ring [11]. The bands at 2846 and 2880 cm^{-1} have been assigned to CH_2 symmetric and antisymmetric stretching modes respectively for many long chain surfactants

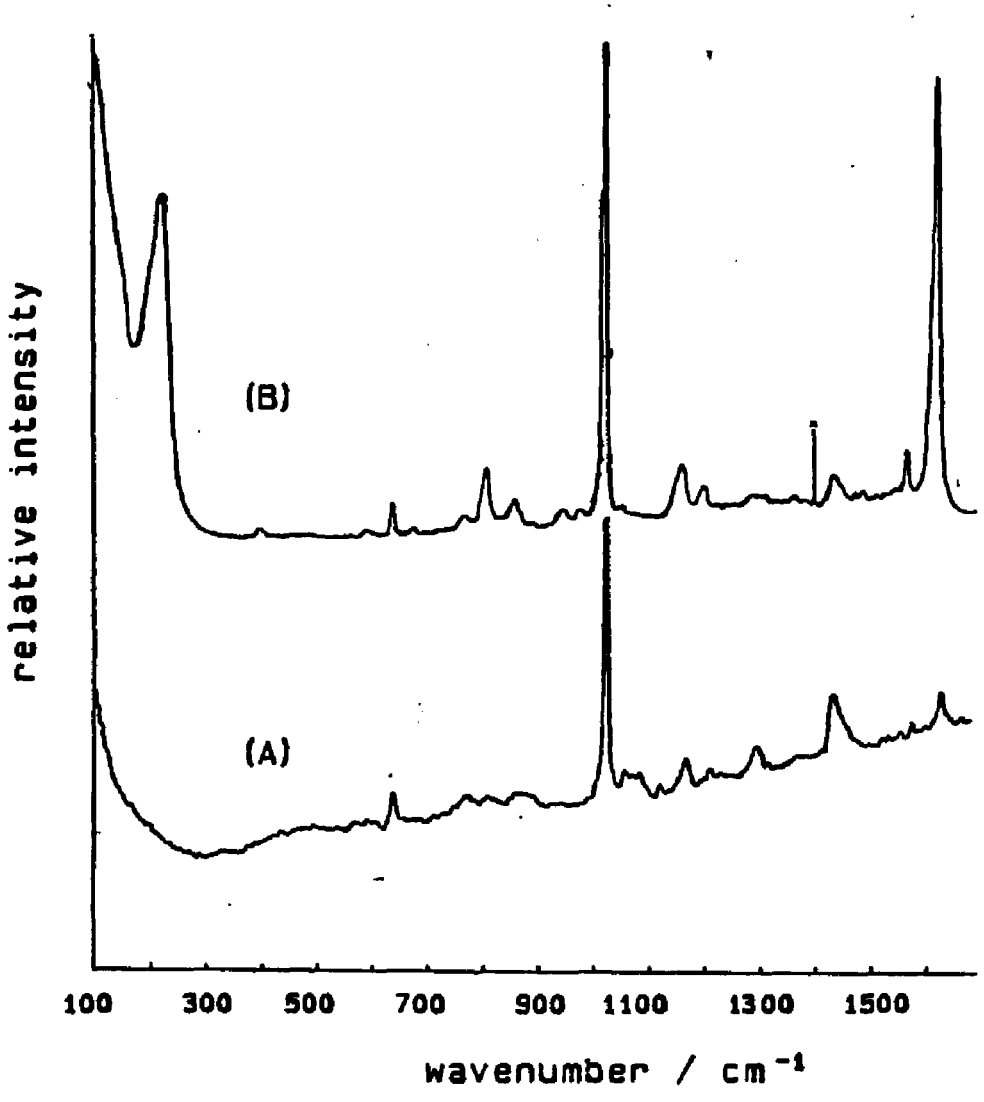

Fig.3 (a) SERS spectrum of 10 mM of CPC in 0.1 M KCl aqueous solution on a Ag electrode and (b) normal Raman spectrum of 0.5 M CPC solution around 100-1700 cm^{-1} region.

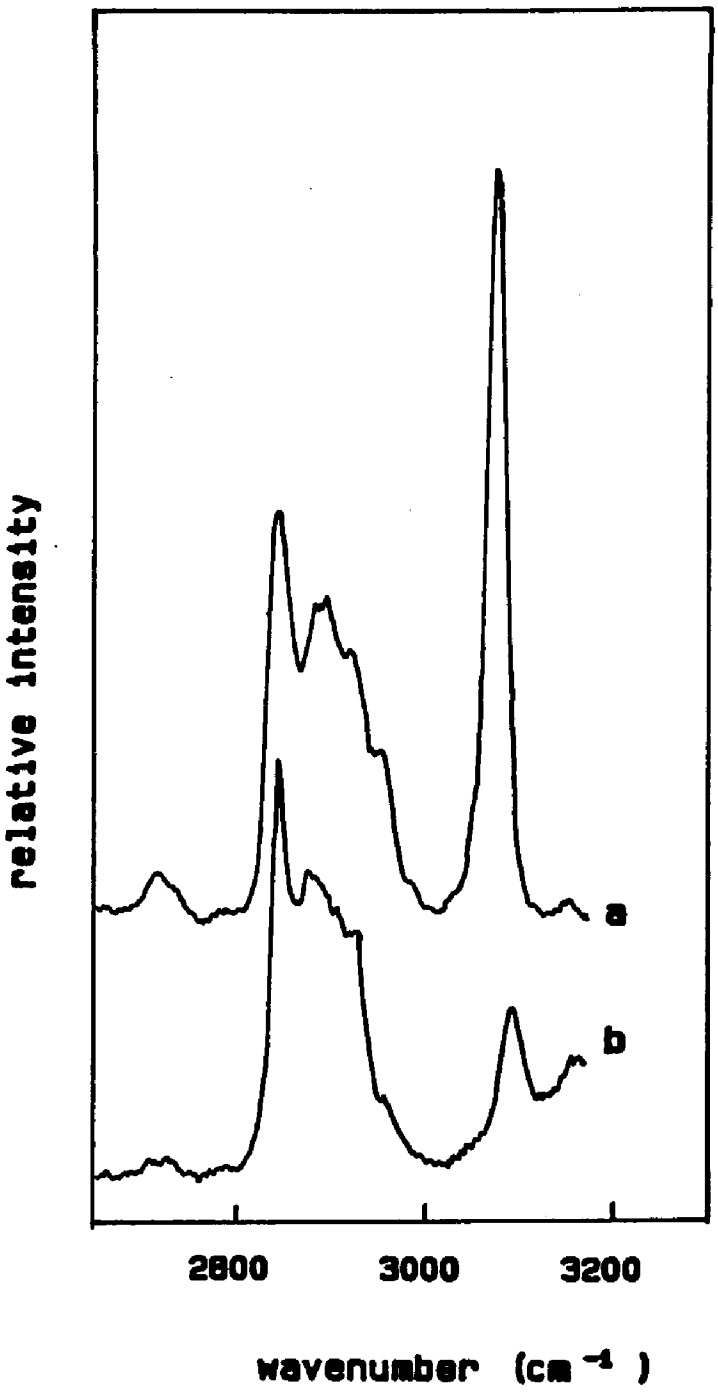

Fig.4 (a) SERS spectrum of 10 mM of CPC in 0.1 M KCl aqueous solution on a Ag electrode and (b) normal Raman spectrum of 0.5 M CPC solution around 2800-3100 cm^{-1} region.

Table 2 Raman shift and assignment of CPC

		SERS of CPC[a]		normal Raman[b] of CPC	
Wilson's number	Approximate description of vibration	freq. /cm^{-1}	rel. int.	freq. /cm^{-1}	rel. int.
	Ag-Cl stretch	224	57		
16a	out-of-plane ring deformation	400	2		
		594	2	594	4
6b	in-plane ring deformation	642	8	642	13
11	out-of-plane CH deformation	680	1		
10b	out-of-plane CH deformation	770	3	770	6
18a	in-plane CH deformation	812	12	814	5
17a	out-of-plane deformation	860	5	865	5
		946	3		
		976	2		
1+12	symmetric & trigonal ring breathing	1024	100	1026	100
18b	in-plane CH deformation	1050	2	1056	6
15	in-plane CH deformation	1168	11	1170	12
9a	in-plane CH deformation	1208	5	1214	5
	* CH_2 twist	1292	1	1298	11
14	ring stretch	1318	2		
	* CH_2 wag	1370	1		
		1390	1		
	* CH_2 scissors	1438	7	1434	22
	* CH_2 scissors	1480	2		
		1494	2		
8b	ring stretch	1574	10	1580	7
8a	ring stretch	1628	93	1631	13
		2718	2		
	* CH_2 symmetric stretch	2844	17	1846	86
	* CH_2 asymmetric stretch	2884	13	2880	63
	* CH_2 symmetric stretch and	2922	11	2922	56
	overtones of CH_2 scissoring	2956	7	2962	16
2,7b,13 20a,20b	CH stretch	3076	31	3092	33

a: SERS spectrum of 10 mM of CPC in 0.1 M KCl solution on Ag electrode. Double potential pretreatment -0.2 to +0.3 to -0.2 V; 1 sec. pule was used.

b: Normal Raman spectrum of 0.5 M CPC aqueous solution.

*: Modes represent tail group.

with different head groups [4,8,15-18]. This assignment coincides with the depolarization property of CPC in the normal Raman spectrum as shown in Fig. 1 and Tab. 1. The assignment of the 2920 and 2960 cm^{-1} bands are less certain since the previous assignments are different one from the other. Our observation more likely supports the assignment given by Snyder and Scherer [18] for 2920 cm^{-1} as the combination band of CH_2 stretching and 2960 cm^{-1} band as the overtone of CH_3 scissoring. Based on the head-on orientation for CPC discussed previously, the hydrophobic CH_3 terminal must be away from the surface. However, from Fig.3 we can see that the 2960 cm^{-1} band is more enhanced than the CH_2 stretching band at 2846 and 2880 cm^{-1}. Thus it is less reasonable to assign the 2962 cm^{-1} band to the terminal CH_3 stretching mode as given in references [7,8,17]. In addition, the depolarization ratio of 2920 cm^{-1} band is much smaller than that of 2880 cm^{-1} band (Fig.1 and Tab.1), indicating that these two bands are unlikely to have the same assignment as a CH_2 asymmetric stretching mode as given in [19].

(d) The conformation

The 1050-1150 cm^{-1} region of the Raman spectrum of surfactants contains the skeletal vibration of the C-C stretching modes which are sensitive to the conformation of the hydrocarbon chain. In the normal Raman spectrum of CTAB, for example, there are three bands located around 1065, 1090 and 1121 cm^{-1} (Fig. 5 a). The bands at 1065 and 1121 cm^{-1} have been assigned to C-C

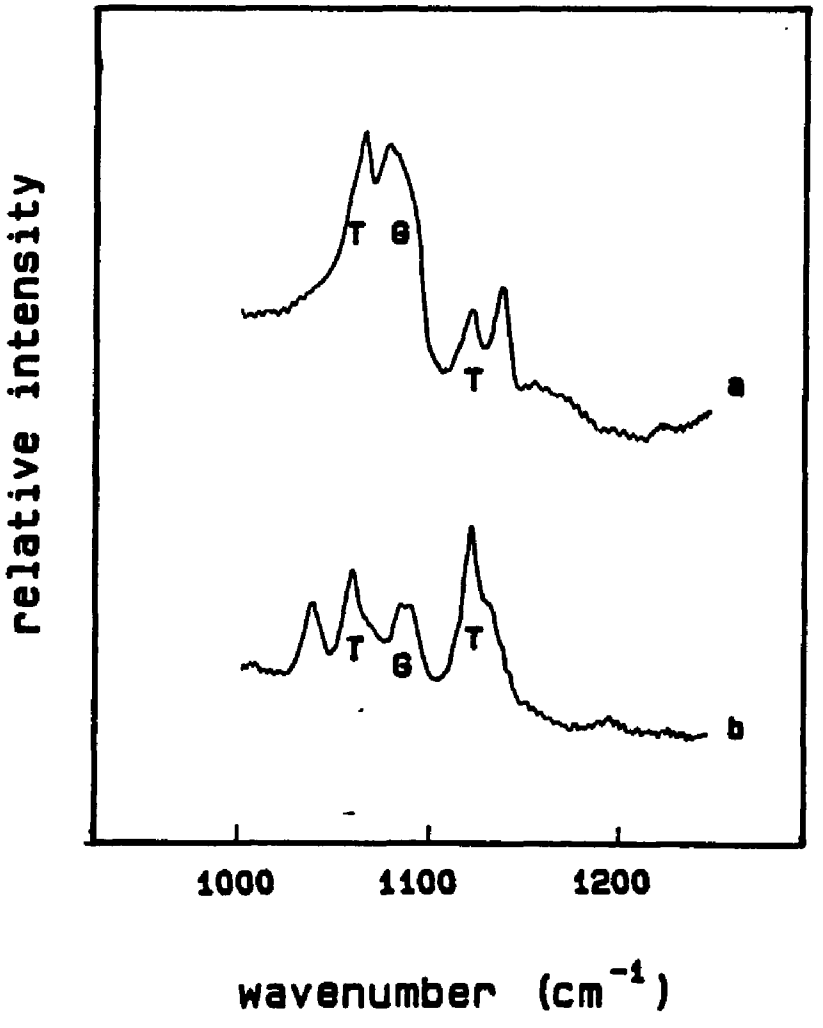

Fig.5 (a) Normal Raman spectrum and (b) SERS spectrum of CTAB in C-C stretching region around 1000-1200 cm^{-1}. "G" represents the gauche conformation and "T" represents the trans conformation.

symmetric and antisymmetric stretching modes, respectively. The 1065 and 1121 cm^{-1} bands represent the trans conformation and the 1090 band represents the gauche conformation [1,2,20]. In Fig. 5(a) the normal Raman of 0.1 M CTAB shows a relatively high intensity for the 1090 cm^{-1} band and low intensities for the 1065 and 1121 bands. The critical micelle concentration of CTAB is 9.2 x 10^{-4} M [21]. So the concentration of 0.1 M CTAB solution is much higher than the cmc. The contribution to the spectrum from the free molecules in the solution phase is negligible, that is, the spectrum represents only CTAB micelles. The larger contribution of gauche conformers indicates that the hydrocarbon chain in the micelle core remains "fluid" (kinked) with several gauche isomers present. In Fig. 5(b) the SERS spectrum of 0.01 M CTAB on a Ag electrode shows the band around 1090 cm^{-1} to be weaker than 1065 and 1121 cm^{-1} bands, indicating that near the head group layer there is a layer of "solid-like" hydrocarbon chain. This result is in very good agreement with the observation of a "solid like" phase of a monolayer of 1-hexadecane thiol on a silver island film, even when this monolayer is in contact with overlying bulk water [1,2].

(e) Potential dependence

One interesting feature of the SERS spectra of surfactants on a Ag electrode is the potential dependence which shows a marked change at very negative potentials. Fig. 6 and Fig. 7 show the SERS spectra of Brij-35 and CTAB in C-

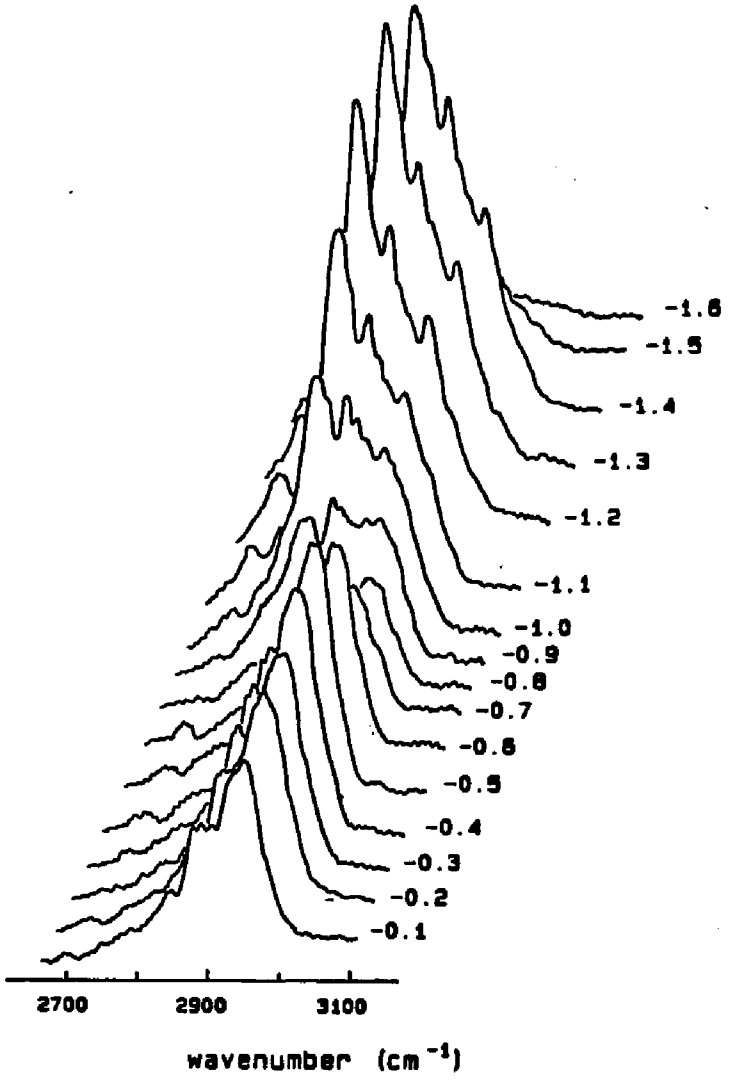

Fig.6 SERS spectra of 10 mM of Brij-35 on a Ag electrode around 2700-3100 cm^{-1} region at different potentials.

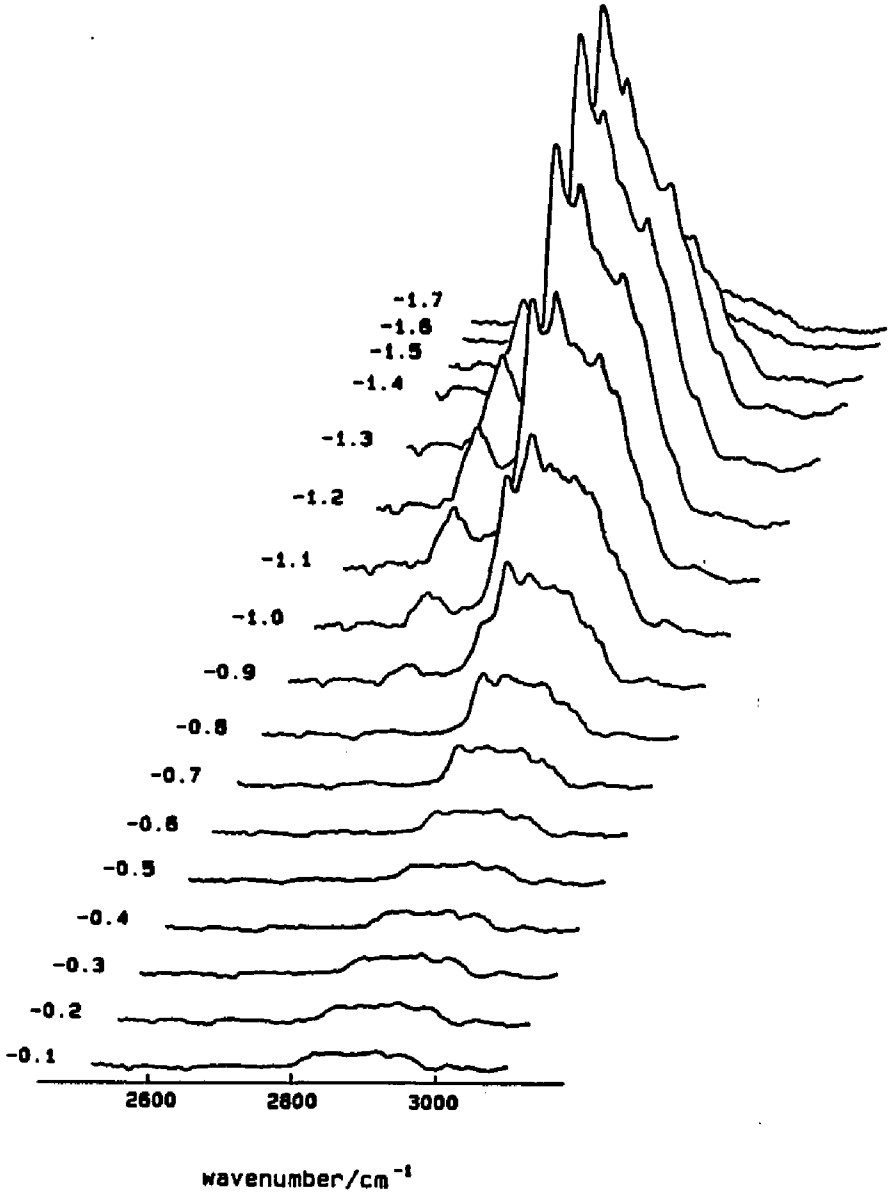

Fig.7 SERS spectra of 10 mM of CTAB on a Ag electrode around 2700-3100 cm^{-1} region at different potentials.

H stretching range around 2900 cm^{-1} at different potentials. There are two intensity maxima of the C-H stretching modes in the potential range from -0.1 to -1.7 V. The first maximum is around -0.5 V. This maximum, as with most SERS scatterers, can be attributed to a resonant charge transfer mechanism which has been discussed in detail previously [22,23]. When the potential is shifted to negative values greater than -0.8 V, the intensities of the C-H stretching bands increase dramatically until they reach a second maximum around -1.3 V. The intensity of the second maximum is much higher (about 2-20 times) than that of the first maximum, indicating an additional enhancement at the very negative potential. As the intensity increases at the negative potential, there are two new bands, at around 2710 and 2815 cm^{-1}, which increase at a relatively higher rate than other C-H stretching bands. As the potential is shifted beyond -1.3 V, the intensity of these bands drop off rapidly. Besides CTAB and Brij-35, other surfactants were also studied and the same potential dependence is obtained.

In order to interpret this phenomenon, the following effects should be considered. Firstly, we must consider the change of the hydrophilic property of the metal surface at very negative potentials. As discussed previously [9], the adsorption of pyridinium ions is closely related to an ion pair formed with specifically adsorbed halide ions. The Raman intensity depends on the amount of adsorbed halide. Similar to pyridinium, the cation surfactants are also adsorbed via specifically adsorbed halide ions. At very negative potential halides

desorb from the surface because of the electrostatic repulsion. The loss of the halide ions from the surface will cause the desorption of the surfactant. Therefore, in the absence of specific adsorption of halides the surface possibly becomes more hydrophobic, causing the hydrophobic tail to adsorb on to the surface. Secondly, the hydrogen ion may be reduced to atomic hydrogen or hydrogen molecules which forms a film between the solid and liquid phases. This will greatly increase the hydrophobic property of the surface, causing a change in the orientation of the surfactant. This orientation change is indicated by the observation that as the intensities of the tail group increase the intensities of the head group decrease.

The great enhancement of the intensity at the second maximum can be attributed to the formation of the hydrogen film. This additional enhancement is also observed, when the electrode potential is stepped to the region of rapid hydrogen evolution prior to performing an oxidation-reduction cycle for any SERS measurement [24]. The additional enhancement has been accounted for by a calculation of the increase of the SERS enhancement when the dielectric constant is changed from an aqueous to a hydrogen film [25].

The rapid decrease of the SERS intensity at the potential more negative than -1.3 V is due to the evolution of a large amount of hydrogen gas which forms bubbles and destroys the interface.

With CPC an additional factor is an electrode reaction since it is reduced at a potential around -0.9 V. However the same potential dependence is still ob-

served as with the other kinds of surfactants, such as, CTAB, Triton X100 or Brij-35 which do not undergo any redox reaction in the potential range used for a silver electrode (0 to -1.3 V vs. SCE). The first intensity maximum is around -0.5 V for both the head and tail SERS modes. However all of the modes from the head group, including the C-H stretching mode of the pyridine ring around 3070 cm^{-1}, disappear at a potential more negative than -0.9 V. At the second maximum only the modes from the alkane chain can be observed.

The SERS spectrum of the C-H stretching modes at the second intensity maximum is very different from the spectrum at potentials more positive than -0.8 V. But for all of the different kinds of surfactants the spectra are identical at the second maximum, indicating that the spectra at the second maximum correspond to the alkane moiety, which is the common feature of the surfactants. Identical spectra at the second maximum can be seen in Fig. 6 and Fig. 7. The two new bands at around 2710 and 2815 cm^{-1}, which appear at the potential more negative than -0.8 V, are not found in the previous assignments of the SERS spectrum of a hydrocarbon chain. A possible explanation is that these two modes represent new C-H stretching modes of the alkane chain, which are shifted by the very negative potential to lower energy. However, the exact assignment of the C-H stretching modes at the very negative potential must remain for a further investigation.

REFERENCES

[1] C. J. Sandroff, S. Garoff and K. P. Leung, Chem. Phys. Lett. 96(5), (1983) 547

[2] S. Garoff and C. J. Sandroff, Journal de Physique C10, (1983) 483

[3] S. M. Heard, F. Grieser and C. G. Barraclough, Chem. Phys. Lett. 95(2), (1983) 155

[4] W. Knoll, M. R. Philpott and W. G. Golden, J. Chem. Phys. 77(1), (1982) 219

[5] A. Girlando, J. G. Gordon II, D. Heitmann, M. R. Philpott, H. Seki and J. D. Swalen, Surface Science 101, (1980) 417

[6] W. Knoll, M. R. Philpott, J. D. Swalen and A. Girlando, J. Chem. Phys. 77(5), (1982) 2254

[7] M. Moskovits and J. S. Suh, J. Am. Chem. Soc. 107, (1985) 6826

[8] A. L. Dendramis, E. W. Schwinn and Sperline, Surface Science 134, (1983) 675

[9] S. C. Sun, I. Bernard, R. L. Birke and J. R. Lombardi, J. Electroanal. Chem., 196, (1985) 359

[10] T. Watanabe, O. Kawanami, K. Honda and B. Pettinger, Chem. Phys. Lett. 102(6), (1983) 565

[11] K. A. Bunding, M. I. Bell and R. A. Durst, Chem. Phys. Lett, 89(1), (1982) 54

[12] G. Mengoli, M. M. Musiani, B. Pelli, M. Fleischmann and I. R. Hill, Electrochimica Acta 28(12), (1983) 1733

[13] S. C. Sun, R. L. Birke and J. R. Lombardi, to be published

[14] T. E. Furtak and J. Reyes, Surface Science 93, (1980) 351

[15] R. G. Snyder, S. L. Hsu and S. Krimm, Spectrochim. Acta Part A, 34, (1978) 395

[16] K. Kamogawa, K. Tajima, K. Hayakawa and T. Kitagawa, J. Phys. Chem. 88 (1984) 2494

[17] H. Okabayashi and T. Kitagawa, J. Phys. Chem. 82(6), (1978) 1830

[18] R. G. Snyder and J. R. Scherer, J. Chem. Phys. 71, (1979) 3221

[19] K. Larsson and R. P. Rand, Biochimica et Biophysica Acta 326, (1973) 245

[20] B. P. Gaber, P. Yager and W. L. Peticolas, Biophys. J. 21, (1978) 161

[21] R. W. Berg, Spectrochim. Acta, 34A, (1978) 655

[22] T. E. Furtak and D. Roy, Phys. Rev. Lett. 50 (17), (1983) 1301

[23] J. R. Lombardi, R. L. Birke, T. Lu and J. Xu, J. Chem. Phys. 84(8), (1986) 4174

[24] F. Barz, J. G. Gordon II, M. R. Philpott and M. J. Weaver, Chem. Phys. Lett. 91, (1983) 168

[25] Milton Kerker and Dau-Sing Wang, Chem. Phys. Lett. 104(5), (1984) 516

CHAPTER (IV)

QUANTITATIVE MEASUREMENT OF ENHANCEMENT FACTOR

Section 4.1 Introduction

In order to utilize SERS properly as a surface chemical probe as well as to understand the mechanisms of surface enhanced processes, it is clearly important to obtain quantitative information on the efficiency of surface Raman scattering. This efficiency has been defined as a "surface enhancement factor" SEF, which is the ratio of the Raman scattering intensity of a given vibrational mode for the adsorbate when present at the metal surface with respect to the corresponding scattering intensity in bulk media [1]. However, quantitative evaluations of SEF are very sparse. The original value of SEF for pyridine at a mildly roughened silver electrode [1], 1 x 10^6, is widely quoted, yet a markedly smaller value, 1.5x10^4, has been reported for a closely related system [2]. One factor responsible for the scarcity of SEF determinations is the paucity of surface coverage data for SERS active adsorbates. There are several methods which have been developed for evaluating surface concentrations for either electroactive or nonelectroactive species, such as, chronocoulometry [1,3], spectrophotometric method [2], rapid linear sweep voltammetry [4], a differential capacitance [5,6], and a radiochemical technique [7]. But, in most of these techniques the surface concentration is measured separately from the SERS measurement. Chronocoulometry [1] was used to determine the coverage of an electrode by the electroreducible adsorbate 4-acetylpyridine whereas the SERS intensity measurements were made on pyridine adsorbed at a similar roughened electrode. It was assumed that the gross coverage was the same for

the two adsorbates. However, 4-acetylpyridine is a weaker base than pyridine and we are not certain that this assumption is valid. In the radiochemical technique [7] the solution was prepared with ^{14}C labeled pyridine. After an oxidation-reduction cycle (ORC) preteatment, the electrode was taken out, rinsed in alcohol and dried in air. Then, the β radioactivity was measured. In this method there is a risk of losing adsorbed molecules due to the withdrawal of potential when the electrode is disconnected and due to the washing in alcohol. The same problems could be present in the spectrophotometric method [2].

We present here a method for evaluating the surface concentration by an in-situ cyclic voltammetry. This method is different from rapid sweep voltammetry which is limited by low bulk concentration and high sweep rates [4]. By selecting a proper system and conditions the adsorption peak can be well separated from the diffusion peak in the cyclic voltammetry measurement of methyl viologen. From the plot of adsorption current vs. scan rate we can calculate the surface concentration. From the surface concentration obtained we calculated the surface enhancement factor of methyl viologen on a Ag electrode as 1.2×10^6.

Based on the comparison between the amount of the molecules adsorbed on a smooth Ag electrode surface and on the surface roughened in the presence and in the absence of adsorbate, we found that an oxidation-reduction cycle (ORC) in chloride media yields only a moderate (ca. 2-fold) increase in the ac-

tual surface area. When the ORC treatment is made in the presence of adsorbate, a total 4 fold increase in surface concentration is obtained. This result indicates that a large amount of molecules are trapped in the sponge-like Ag layer formed during the anodic process of the ORC treatment.

Section 4.2 Theory of Adsorption Isotherm [8]

For an electrochemical reaction

$$O + ne^- \longrightarrow R$$

where O represents an oxidized form and R represents a reduced form, the amount of the species adsorbed is related to the bulk activity and standard free energy as shown in a Langmuir isotherm

$$\Gamma_i / (\Gamma_s - \Gamma_i) = \beta_i \, a_i^b \qquad (1)$$

where Γ_i is the surface concentration for species i, and is represented as mol/cm^2, Γ_s is the saturation coverage of the electrode by adsorbate, a_i^b is the bulk activity for species i, and

$$\beta_i = \exp(-\Delta G_i^o / RT) \qquad (2)$$

ΔG_i^o is standard free energy for the adsorption process. With the assumption that the Γ_o^*'s are independent of E, combining with Fick's law, the peak current in cyclic voltammetry can be derived as

$$i_p = (n^2F^2/4RT)\, \nu\, A\, \Gamma_o^* \qquad (3)$$

and the peak potential for a reversible system is given by

$$E_p = E^{o\prime} - (RT/nF) \ln(b_o/b_R) \qquad (4)$$

In equation (3) υ is the scan rate, A is the area of electrode and $A\Gamma_o^*$ represents the total amount of molecules adsorbed on a surface. Two important insights can be obtained from equation (3). (i) The peak current i_p is proportional to the scan rate. This is a useful role for distinguishing the diffusion controlled current from an adsorption current. The peak current for a diffusion controlled process is represented by the equation

$$i_p = (2.69 \times 10^5) n^{3/2} A D_o^{1/2} \upsilon^{1/2} C_o^* \qquad (5)$$

that is, the peak current i_p is proportional to the square root of the scan rate. If both processes, diffusion and adsorption, are present in the same system, increasing the scan rate will cause a greater increase in adsorption current than that of the diffusion current. (ii) The peak current i_p is proportional to the amount of the species adsorbed on the electrode. If the i_p is plotted as a function of scan rates, the slope can used to calculate $A\Gamma_o^*$. In equation (4) E_p is the peak potential and $E^{0\prime}$ is the formal potential, b_i is defined as

$$b_i = \beta_i \Gamma_s \qquad (6)$$

Combing equations (2), (3) and (6), the relation of E_p with free energy is given by

$$E_p = E^{0\prime} + (1/nF) (\Delta G_o^{\,o} - \Delta G_R^{\,o}) \qquad (7)$$

From equation (7) we can see that the location of E_p with respect to $E^{0\prime}$ depends on the relative strength of the adsorption of O and R. If $\Delta G_o^{\,o} = \Delta G_R^{\,o}$, $E_p = E^{0\prime}$, that is the adsorption peak will be located at the same position as the diffusion peak. If O is adsorbed more strongly ($\Delta G_o^{\,o}$ has a larger negative

value than ΔG_R^o), the wave is displaced toward negative potentials beyond the position where the reversible wave of a diffusion species would occur (postwave). If R is adsorbed more strongly, the wave occurs at more positive potential than m and is called prewave. In most cases of electroanalytical chemistry one usually tries to avoid the adsorption current which interferes with the measurement of the diffusion current. But in our experiment we use the adsorption current and avoid a diffusion controlled current.

Section 4.3 Experimental

A model 206 Oscilloscope from Nicolet Instrument Corporation was used to record fast scan cyclic voltammograms. The scan rate used in our experiments is in the range of 0.05-20 V/sec. The Oscilloscope is triggered by a model 175 Universal programmer (EG & G PARC), which generates a linear sweep voltage. So the Oscilloscope is synchronized with the wave form generator. The data can be stored on disks by the data system in Oscilloscope, and can also be transferred through a PDP8 computer to a VAX system, then stored or treated in the VAX.

Other electrochemical and spectroscopic equipment are the same as discussed in previous chapters.

Section 4.4 Results and Discussion

(a) The behavior of the adsorption current in cyclic voltammetry

Because of the biochemical importance of methyl viologen [9] and its usefulness as a relay in the investigation of the photochemistry of energy conversion, the electrochemistry of methyl viologen has been widely studied and the mechanisms of the electrochemical reaction is relatively clear. There are two steps of the reduced from methyl viologen dication to biradical as shown in following reactions.

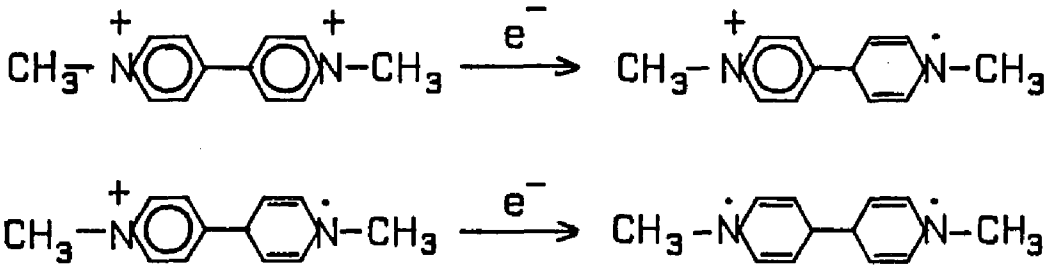

The first totally reversible reduction at around -0.68 V vs. SCE forms a radical cation and the second reduction at around -1.03 V forms a neutral biradical. The cyclic voltammetry on a smooth silver electrode is shown in Fig. 1(a). The second reduction is distorted due to the small solubility of the biradical. Fig. 1(b) shows the cyclic voltammogram of methyl viologen at the same conditions as Fig. 1(a), but on a roughened Ag electrode. There are two closely located peaks at around -0.53 and -0.58 V, which dramatically increase in peak current after the electrode is roughened. These two peaks proved to be adsorption peaks because the peak current is linearly proportional to the scan rate. Fig. 2 shows the cyclic voltammetry of methyl viologen on a roughened Ag

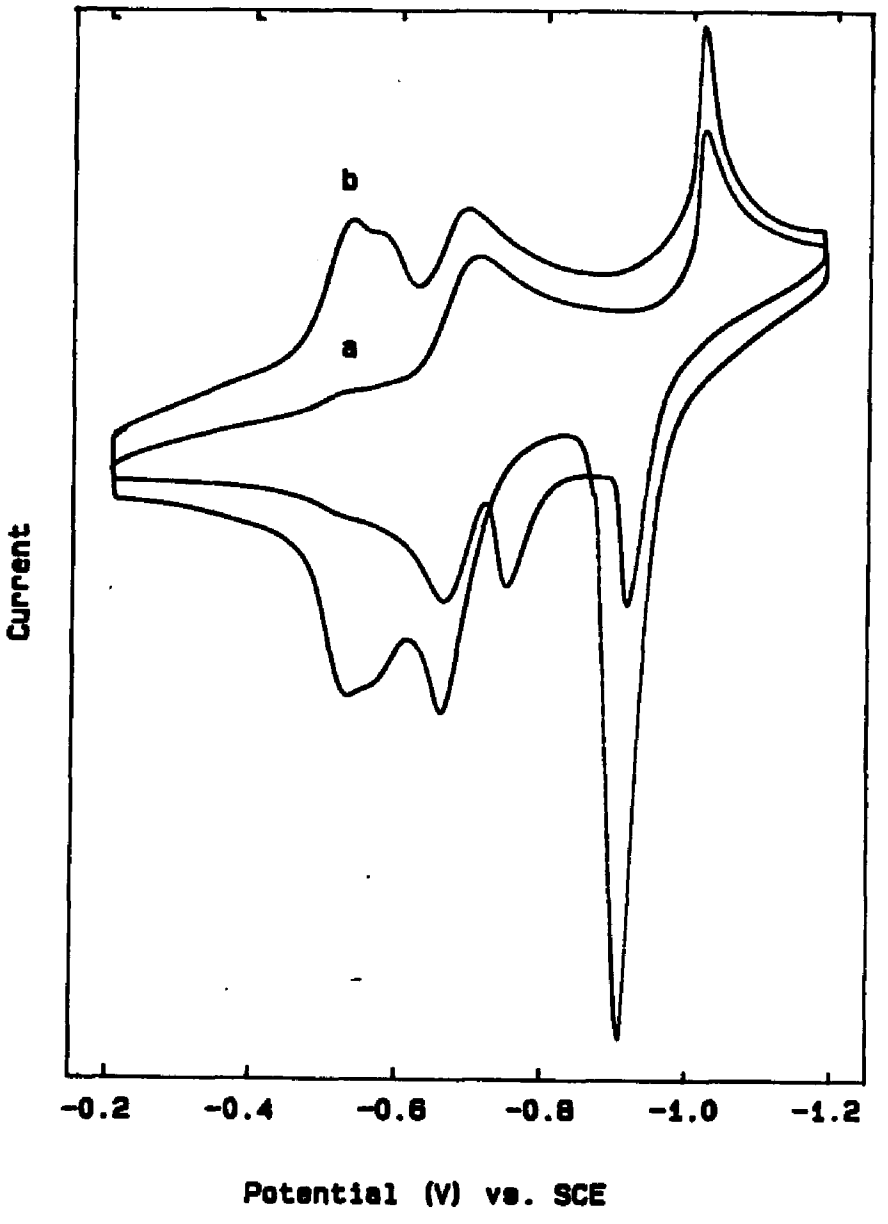

Fig. 1. Cyclic voltammetry of 1 mM methyl viologen and 0.1 M KCl solution at 200 mV/sec. scan rate. (a) on a smooth Ag electrode. (b) on a roughened Ag electrode. An ORC from -0.3 to +0.3 to -0.3 V with 2 sec. pulse was used to rough the electrode surface. Total anodic charge is around 100 mC/sec.

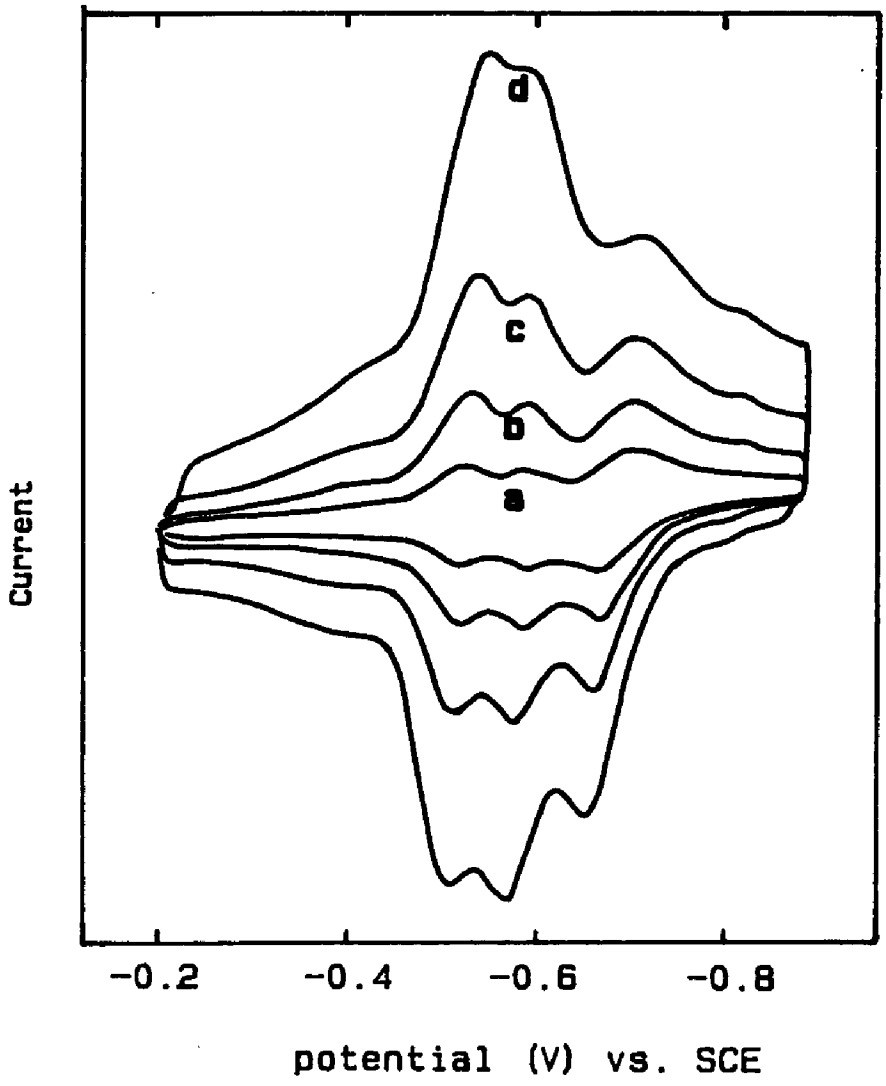

Fig. 2. Cyclic voltammogram of 5×10^{-4} M methyl viologen on a rough Ag electrode at different scan rate (a) 20 mV/sec. (b) 50 mV/sec. (c) 100 mV/sec. and (d) 200 mV/sec.

electrode at a different scan rates. It can be clearly seen that the adsorption peaks increase as the scan rate increases much faster than a diffusion peak does. A plot of the adsorption current versus scan rate is linear, whereas a plot of a diffusion controlled current versus the square root of scan rate is linear. This difference distinguishes the adsorption current from a diffusion current. Further evidence for distinguishing an adsorption peak from a diffusion peak is that the peak separation between anodic peak and cathodic peak is about 57 mV for diffusion peaks, but for an adsorption peak the peak potentials of anodic and cathodic are the same. From Fig.2 we can see that the peak position of the cathodic and anodic peaks for the prepeak are quite close. A small increase in the separation of peak potentials as the scan rate increases is due to the increase of an IR drop.

The prepeak indicates that the reduced form (cation radical) is adsorbed more strongly than the oxidized form (dication). Therefore, the adsorption peak occurs at more positive potential then that of a diffuse controlled reversible potential.

The relative strength of adsorption of both the oxidized and reduced forms is further proved by the measurements of cyclic voltammetry after replacing the solution by a pure electrolyte solution. The electrode is first treated with an ORC in 0.1 M KCl then put into a solution containing 10^{-4} M methyl viologen. In one experiment the potential was held at -0.2 V and the methyl viologen solution was replaced by 0.1 M KCl, then the electrode potential was

swept from -0.2 to -0.8 V. We found that most of methyl viologen (at this potential it is a dication) was lost by washing with the electrolyte at -0.2 V; However, in another experiment after ORC pretreatment in KCl the electrode potential was held at -0.8 V and the methyl viologen solution was replaced by 0.1 M KCl. A potential sweep from -0.8 V to -0.2 V gives an adsorption peak which has the same magnitude as before washing out the bulk methyl viologen. These two experiments indicate that at -0.2 V the oxidized form is adsorbed quite weakly whereas at -0.8 V the reduced form is adsorbed so strongly that it can not be washed out. So a prepeak is observed in cyclic voltammetry.

It is interesting that in organic solvent a postpeak is observed as in Fig. 3. A cyclic voltammetry of 1 mM methyl viologen in acetonitrile and 0.1 M tetrabutylammonium perchlorate (TBAP) shows three peaks. The first reversible reduction from dication to cation radical at around -0.05 V vs. Ag/AgCl reference electrode proves to be diffusion controlled according to the plot of peak current vs. the square root of scan rate. The second peak at around -0.2 V vs. Ag/AgCl electrode increases faster than the first diffuse controlled peak as the scan rate increases. This peak is an adsorption peak. Comparing with Fig. 1 in aqueous medium the difference is that the peak position changes from "pre" to "post". The third peak at around -0.45 V is again a diffuse controlled peak. This peak is more likely a reversible process than in aqueous solution, since the biradical is a neutral species and is more soluble in organic solvent than in

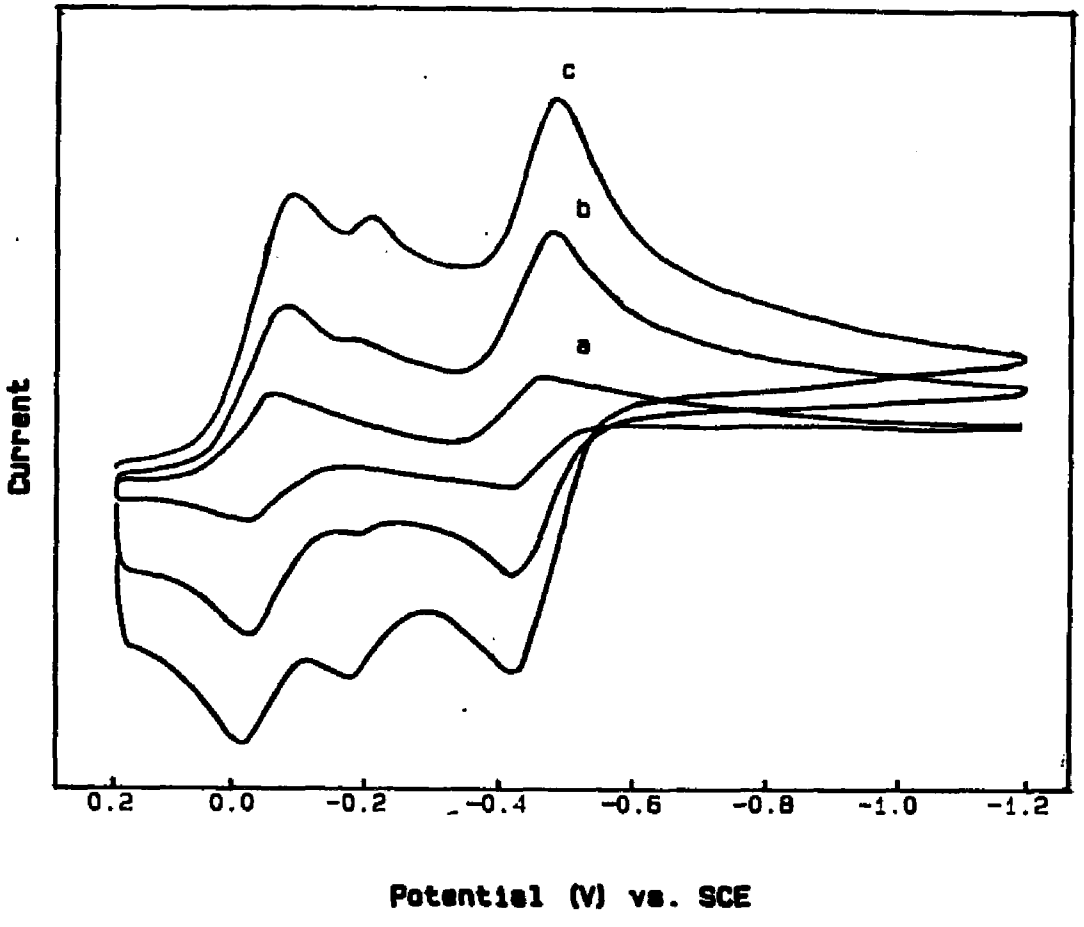

Fig. 3. Cyclic voltammetry of 1 mM methyl viologen in acetonitrile and 0.1 M TBAP, on a roughened Ag electrode. The electrode is treated with a ORC pulse from +0.1 to +1.0 to +0.1 V. The pulse time is 1 sec. The potential is vs. Ag/AgCl electrode. The scan rate is (a) 20 mV/sec. (b) 100 mV/sec. and (c) 500 mV/sec.

polar aqueous medium.

The stronger adsorption of a cation radical on the electrode surface in an aqueous solution than that of a dication can be explained by the hydrophobicity. The reduced form has less charge than an oxidized form. Therefore, its hydrophobicity increases. Water as a very polar solvent pushes the hydrophobic reduced form on to the electrode surface, causing more strong adsorption for the cation radical. But in an organic medium the less polar solvent pulls the hydrophobic cation radical, causing a weaker adsorption of cation radical than biradical.

In order to measure the adsorption current accurately there are three ways to reduce the interference of the diffusion peak. First, because adsorption current is proportional to scan rate but diffusion current is proportional to the square root of scan rate, by increasing scan rate the adsorption current will increase more than the diffusion current, and at high scan rate the adsorption peak will become predominant. Second, by roughening the electrode the microscopic area will be greatly increased and more molecules can be adsorbed. Fig. 4 shows the cyclic voltammogram of methyl viologen on a Ag electrode at different extents of ORC pretreatment. It can be seen that the diffusion current does not increase as much as the adsorption current does, since the size of the roughness (a few hundreds of Å) is very small in comparison with the thickness of the diffusion layer. The diffusion process does not "feel" the increase of the microscopic area. And lastly, from the Langmuir isotherm we

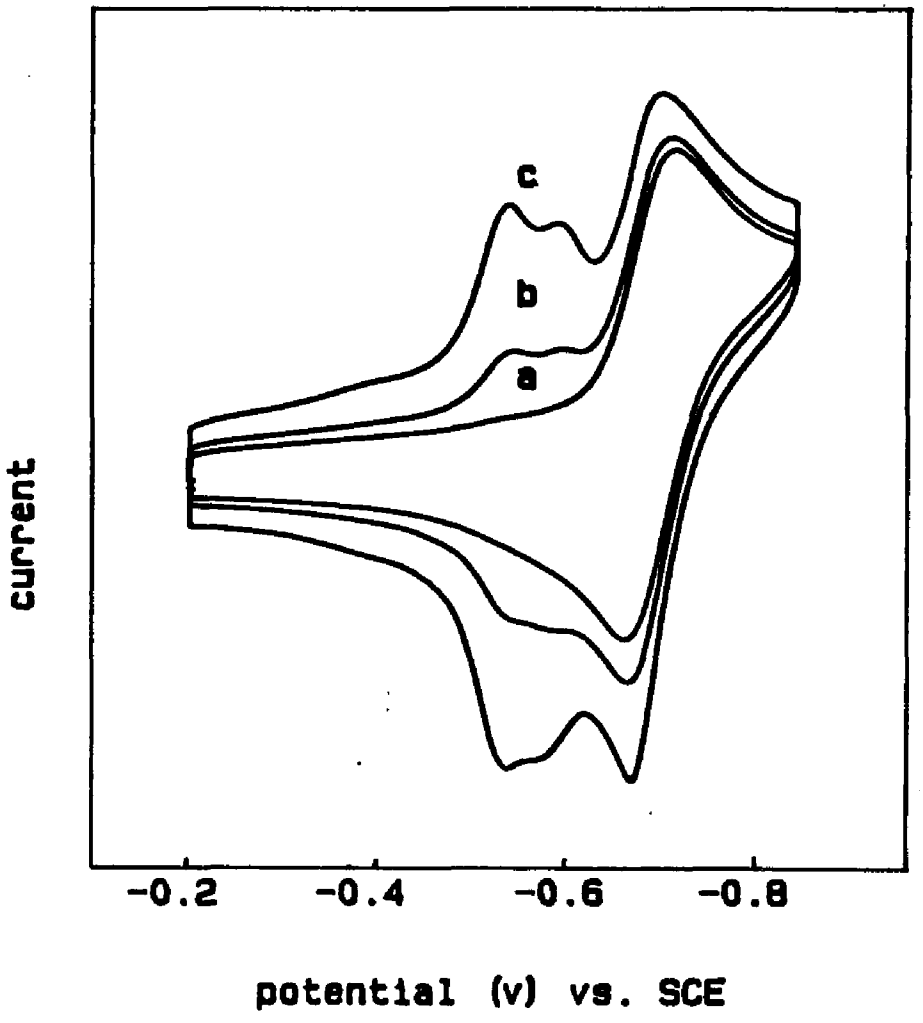

Fig. 4. Cyclic voltammogram of 1 mM methyl viologen at scan rate of 200 mV/sec., on a Ag electrode with different roughness (a) smooth surface (b) 100 mC/cm^2 of anodic charge was passed for a ORC treatment (c) 250 mC/cm^2 of anodic charge.

can see that the surface concentration is not proportional to the bulk concentration, especially for strongly adsorbed species. Lowering bulk concentration does not decrease the surface concentration in the same manner as in the bulk. But the diffusion current is proportional to the bulk concentration over the whole range of concentrations. So, at low bulk concentration the adsorption current will be much higher than the diffusion current or the diffusion current will be negligible.

There is another effect which has to be considered. The charging current is proportional to the scan rate. At high scan rate and low concentration the charging current is much larger than the Faradic current. However, the charging current as a background can be subtracted by computer easily.

(b) The measurement of surface concentration

Based on equation (3), the slope of the plot of i_p with respect to the scan rate υ can be used to calculate the surface concentration Γ_o^*, by the relation

$$\text{slope} = n^2F^2/4RT\ A\ \Gamma_o^*$$

or by plotting log i_p vs. log υ where the intercept at log $\upsilon = 0$ is

$$\text{intercept} = \log n^2F^2/4RT\ A\ \Gamma_o^*.$$

Fig. 5 shows the log plot of adsorption current vs. scan rate of 0.1 mM methyl viologen solution on a smooth Ag electrode. From the intercept at log $\upsilon = 0$ we calculated $A\Gamma_o^* = 3.3\times10^{-12}$ at 25 ^{0}C. The diameter of the electrode was 1.2 mm, and was cut at a 45^o angle. The geometric area of the electrode

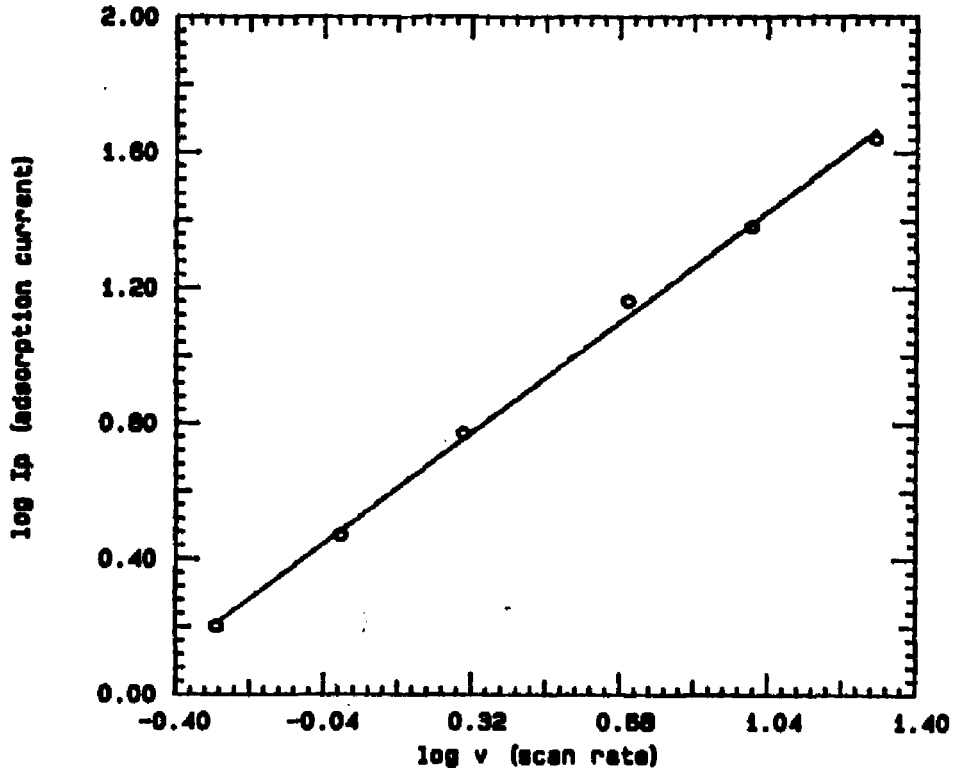

Fig. 5. Log plot of the peak current of adsorption vs. scan rate. The current is measured from the cyclic voltammogram of 10^{-4} methyl viologen solution on a smooth Ag electrode.

was 0.0159 cm^2. We calculated the surface concentration to be

$$\Gamma_o^* = 2.1 \times 10^{-10} \quad \text{moles/cm}^2$$

or $$\Gamma_o^* = 1.2 \times 10^{14} \quad \text{molecules/cm}^2.$$

Assuming this coverage is close to the saturation coverage, each molecule occupies an area of about 80 $Å^2$/molecule. If we estimate the area of a single methyl viologen molecule using bond lengths and considering that the molecule is flat and positioned parallel to the surface, the area occupied by a single molecule is about 75 $Å^2$. This is close to the area we measured by cyclic voltammetry. So we can conclude that the methyl viologen is most likely positioned parallel to the surface rather than positioned vertically or in an other orientation.

If the electrode surface is roughened, the area will be changed and the amount of molecules adsorbed will be increased. Fig. 6 shows a log plot of the number of molecules adsorbed on the Ag electrode with respect to the bulk concentration at different situations of the electrode: (a) on a smooth Ag electrode, (b) with an ORC treatment in 0.1 M KCl (without methyl viologen), (c) with an ORC treatment directly in methyl viologen solution, which is the same as the solution for the measurement of the surface coverage. At concentrations lower than 10^{-4} M, the surface coverage increases almost linearly as the bulk concentration increases. Above 10^{-4} M of the bulk concentration, the surface coverage tends to be saturated. Comparing (a) and (b), the surface area is increased by roughness. The Γ_o^* in 10^{-4} M methyl viologen solution on the

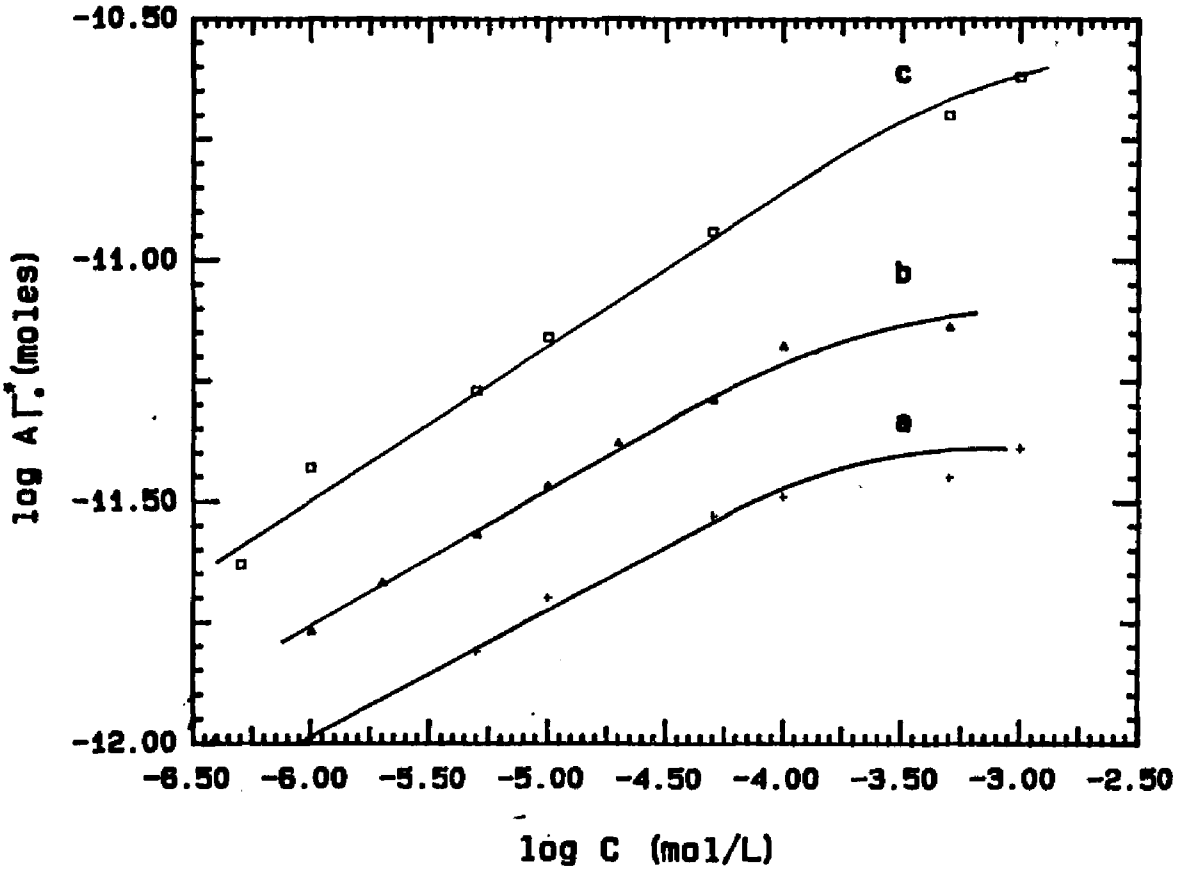

Fig. 6. Log plot of surface coverage vs. bulk concentration of methyl viologen on a Ag electrode (a) on a smooth surface, (b) with an ORC treatment in 0.1 M KCl (without methyl viologen) then measure the surface concentration of methyl viologen in the solution containing a series of the concentration of methyl viologen by cyclic voltammetry. (c) with an ORC treatment directly in the solution containing methyl viologen. The surface coverage is measured in the same solution. The same ORC treatments were used for both (b) and (c). A 0.5 sec. pulse from -0.3 to +0.3 to -0.3 V was used with about 25 mC/cm^2 of anodic charge transferred.

roughened electrode is calculated from (b)

$$\Gamma_0^* = 2.5 \times 10^{14} \quad \text{molecules/cm}^2.$$

More than twice of the molecules are adsorbed on the roughened electrode surface in comparison with that on a smooth electrode. From (c) we can calculate the number of adsorbed molecules in 10^{-4} M methyl viologen solution as

$$\Gamma_0^* = 5.2 \times 10^{14} \quad \text{molecules/cm}^2$$

More than twice of the molecules are adsorbed than if the electrode is treated in the absence of the adsorbate. Since the charge transferred during the ORC pretreatment only depends on the electrolyte concentration (we kept all experiments in 0.1 M KCl), the surface roughness or surface area will be similar for both cases of (b) and (c). Therefore, we can conclude that when the electrode is treated in the presence of adsorbate, a large amount of adsorbate will be trapped in the sponge-like Ag layer.

Comparing our results with other measurements from the literature, our results compare favorably (see Tab. 1). For example, 2-amino-5- nitropyridine (ANP) is measured by a spectrophotometric method [2]. Both the measured value and the estimated value from the structure and dimensions of the adsorbate indicate that the monolayer contains 2.5×10^{14} molecules/cm^2. This coincides well with our measurement for a monolayer of methyl viologen (1.2×10^{14} molecules/cm^2) if the difference of the size of ANP and methyl viologen is considered. The surface coverage for a roughening charge transfer of 25 mC/cm^2 in 1 mM ANP solution is about 27×10^{14} molecules/cm^2, which

Table 1 surface coverage data of methyl viologen compared with other systems

methods	molecules	Γ_0^* x 10 ^{14} molecules/cm^2
cyclic voltammetry (this work)	MV^{++}	1.2
spectrophotometric [3]	ANP	2.5
radiochemical [7]	pyridine	80
differential capacitance [6]	NCS	24
rapid linear sweep [4]	$Cr(NCS)_6^{3-}$	3
chlonocoulometry [5,6]	pyridine	3-6

is 11 monolayer equivalents. At the same conditions our result is 9.5×10^{14} molecules/cm^2, which is about 8 monolayer equivalents. Comparing with the measurement by Barradas [11], a monolayer of pyridine corresponds to 9×10^{14} molecules/cm^2, our value, $1.2 \times 10_{14}$ molecules/cm^2, is a little smaller. By radiochemical technique the number of adsorbed pyridine molecules is measured as 8×10^{15} molecules/cm^2 in 50 mM pyridine solution when the roughening charge transfer is lower than 50 mC/cm^2. It is much higher than our result since the concentration is much higher.

(c) Calculation of enhancement factor

One of the advantages of this method is that we can measure surface concentration and SERS intensity in-situ. There is no risk of losing adsorbed molecules from washing or transferring the electrode. After ORC treatment in 10^{-4} M methyl viologen solution we measured the SERS spectra at -0.2 V, then measured the surface concentration by cyclic voltammetry scanning from -0.2 V to -0.8 V. By measuring the normal Raman intensity the enhancement factor can be calculated according to the following equation:

$$\text{enhancement factor} \approx \frac{\left(\frac{I_s / W_s}{\sqrt{2} \cdot A' \Gamma_0^*}\right)}{\left(\frac{I_n / W_n}{A' 1\,M\ 10^{-3}}\right)}$$

where I_s, I_n are Raman intensities of SERS and normal Raman respectively. W_s, W_n are the laser power used for SERS and normal Raman measurement, assuming the SERS and normal Raman intensities are proportional to the laser power. A' is the area of the laser spot. The length of the laser beam is l from which the normal Raman is collected. M is the concentration of the solution for normal Raman measurement (mol/L). Γ_o^* is the surface concentration (moles/cm^2). When W_s = 50 mW, W_n = 150 mW, l = 1cm, M = 0.5 mol/L, and the concentration for SERS is 0.1 mM, we get similar intensities for both SERS and normal Raman. Γ_o^* is measured under these conditions by cyclic voltammetry as $\Gamma_o^* = 8.6 \times 10^{-10}$ mol/cm^2. We can calculate that the enhancement factor is about 1.2×10^6 when 25 mC/cm^2 charge was passed for ORC pretreatment. Comparing with the enhancement factors measured by other methods, our result is well correlated with the result of pyridine (1.3×10^6) [1], and NCS (1.2×10^6) [5], but much higher than the result of ANP (1.5×10^4) [2].

(d) Correlation of surface coverage and SERS intensity

A linear relation between SERS intensities and surface concentration is observed as shown in Fig. 7. This linear relation is obtained only when the surface concentration is lower than 7×10^{-10} moles/cm^2 or the bulk concentration is lower than 10^{-3} M. Above this concentration some deeply trapped molecules presumably can not be excited by laser light efficiently. Both laser light and scattered light may be "shaded" by Ag particles.

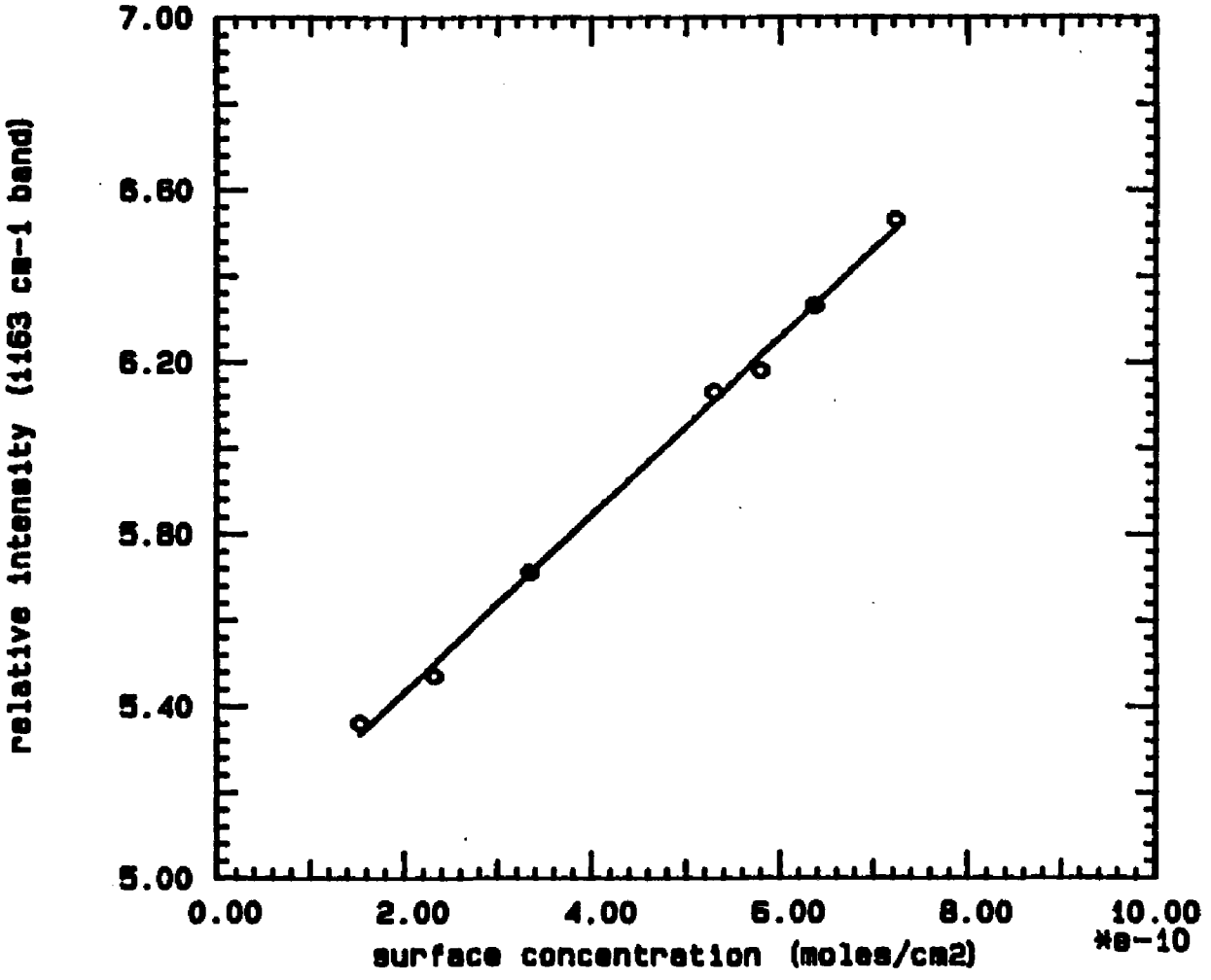

Fig. 7. Plot of relative intensity of SERS band (1163 cm^{-1}) vs. surface concentration. Surface concentration is changed as bulk concentration changes. A 0.5 sec. pulse from -0.3 to +0.3 to -0.3 V was used for electrode roughening. The relative intensity of Raman band is calculated by integrating peak area.

Another linear relation can be seen between SERS intensities and bulk concentration as shown in Fig. 8. The intensities are measured by integrating the peak area, two different bands are measured (1160 cm^{-1} and 826 cm^{-1}). There is no difference between these two bands. The low limit of the detection of SERS intensity is below 10^{-9} M. The intensity at the concentration of 10^{-9} M is well above the noise level, indicating that SERS is a very sensitive technique that allows one to obtain vibrational spectra of molecules.

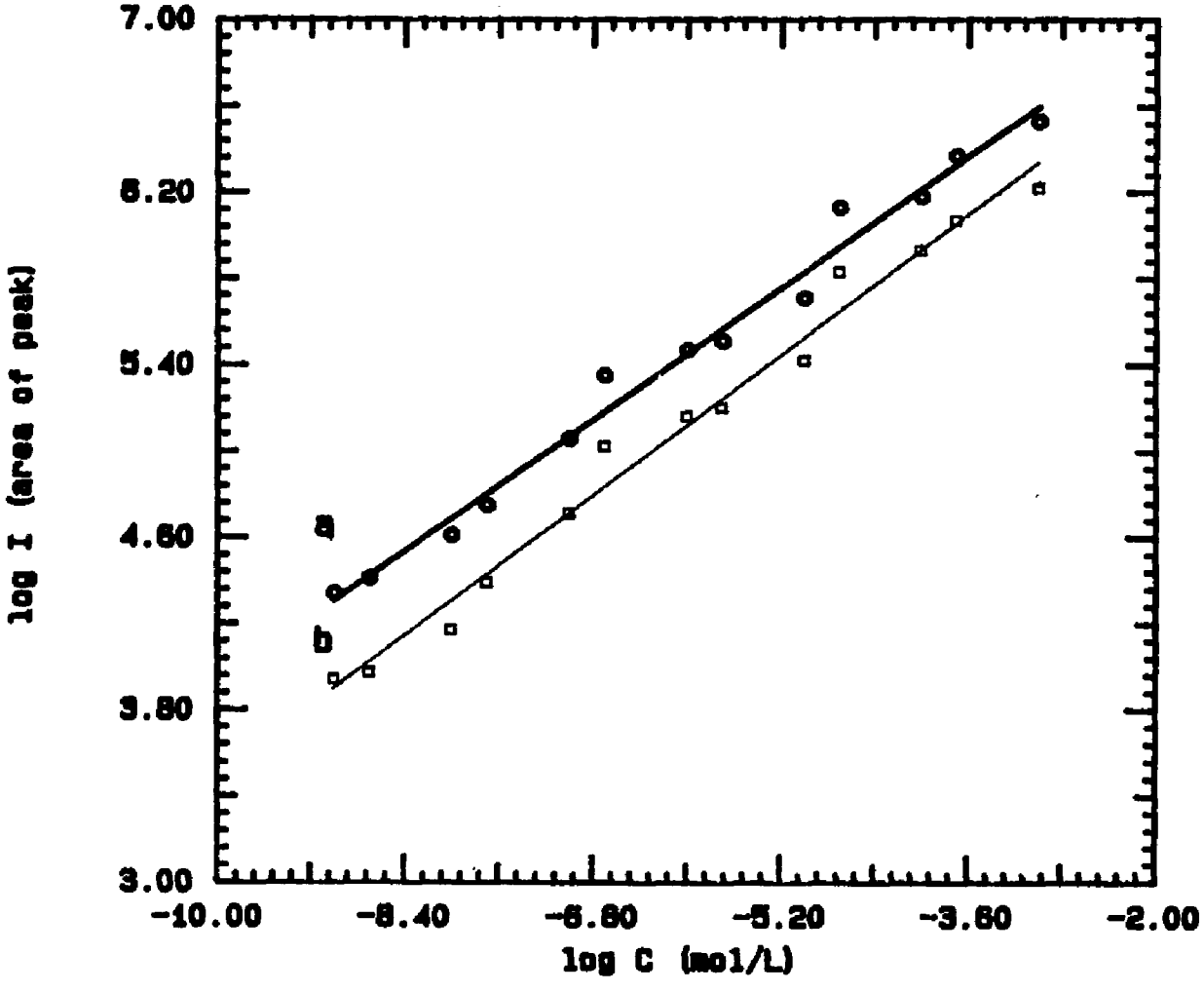

Fig. 8. Log plot of SERS intensity with respect to bulk concentration of methyl viologen. A 0.5 sec. pulse from -0.3 to +0.3 to -0.3 V was used for electrode roughening. The area of Raman peak is used to represent intensity (a) 1160 cm^{-1} mode (b) 826 cm^{-1} mode.

REFERENCES

[1] R.P.Van Duyne in C.B. Moore (Ed.), Chemical and Biological Applications of Laser Vol.4 Academic Press, New York, 1978 p101

[2] C.C.Busby and J.A.Creighton, J. Electroanal. Chem. 133, (1982) 183

[3] M.J.Weaver, S.Farquharson and M.A.Tadayyoni J. Chem. Phys. 82(11), (1985) 4867

[4] K.J.Guyer and M.J.Weaver, Inorg. Chem. 23, (1984) 1664

[5] J.T.Hupp, D.Larkin, and M.J.Weaver, Surf, Sci., 125, (1983) 429

[6] M.J.Weaver, F.Barz, J.G.Gordon II and M.R.Philpott, Surf. Sci. 125, (1983) 409

[7] G.Blondean, M.Froment, J.Zerbino, N.Jaffrezic-Renault and G. Revel, J.Electroanal. Chem. 105, (1979) 409

[8] Allen J.Bard, and Larry R.Faulkner. 'Electrochemical Methods' by John Wiley & Sons, Inc. New York, 1980

[9] E.M.Kosower, in 'Free Radicals in Biology', Vol.2, W.A. Pryor, Editor, p.1 Academic Press, New York (1976).

[10] J.Kiwi, K.Kalyanasundaram, and M.Gratzel, in 'Structure and Bonding', Vol. 49, M.J.Clarke et al. Editors, p37 Springer Verlas, Berlin (1982)

[11] R.G.Barradas and B.E.Conway, J. Electroanal. Chem. 6, (1963) 314

CHAPTER (V)

SURFACE INDUCED PHOTOCHEMICAL REDUCTION OF P - NITROBENZOIC ACID ON SERS ACTIVATED SILVER SURFACES

Section 5.1 Introduction

This work is concerned with the photolysis of p-nitrobenzoc acid (PNBA), which had been observed on Ag island films and on roughened Ag electrode surfaces in our laboratories. We have found that PNBA undergoes a reduction which does not exist in the absence of the surface, since the molecular absorption in the visible range is exceedingly weak either in solution or in the solid state. Thus the photolysis is a surface induced photochemical reduction.

It has been known that the optical properties of molecules are dramatically attered when they are adsorbed on or near a rough metal surface, such as, enhanced light absorption [1] and enhanced fluorescence [2] etc. The photochemistry of adsorbed molecules is usually quenched by a metal surface due to a non-radiative energy transfer to the substrate [3]. In contrast, on some rough metal surfaces, enhanced photochemical reactions have been observed. For example, the enhanced photofragmentation of pyridine, pyrazine and benzaldehyde [4], photochemical degradation of rhodamine 6G (R6G) on silver island films [5] and the demethylation of N-methyl pyridinium [6] or methyl viologen [7] on Ag electrode have been observed. Furthermore, several calculations have been given which predict that the photochemical reactions can be enhanced on rough metal surface [8,9]. The surface enhancement of a photochemical reaction might come from several sources. These include: (i) an electromagnetic effect, whereby a large increase in the local field produced by the

excitation of localized electron plasma resonances, might be expected to increase the rate of a photochemical reaction; (ii) a charge transfer mechanism, where if the excitation can take place by a charge transfer between the metal and the new states of the charge transfer complex, then the photochemistry may be assisted by lowering of the charge transfer threshold with subsequent chemical reaction. In addition to these two mechanisms there is (iii) enhanced photoemission in such a system which can also occur by exciting localized multipolar plasmon modes of microstructures on the surface. Localized plasmons associated with multipoles higher then the dipolar mode are thought to create strong electric fields just under the surface of metal microstructures [10], and thus photoelectron emission could be enhanced by several order of magnitude over that of a planar metal surface [10]. Calculations show that for a 50 nm Ag sphere in water the enhancement ratio of photoelectron emission is about 5000 [10].

On the other hand, any deactivation process can also be enhanced by a rough metal surface. So the surface induced enhancement of any optical process depends on the balance between the enhanced pumping and the decay rates of the various deexcitation channels. Therefore, only those molecules which have a greater pumping rate than decay rates would show photochemistry.

It is advantageous to study the photochemistry or photoelectrochemistry on a surface on which SERS is observed because (i) surface enhancement tech-

niques can be used to achieve the required submonolayer sensitivity, (ii) SERS spectra can be used to identify products or intermediates of photochemical reactions, and (iii) one can follow reactions in real time since the Raman scattering process is faster than any other chemical process. Investigations of surface enhanced photochemistry can lead to a richer and deeper understanding of the influence of a rough metal surface on the optical processes of adsorbed molecules.

Although PNBA has been widely used as a model molecule in SERS studies on metal surfaces or tunnel junctions [11-17], less attention was paid to its photolysis. Several studies have commented on the two different kinds of SERS spectra from PNBA adsorbed on a Ag surface [14-17], among them is one very close to the normal Raman spectrum of PNBA but a second kind, which is characterized by a band near 1460 cm^{-1} and a doublet near 1150 cm^{-1}, is very different from the normal Raman spectrum. The explanations for diverse spectra these studies are not satisfactory. Only a recent report by Roth, Venkatachaiam and Boerio [18] gives a detailed study of the possible chemical change of PNBA on a Ag surface. They conclude that PNBA molecules undergo a thermally induced chemical reduction, and the reduction product is identified as azodibenzoate. However, their studies are limited to Ag island films. In the present investigation the SERS spectra on both Ag island films and Ag electrode surfaces are studied. According to our observations the chemical change on a SERS activated surface is more likely a photo induced instead of a ther-

mally induced process.

Section 5.2 Experimental

The silver island film is produced by slow thermal evaporation [19] onto a quartz substrate to a mass thickness of about 50 Å. The substrate is mechanically polished and chemically cleaned. An electron micrograph has shown that the islands have an average 200 Å in diameter and cover about 30-40% of the surface [20]. The PNBA molecules were deposited on the substrate by the dipping technique [21]. The substrate is slowly inserted into and withdrawn from 10^{-3} M solution of PNBA in ethanol. The scattered light was collected in a back-scattering geometry. The incident laser beam was focused onto the island film by an f/1.2 lens with 5 cm focal length, giving a spot with approximately 15 μm in diameter. The laser radiation was provided by either an (Spectra Physics) Ar^+ laser or a (Coherent) Kr^+ laser, with the substrate either stationary or spinning. The SERS spectra were recorded using a Spex Triplemate spectrometer with a PAR optical multichannel analyzer. The experimental setup for the SERS study of PNBA on silver electrode has been described elsewhere [22].

The p-nitrobenzoic acid (PNBA) and p-aminobenzoic acid (PABA) are reagent grade and used without further purification. In the electrochemical study the solution pH was adjusted by adding NaOH to pH=11 to increase the solubility of PNBA. At this pH the predominant form is p-nitrobenzoate

(pK_a=3.47) ions (hereafter we also abbreviate these anions as PNBA).

It has been found that monocarboxylic acids chemisorb on Ag or metal oxides surface as symmetric, bidentate carboxylate ions, that is, the carboxylic acid group loses its hydrogen to form a carboxylate anion. Then both oxygen atoms on the carboxylate are equally adsorbed on surface. This has been determined from the absence of C=O stretching band in the 1700 cm^{-1} region of the SERS spectrum [12] and from studies using tunneling spectroscopy [23], second-harmonic generation [24], as well as FTIR-ATR studies [25].

Sodium sulfate was used as the electrolyte. We found that halides quench the SERS spectrum of PNBA due to the competition of halide anions with the anions of PNBA on the Ag surface. Much larger SERS intensity was observed for PNBA when sulfate or nitrate was used as the electrolyte than when the halides were used.

Section 5.3 Resuits and Discussion

(a) The Observation of the photolysis of PNBA

Fig. 1 shows the time dependence of the SERS spectrum of PNBA on a stationary Ag island film which is irradiated by laser radiation. At the beginning, the SERS spectrum, which is the same as the spectrum obtained when the substrate is spinning, is very similar to the normal Raman of PNBA in solution phase. The main bands at around 866, 1115, 1355, 1395 and 1602 cm^{-1} correspond to $\delta_{(NO_2)}$, $\gamma_{a\,(NO_2)}$, $\gamma_{s\,(NO_2)}$, $\gamma_{s\,(CO_2)}$, and γ_8 ring modes respectively

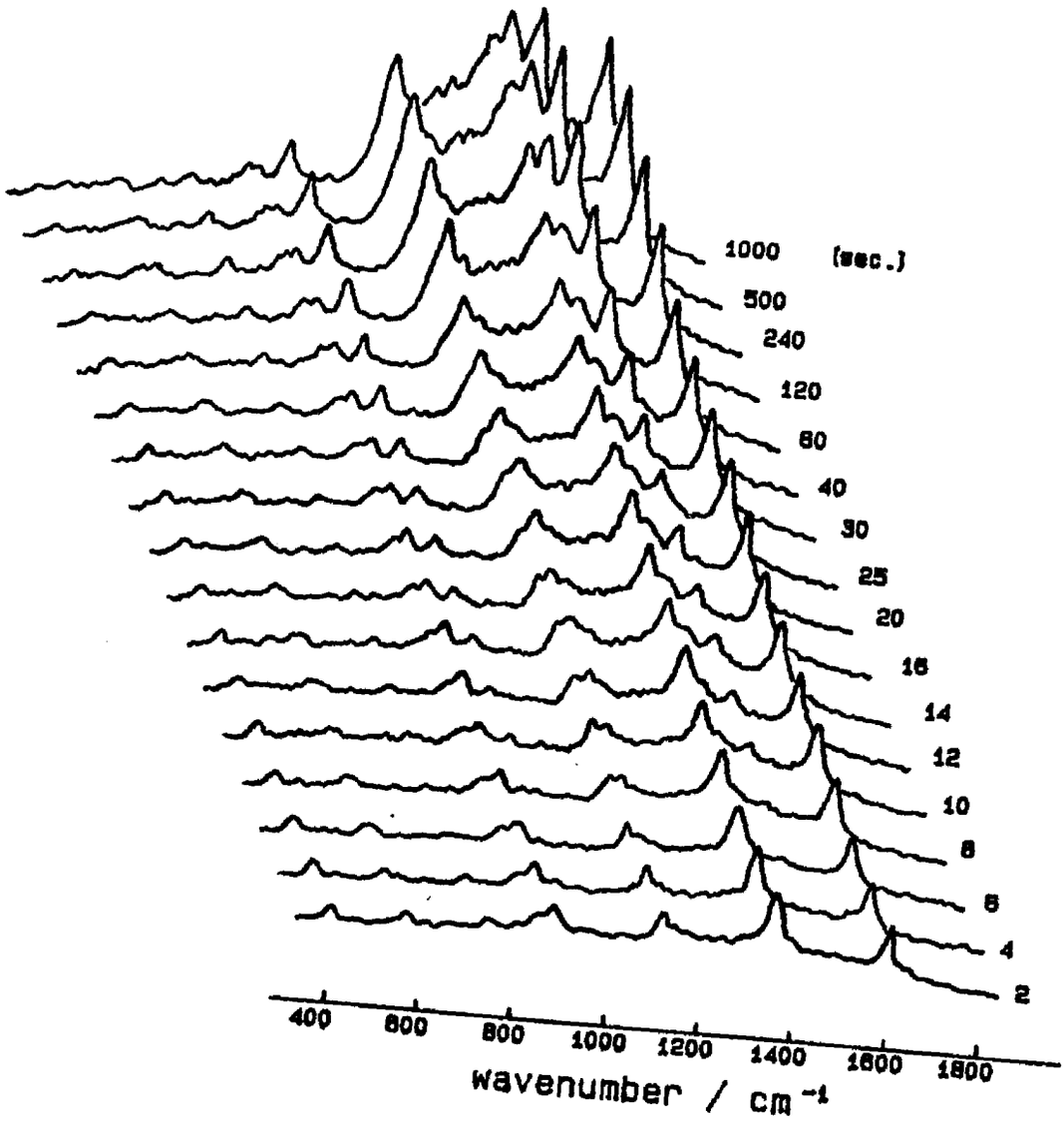

Fig. 1 SERS spectra of PNBA on a Ag island film at different times of irradiation with 5 mW of 476.5 nm laser light.

(where δ represents the deformation and γ represents the stretching mode). The absence of the C=O stretching mode around 1700 cm^{-1} indicates the loss of a hydrogen atom when the carboxylic acid group is adsorbed on Ag island surface. As the sample is irradiated with laser light a second set of new modes at around 825, 1131, 1145, 1175, 1283, 1390, 1453 and 1595 cm^{-1} increase in intensities. This observation is very similar to that of Roth, Venkatachaiam and Boerio recently reported [18]. We have also observed that a structured background around 1350 and 1550 cm^{-1} grows as the new modes increase. This background is very similar to the broad bands which were reported and identified as surface carbon due to surface enhanced photofragmentation [4].

When the sample is immersed in cyclohexane, the same change in spectrum is observed as when the sample is exposed to air. But under cyclohexane there is no remarkable background growth as the new modes increase. The cyclohexane seems to protect the sample from photofragmentation. Possibly the cyclohexane reduces an oxidation reaction which is part of the photofragmentation process.

We have found that the rate of the increase in intensities of the second set of Raman modes are faster for irradiation at 488.0 nm than for 514.5 nm at the same photon flux of laser irradiation, indicating a frequency dependence of the change in spectra.

In order to determine whether this change of the spectrum is caused by a thermally induced effect or by a photoexcitation, we heated the Ag island film

sample, on which the PNBA molecules have been deposited on, in an oven. No change in the SERS spectrum of PNBA was observed except for a decrease of the overall SERS spectrum. This decrease in the overall spectrum is probably due to a change of the Ag morphology or desorption of adsorbate. On heating up to 110 °C for 30 minutes, the whole spectrum disappeared. A similar observation in the literature [18] has been reported for the heating effect. There is no observable change in SERS spectrum of PNBA on the Ag island film even by heating up to 160 °C.

The SERS spectra of PNBA on a roughened Ag electrode surface in aqueous solution has also been studied. The change in SERS spectra at the electrode/electrolyte interface, as shown in Fig. 2, is very similar to that on the Ag island film. Initially, the SERS spectrum is almost the same as the normal Raman of PNBA in aqueous solution. The same modes as those on the Ag island film grow with time on irradiation with laser light. Similar to the observation on island films covered with cyclohexane, on the Ag electrode, which is under an aqueous solution, the background remains structureless.

The other isomers of PNBA, o-nitrobenzoic acid and m-nitrobenzoic acid as well as some similar molecules such as benzoic acid, nitrobenzene and p-, o-, and m-aminobenzoic acids were studied under the same conditions as those for PNBA. In all these systems, except for a growth of the background, no spectral change was observed, indicating that the change in the spectrum is very specific for PNBA molecules.

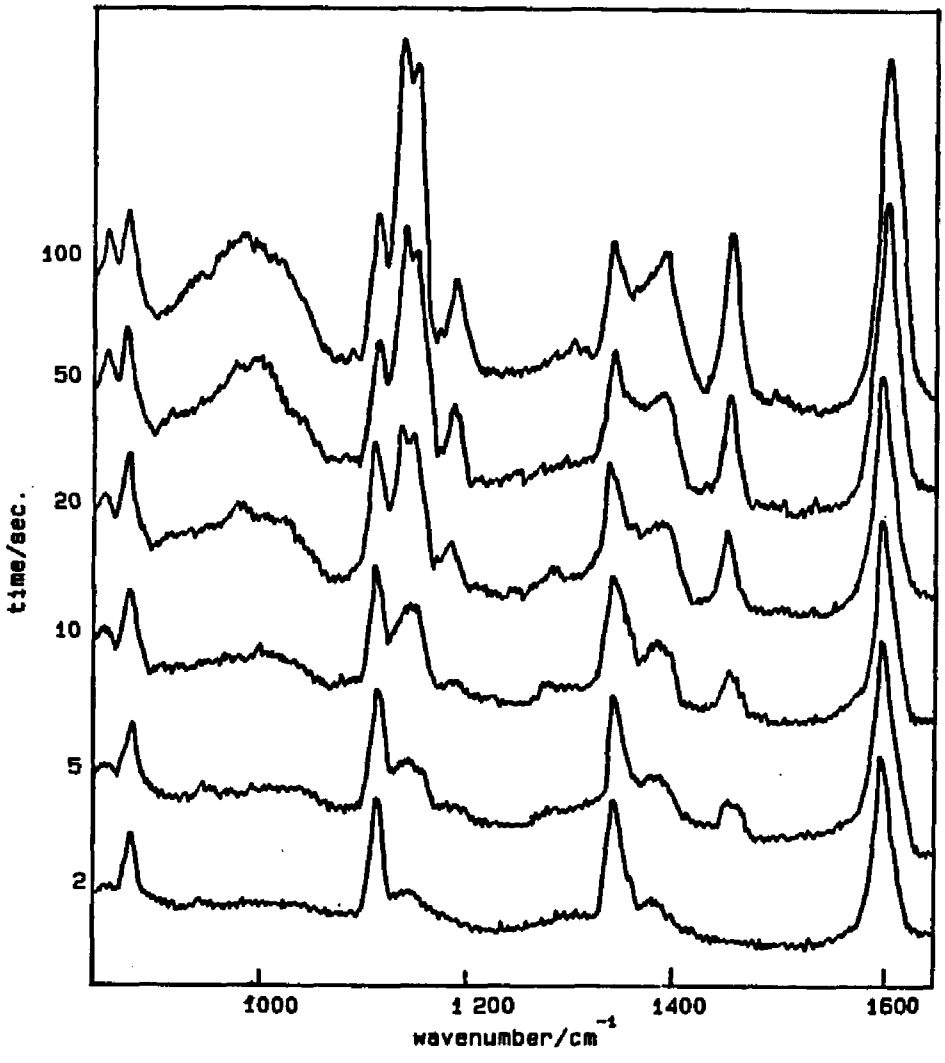

Fig. 2 SERS spectra of PNBA on a Ag electrode surface at different times of irradiation with 20 mW of 606 nm laser light. The electrode was roughed by an oxidation reduction cyclic (ORC) pretreatment with a pulse of -0.2 to +0.5 to -0.2 V vs. SCE, with 2 sec. duration. Both ORC treatment and SERS measurement are in 50 mM PNBA, 0.1 M Na_2SO_4 electrolyte and pH=11.

The solid PNBA and p-nitrobenzoate salt powder were tested under the same excitation conditions as those in the study of PNBA on the Ag island film. It was found that the spectra remain unchanged even after irradiation for an hour. In addition, there is no observable change in normal Raman spectrum of PNBA in solution phase under irradiation even with a high laser power (600 mW). This proves that the change in spectrum only occurs for the molecules which are adsorbed on metal surface. On the other hand, this change in the SERS spectrum only occurs under the irradiation of a laser light, and it occurs within one second after the sample is irradiated. If the electrode is not exposed to laser light, there is no change of the spectrum even several hours after an oxidation-reduction cycle (ORC) pretreatment. The transformation only starts once the laser irradiates the electrode surface and ceases when the laser is shut off. From the above observations it can be seen that both rough metal surface and the laser excitation are necessary for the observation of a spectrum which varies with time. So we conclude that the change of the spectrum is neither a simple photochemical process nor a simple electrochemical process, and it seems not to be a thermally induced chemical process. It is more likely a surface induced photolysis or a photo-induced electrochemical process.

(b) Identification of the photolysis products

Fig. 3(a,b,c) shows the SERS spectrum of p-aminobenzoate, PABA, compared

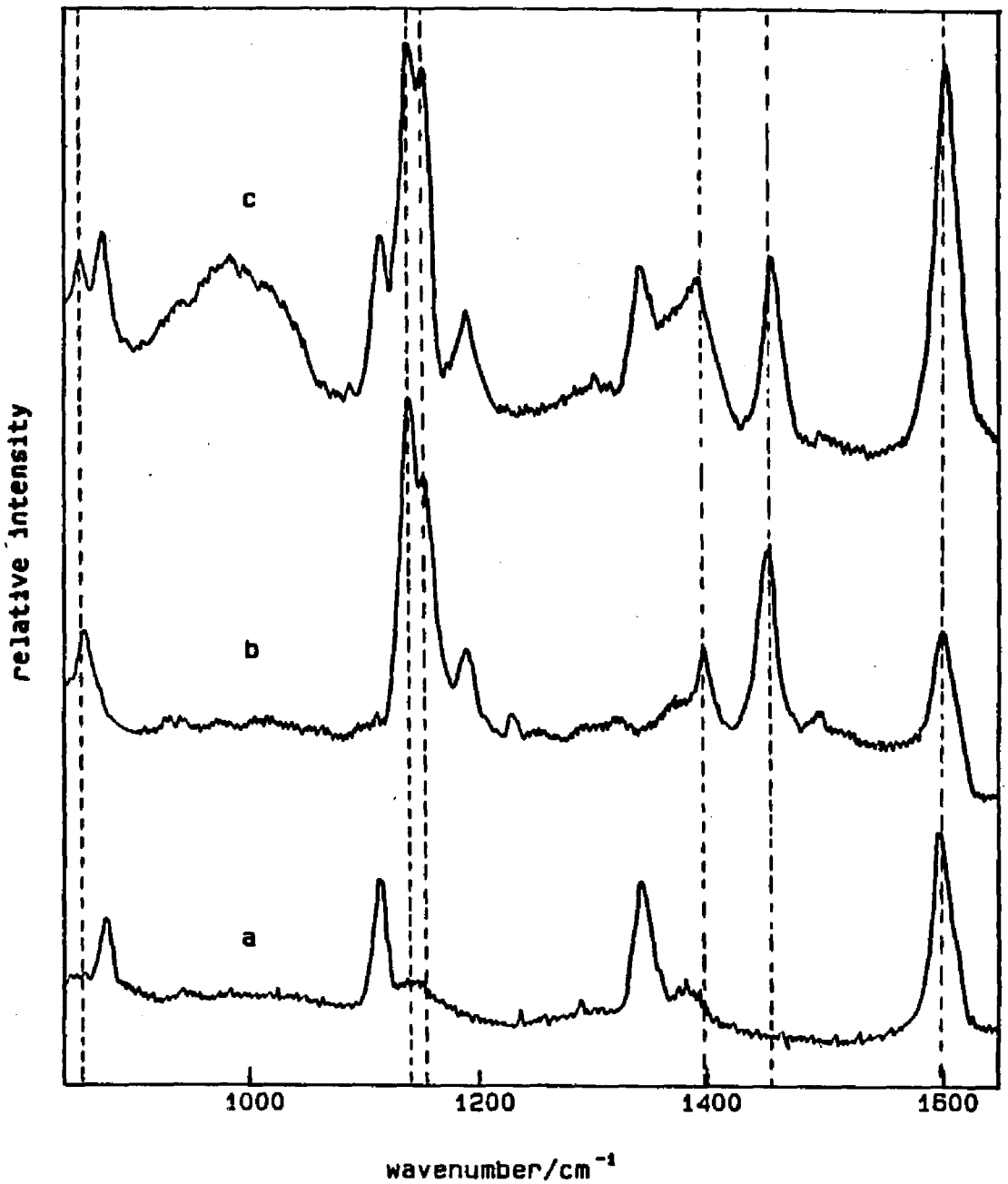

Fig. 3 SERS spectra on a Ag electrode surface at -0.2 V, using 5 mW of 606 nm laser excitation (a) 0.05 M PNBA. The first 1 sec. exposure was recorded. (b) 0.05 M PABA. (c) 0.05 M PNBA after 100 sec. of exposure under 20 mW of laser light.

with the SERS spectra of PNBA before and after photolysis. Fig. 3(a) is the SERS spectrum of PNBA recorded within one second with the irradiation of 606 nm laser light at a low power (5mW) to suppress the photochemical reaction. Thus this spectrum corresponds to the unchanged spectrum of PNBA. It is, indeed, very similar to the spectrum of PNBA in aqueous solution. Fig. 3(c) is the spectrum of PNBA after 100 seconds with the irradiation at 20 mW of 606 nm laser light. Fig. 3(b) is the SERS spectrum of the PABA under the same conditions as Fig. 3(c). Comparing the spectrum in Fig. 3(b) with Fig. 3(a,c), it can be seen that the spectrum 3(c) is just the result of superposition of spectra 3(a) and 3(b), that is, PABA has the same SERS spectrum as the photolysis product of PNBA. However, one can not simply conclude that the photolysis product of PNBA is PABA from their identity of the SERS spectra, since we observed that the SERS spectrum of PABA is remarkably different from the solution Raman spectrum of PABA. The solution spectrum is dominated by two bands: one at 1383 cm^{-1} most likely corresponding to a COO^- stretching vibration and one at 1607 cm^{-1}, a benzene ring stretching mode. But the SERS spectrum is dominated by four bands: one at 1600 cm^{-1}, the ring stretching, one at around 1454 cm^{-1} probably corresponding to the ring in-plane deformation γ_{19b}, and two closely spaced bands at around 1130 and 1145 cm^{-1}. In most SERS spectra, the band position is only slightly shifted (usually less than 20 cm^{-1}) from the normal Raman, since the molecules are only weakly bonded to surface, and the vibrational energy level are slightly

perturbed by the interaction between molecules and metal surface. The remarkable difference between the SERS spectrum and normal Raman spectrum of PABA indicates that there must be some other effect which causes the change in the spectrum.

A two phase model, which accounts reasonably well for our observation, has been reported by Moskovits and DiLella [26] based on the concentration dependence and temperature dependence of the SERS spectrum of PABA on Ag sols. They suggested that there are two different phases for adsorbed PABA molecules. One is called a 'gas-like' phase, which is present in low concentration or at high temperature. Another is called a 'solid-like' phase, which appears in high concentration or at low temperature. The SERS spectrum of the surface 'solid-like' phase resembles that of crystalline PABA in many aspects, while the surface 'gas-like' phase is much more similar to PABA molecules in solution. For example, the prominent band at 1452 cm^{-1} in the SERS spectrum of 'solid-like' phase has its counterpart (1432 cm^{-1}) in crystalline PABA, but no such band is seen in the solution spectrum. The solution spectrum, on the other hand, is dominanted by the two bands at 1383 and 1607 cm^{-1}, close to their counterparts (at 1372 and 1600 cm^{-1}) in the SERS spectrum of the 'gas-like' phase. Furthermore the COO^- vibration (at 1383 cm^{-1}) is a prominent band in both solution spectrum and 'gas-like' SERS spectrum, but quite weak in both the spectra of crystalline and 'solid-like' phase. The SERS spectrum of PABA observed in our experimental conditions is very similar to the SERS

spectrum of adsorbed PABA in 'solid-like' phase as reported by Moskovits [26]. Therefore, we can conclude that the main photolysis product of PNBA is PABA. The nature of the 'solid-like' phase has been described [26]. It is formed by 'condensed' molecules which are linked together by hydrogen bonds between $-NH_2$ and $-COO^-$ groups on neighboring molecules. Such linkages are in fact known to exist in the ordinary solid form of PABA [27]. In the case of the photolysis of PNBA, this kind of linkage can exist not only between PABA molecules, but also between PABA and PNBA, that is, between the $-NH_2$ group in PABA and the $-COO^-$ group in PNBA. This may be the reason why the intensity of $-NO_2$ modes (at 866, 1115 and 1355 cm^{-1}) do not decrease at the same extent as the PABA modes increase during the course of the photolysis of PNBA as seen in Fig. 2. As the PNBA molecules are reduced, the PNBA molecules in the solution phase can diffuse to surface and link with the PABA. This may compensate the lost of the intensity of PNBA due to the reduction. When we replace the PNBA solution with a electrolyte solution after ORC pretreatment (a flow-cell and replacement procedures have been described elsewhere [22]), we found that the intensity of the PNBA modes decrease much faster as the PABA modes increase than if PNBA is present in solution.

There is another possible way to obtain a different reduction product. It has been reported [18] that an azodibenzoate is the main reduction product based on the similarity of the SERS spectrum of PNBA on Ag island film with the

normal Raman spectrum of azodibenzoate. The PNBA molecules undergo a condensation to give an azo compound. There is some evidence which we have observed, as will be discussed, which also supports this conclusion, but there is some uncertainty as to which species is more likely the main product. This problem is left for further investigation.

(c) Determination of the photolysis rate

The photolysis rate is determined based on the change of the SERS intensity, assuming that the SERS intensity is proportional to the concentration of the species adsorbed on surface. We use the intensity of the 1450 cm^{-1} band (background subtracted) to represent the change of the surface concentration of the photolysis product, since this band has less interference than other bands from background and adjacent bands for measuring intensities. Because each change of laser power requires repolishing the electrode, the intensity of PNBA is normalized by the initial intensity of the 1350 cm^{-1} band, which characterizes PNBA, to eliminate the deviations due to the change in optics.

The plot of the intensity of product vs. time at different photon flux is shown in Fig. 4. As the power of the irradiation increases the photolysis rate increases. From the plot of intensity vs. time, the initial photolysis rate is obtained by polynomial curve fitting, and the first derivative at t=0 is taken as the initial rate of photolysis. The initial rate is plotted as a function of the laser power as shown in Fig. 5. A good linear relation is observed, that is, the

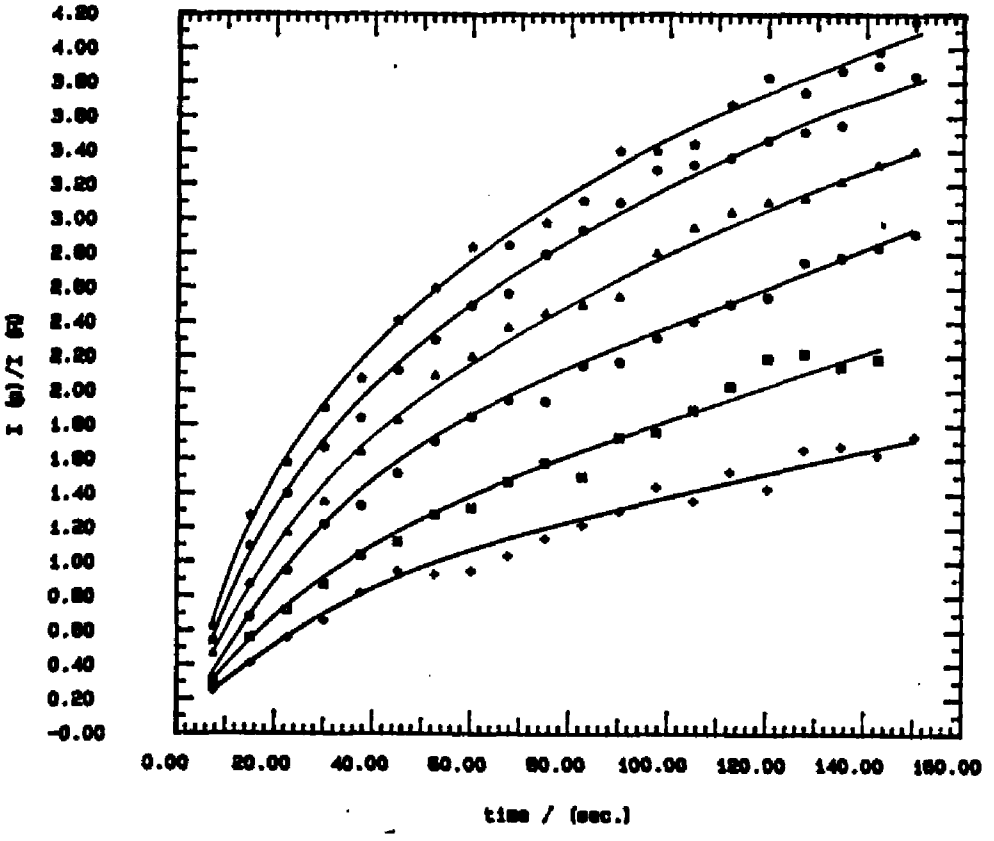

Fig. 4 Time dependence of the intensities of 1450 cm^{-1} peak of the reduction product at different powers of laser light. 606 nm laser excitation was used.

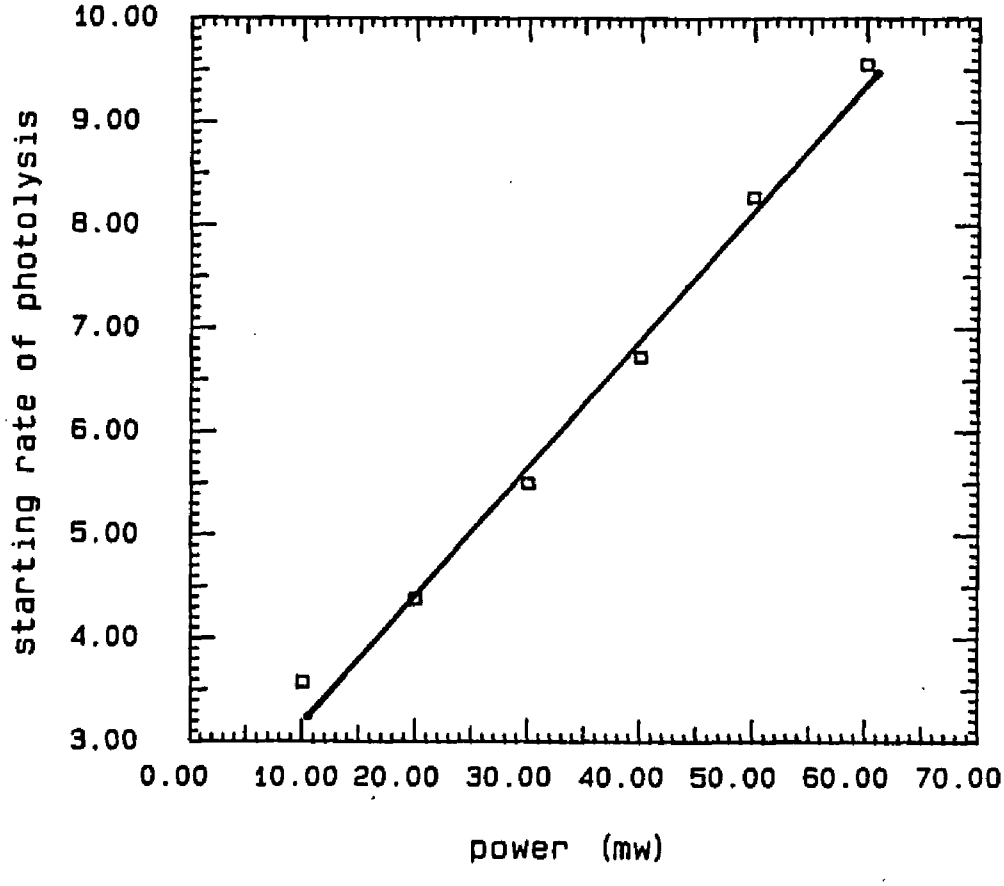

Fig. 5 The linear relation between initial rate of photolysis and laser power.

photolysis rate is proportional to the power of excitation, indicating a one photon absorption process, which is distinct from the surface enhanced photofragmentation of pyridine which was observed to be a non-linear photochemical process under the irradiation of UV light [4].

The photolysis rate was also studied at different electrode potentials as shown in Fig. 6. The power of the dye laser (606 nm) was kept at 20 mW. The intensities of 1450 cm^{-1} band were plotted as a function of time. At potentials between -0.1 to -0.3 V a small increase in photolysis rate was observed as the potential was changed in the negative direction. Then a dramatic increase of the photolysis rate was observed when the potential reaches -0.4 V. This change is most likely attributable to the initiation of an electrochemical reduction.

In order to establish how the change in the spectrum is related to a electrochemical reduction, the cyclic voltammetry of PNBA was studied as shown in Fig.7. There are two main steps for the reduction of PNBA in the potential range between -0.1 to -1.5 V. The first step at around -0.55 V is a four electron reduction process to form a hydroxylamine compound, then the hydroxylamine is further reduced at around -1.1 V to form an amino compound. There is no corresponding oxidation peak for these two main steps in the anodic scan, indicating both reduction steps are irreversible. However, there is another reversible oxidation-reduction process at about -0.3 V which occurs during a second scan. This process, as has been reported [28], corresponds to the reduc-

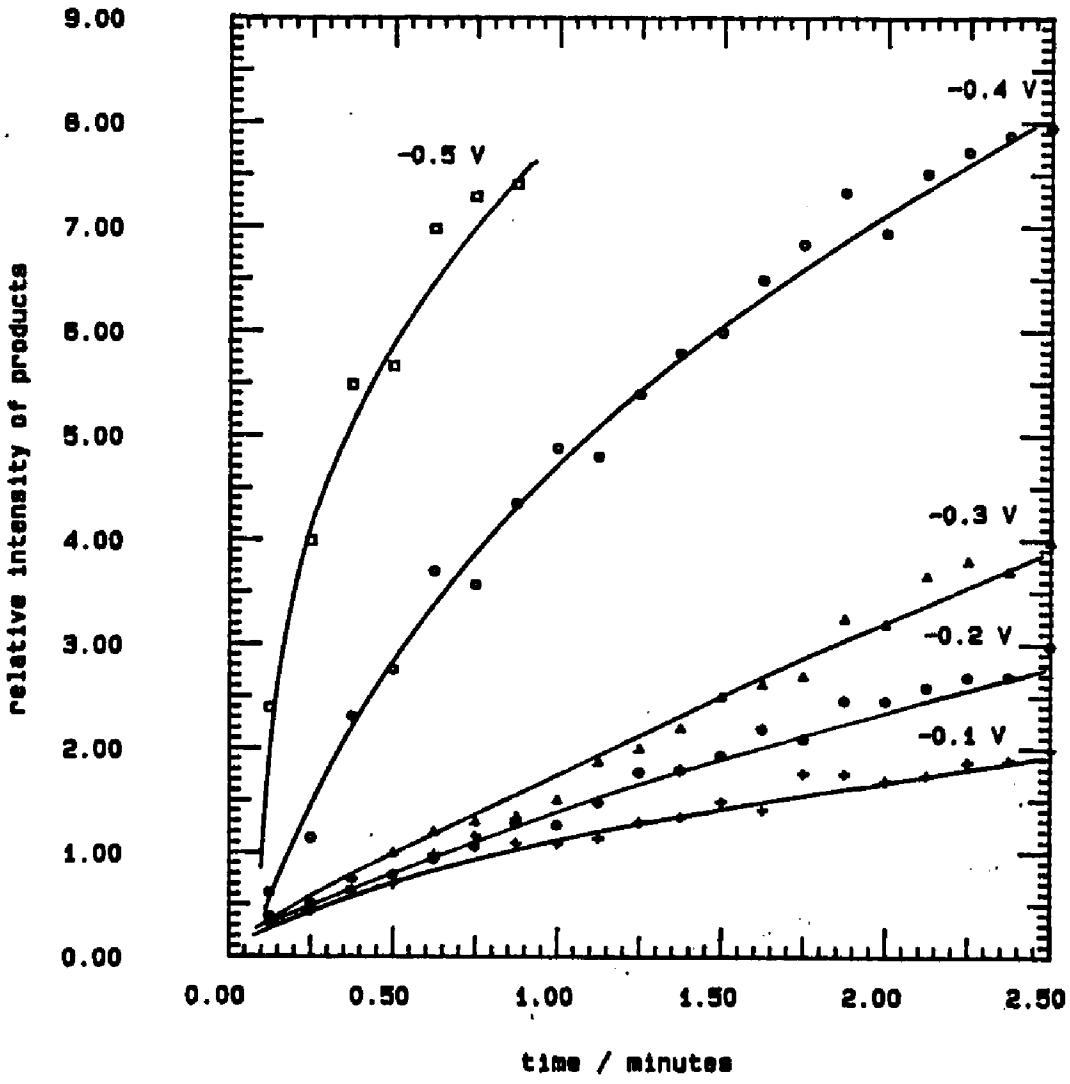

Fig. 6 The time dependence of the intensities of photolysis product at different electrode potential, a constant laser power of 20 mW at 606 nm was used.

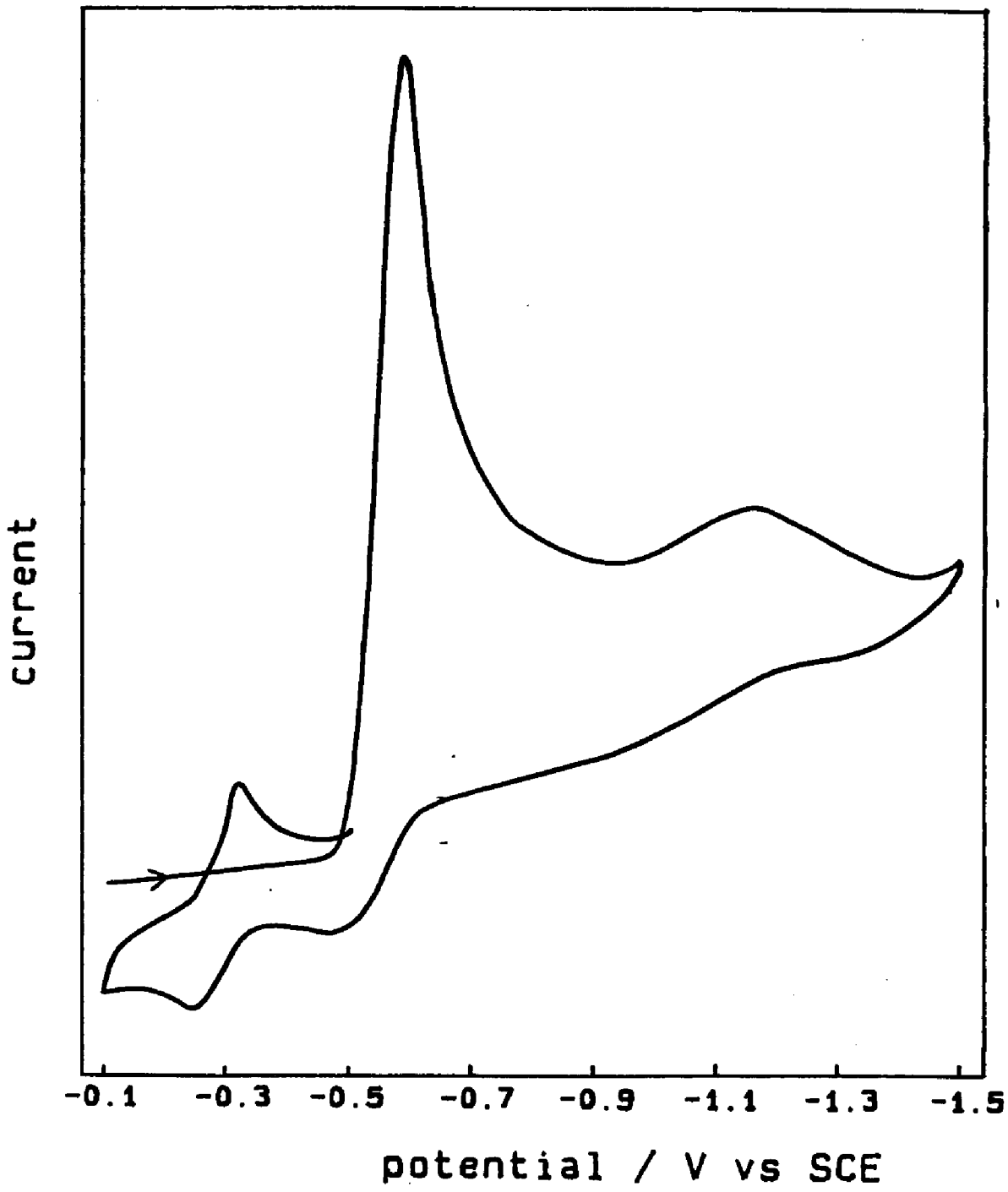

Fig. 7 Cyclic voltammogram of 0.001 M PNBA (in 0.1 M Na_2SO_4, pH=11) on a Ag electrode at 100 mV/sec. of scan rate. The arrow shows the direction of the scan.

tion and oxidation between the nitroso group and hydroxylamine. This reduction peak does not occur during the first scan since originally there is no nitroso, and nitroso being formed as the oxidation product of hydroxylamine.

The potential dependence of the photolysis rate indicates that the change of the spectrum is related to a chemical reduction. From the study of the cyclic voltammetry, it can be seen that the electrochemical reduction starts at around -0.5 V. But under the irradiation of laser light this reduction is observed on a rough Ag surface at a much more positive potential (up to the positive limit around +0.1 V where the Ag electrode is oxidized). This decrease of the charge transfer threshold is not simply caused by the roughness of the surface. The cyclic voltammetry on a smooth Ag surface and on a roughened surface is compared in Fig. 8. Only about 100 mV shift of the reduction potential in a positive direction is observed. This shift is probably due to the catalytic properties of small Ag clusters at the Ag surface which lower the overvoltage for reduction [29].

The chemical and electrochemical reduction of aromatic nitro compounds has long been studied [31-33]. The electrochemical reduction process can be represented by the following scheme [34]

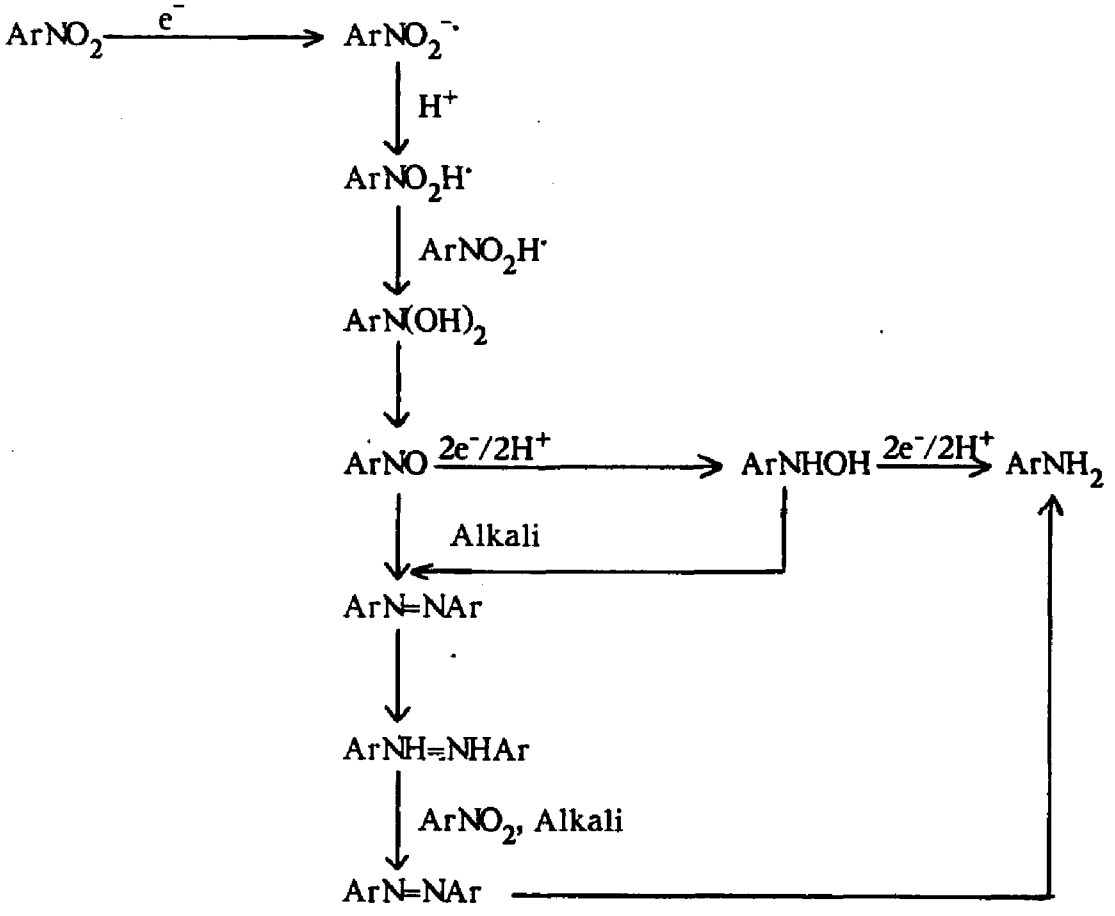
ArNO2
e−
ArNO2−·
H+
ArNO2H·
ArNO2H·
ArN(OH)2
ArNO
2e−/2H+
ArNHOH
2e−/2H+
ArNH2
Alkali
ArN=NAr
ArNH=NHAr
ArNO2, Alkali
ArN=NAr

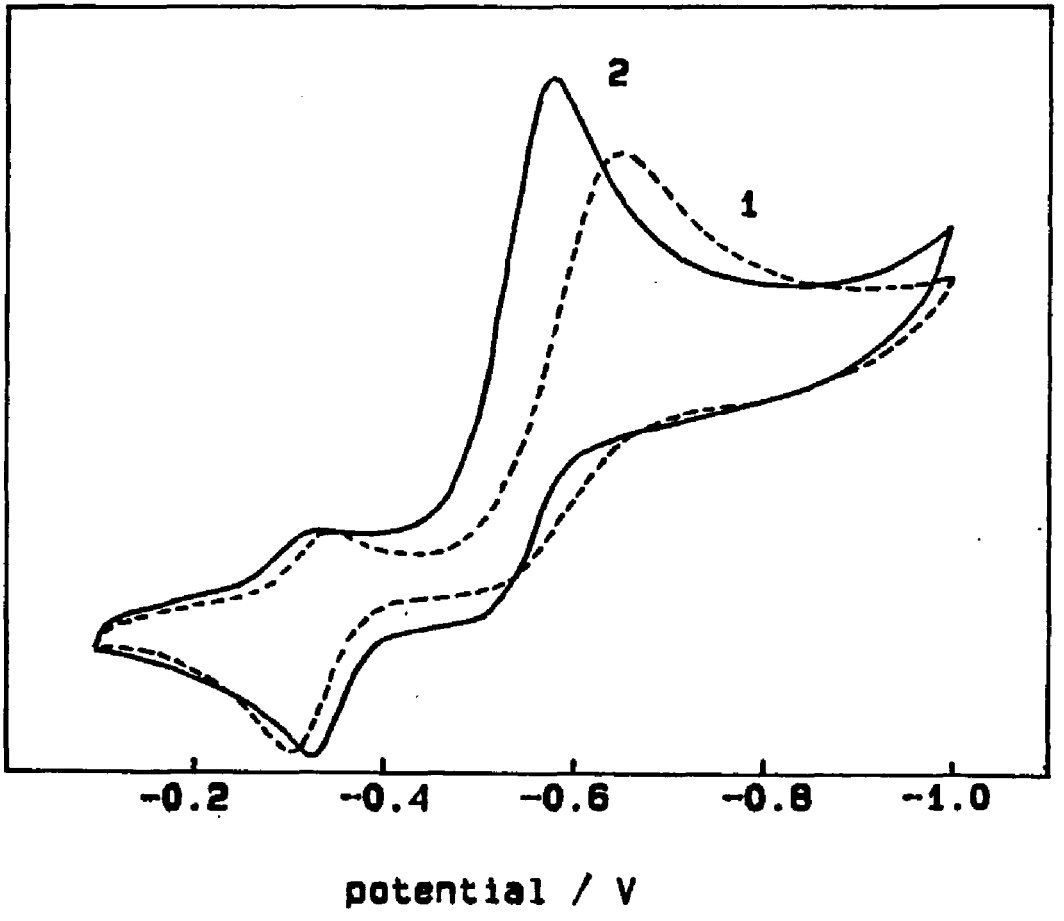

Fig. 8 Cyclic voltammogram of PNBA (1) on smooth Ag electrode and (2) on roughened Ag electrode at 100 mV/sec. of scan rate. The same ORC preteatment as in SERS measurements was used for roughening the electrode surface.

Generally speaking, the reduction proceeds in two ways, depending to whether the solution is alkaline or acid. In both cases the ultimate product, if the reducing agent is strong enough or the electrode potential is negative enough, is the primary amine. In alkaline medium the nitroso compound may act as an electrophilic center and the hydroxylamine compound can react with it with the formation of azoxy compounds. The hydroxylamine, as it is the unprotonated form, may act as a nucleophile, and a higher pH may make the electrophilic center more reactive. Thus if the nitro compound is reduced in alkaline solution, the main products are those formed by the condensation of ArNO and ArNHOH. In contrast, the amino compound will be predominant in acidic medium. In our work the solution pH was adjusted to pH=11. This pH would seem to be favorable for the formation of and azo compound.

In highly basic solution (0.1 M KOH) the formation of trans-azobenzene from the reduction of nitrobenzene can be determined by cyclic voltammetry and SERS [35-37]. There is an additional peak around -0.5 V, which has been assigned to the trans-azobenzene. Only in a narrow potential range between -0.4 and -0.55 (vs. SCE) the SERS spectrum of trans-azobenzene can be detected, since beyond this range, at more positive potential azobenzene has not been formed and at more negative potential the azobenzene will be further reduced. This study indicates that azobenzene can be formed in basic medium and observed by SERS. However, the formation of the azobenzene is not a surface induced photochemical process, it is merely an electrochemical reduction, since

the azobenzene is only observed when it is electrochemically reduced.

The photolysis rate was further investigated as a function of excitation frequency at a constant electrode potential (-0.2 V) and at a constant power of the laser light (30 mW). The initial rate of photolysis is obtained from the plot of the intensities of photolysis product vs. time. Then the initial rate is plotted as a function of excitation frequency as shown in Fig. 9. The arrow bars indicate the range of repeated measurements. The frequency dependence of SERS (excitation profile) of PNBA on a Ag island film and the absorption spectrum of the Ag island film are plotted on the same graph for comparison in an arbitrary scale of vertical axis. Both SERS and photolysis rate exhibit a pronounced resonance. The photolysis rate peaks around 490 nm at a very close frequency to the excitation profile of Raman scattering.

The photolysis rate was also found to be dependent upon the solvent. Fig. 10 shows the change of the intensities of photolysis product as the time of the irradiation changes. It can be clearly seen that the photolysis rate in an aqueous solution is much faster than in a mixture of isopropyl alcohol and water, indicating the reaction is not favorable in alcohol medium.

The process of the photochemical reduction of aromatic nitro compounds in solution phase with irradiation by UV light can be written as follows [38]

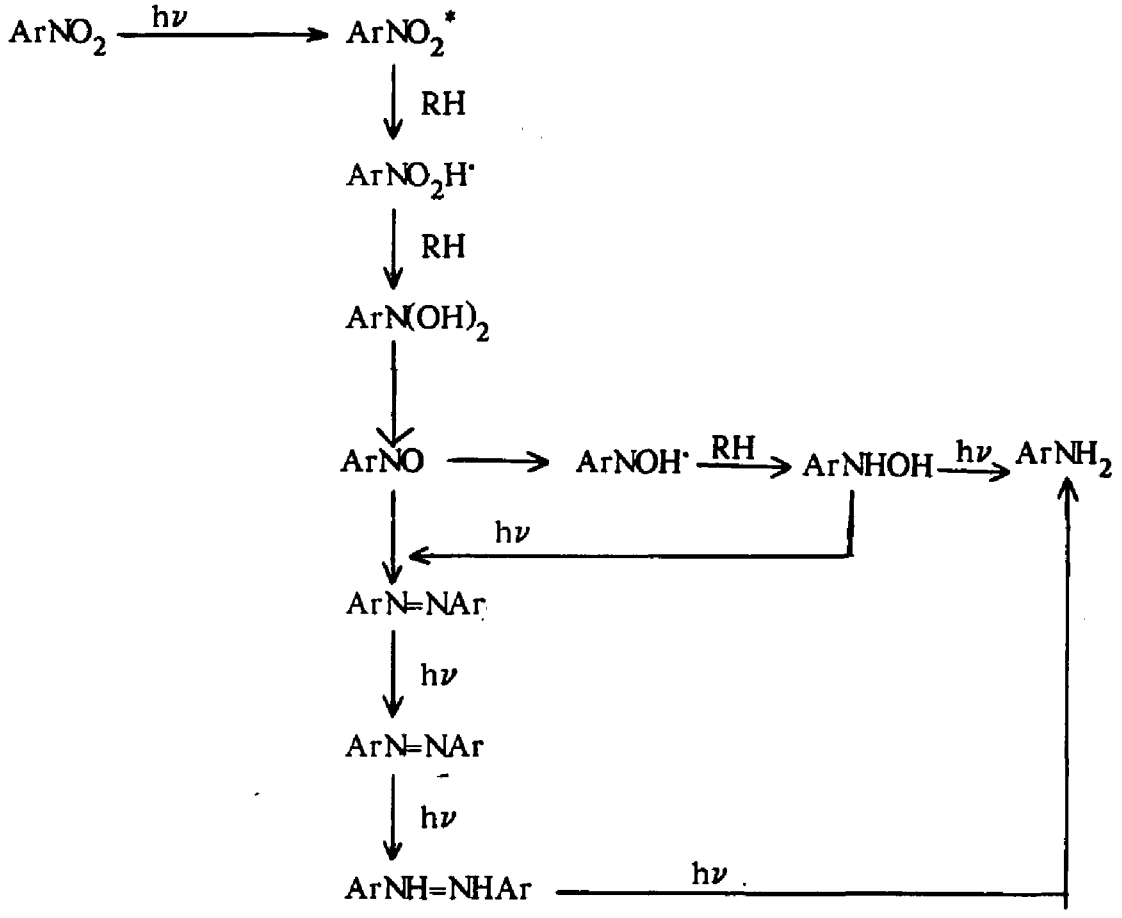
ArNO2
hν
ArNO2*
RH
ArNO2H·
RH
ArN(OH)2
ArNO
ArNOH·
RH
ArNHOH
hν
ArNH2
hν
ArN=NAr
hν
ArN=NAr
hν
ArNH=NHAr
hν

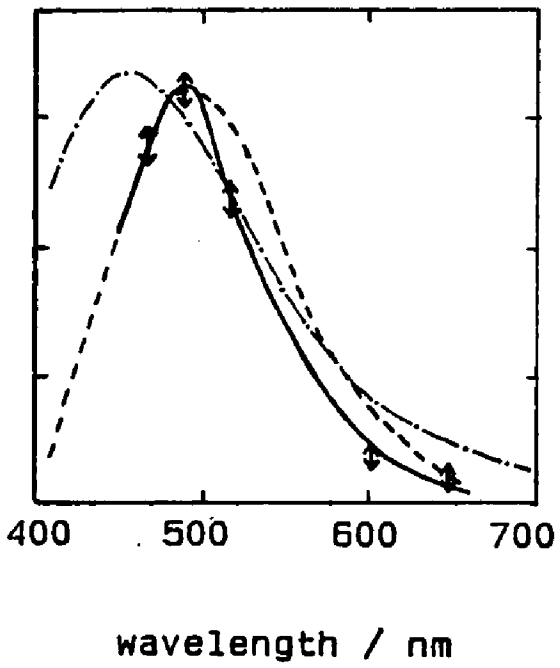

Fig. 9 Frequency dependence of the initial rate of photolysis of PNBA (solid line with arrow bars), compared to the absorption spectrum of a Ag island film (dash-dot line) and to the excitation profile of SERS of PNBA on the Ag island film (dashed line). The later two lines are quoted from reference [30].

where RH is the solvent which contains abstractable hydrogen atoms. In the photochemical reduction the $ArNO_2$ molecule first adsorbs a photon. The energy of the photon must be high enough to cause an electronic transition, then the excited state is followed by a hydrogen abstraction from the solvent. This hydrogen abstraction is probably by a $^3(\pi,\pi^*)$ excited state of the nitrocompounds [38]. Comparing the photochemistry in a solution phase with the photochemical reduction on a SERS activated surface, different conditions are required. The photochemical reduction in the solution phase necessitates excitation by UV light (220-330 nm) [38] to give a photochemical reduction. The absorption maximum of PNBA in aqueous solution is measured at about 280 nm, and it does not show observable absorption at the wavelengths longer than 350 nm. No photochemical reduction of PNBA in solution phase is observed with the irradiation of visible light (465-647 nm in our experimental condition). However, when the molecules are adsorbed on a roughened Ag surface, the reduction takes place on irradiation with visible light.

The overall processes of photochemical reduction are very similar to the electrochemical reduction processes. There are also two pathways according to the properties of the solvent. In the presence of both oxygen and base the product is the azoxy compound. However, in the absence of base it is converted into amino compound. Our experimental conditions at pH=11 seems to be more favorable for production of the azo compounds. In addition, it has been reported [38] that in isopropyl alcohol, which is a highly hydrogen abstractable sol-

vent, only amino compound is formed, but in t-butyl alcohol, which is a low hydrogen abstractable solvent, only a very low yield of amino compound is obtained. From Fig. 10, in the presence of isopropyl alcohol, we see that the photolysis rate is smaller then that in the absence of isopropyl alcohol. This is not in agreement with the result giving amino compounds as the main reduction product.

Summarizing the observations above, the reduction of PNBA may occur in the following three cases (i) in solution phase with the irradiation of UV light, (ii) on an electrode at a potential negative to -0.5 V vs. SCE, (iii) on a SERS activated Ag surface under the excitation of visible light. No potential is required on island films or a potential up to +0.1 V vs. SCE in the positive direction. From these comparison we can see that the reduction we have observed is a new type of reaction, a surface induced photochemical reduction.

(d) Discussion of the mechanisms of surface induced photochemistry

Similar to the electromagnetic enhancement effect a theoretical calculation by Nitzan and Brus [8,9] indicates that an enhanced photochemical reaction is possible when a molecule approaches to an appropriately roughened surface. They indicated that there are two effects leading to enhanced photochemistry (i) enhanced absorption due to the enhanced local field at a given wavelength, (ii) the absorption of light by the protrusions followed by energy transfer to the adsorbed molecules. In our experimental conditions these two effects are

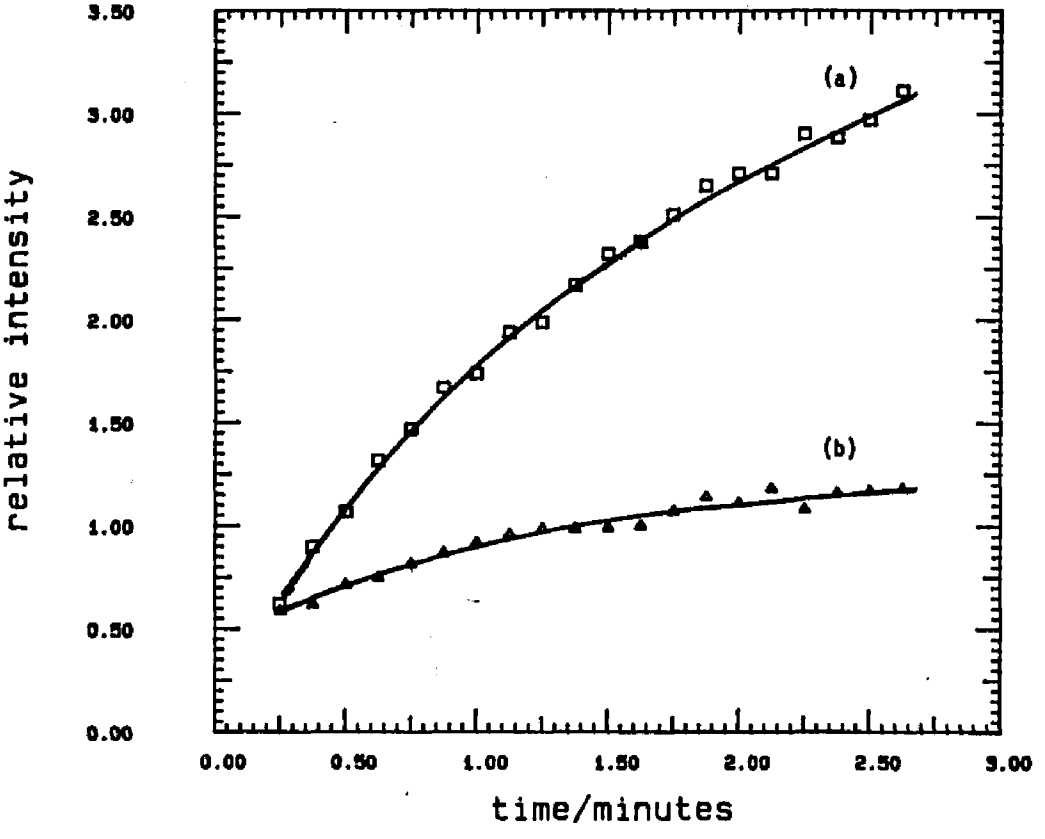

Fig. 10 Time dependence of the intensities of photolysis product at (a) aqueous solution and (b) a mixture of 25% of isopropyl alcohol and 75% water solution, a 30 mW of Kr^+ laser (647.1 nm) was used.

probably not important for the photochemical reaction of PNBA adsorbed on Ag surface. Firstly, the frequencies we used are in visible range, but the absorption bands of PNBA are in UV range. The energy needed to cause an electronic transition is much larger than the excitation energy of the laser. In the second effect, the energy transfer process from the metal to adsorbed molecules is more likely a multiphoton absorption process. An energy accumulation is needed as reported in the non-linear photofragmentation processes [4], but our observations indicate a one photon process for the photochemical reduction of PNBA.

Based on the observation of the potential dependence and frequency dependence, a charge transfer mechanism seems more important in the enhancement of the photochemical reduction on the Ag surface. Similar to the charge transfer theory for SERS [39], we can consider the metal adcluster and chemisorbed molecules as a whole. First of all, the interaction between the adsorbed molecules and the metal surface may lower the charge transfer threshold. A charge transfer acceptor level may exist in the molecule. An energy level diagram is shown in Fig. 11, where $E_{F(0)}$ is the Fermi energy of an electron in the Ag electrode at an arbitrary zero potential and the energy is referenced to the vacuum level, E_{CT} is the lowest lying charge transfer state formed from an excited state of the adcluster-molecule complex. The Fermi level of the metal can be changed by a change of the electrode potential. A negative shift of the electrode potential will raise the Fermi level, and vice versa. If the energy

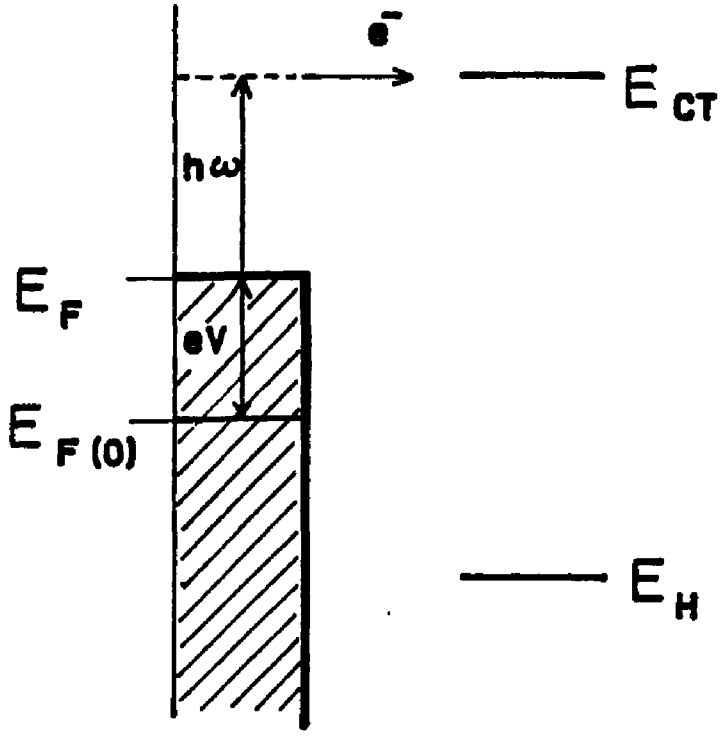

Fig. 11 Energy level diagram of a charge transfer processes.

difference between the Fermi level E_F and the low lying excited state of the charge transfer complex E_{CT} matches the energy of the excitation radiation, a resonant charge transfer from metal to the excited state of the complex will take place. Following the electron transfer step the excited state of the complex may undergo two deexcitation processes. One involves the return of the electron back to the surface followed by a radiation process (either Rayleigh scattering or Raman scattering). Another possible process could be chemical one. The excited state may be attacked by a proton in solution to form a radical $ArNO_2H^{\cdot}$ followed by subsequent reactions. The distinguished feature of the surface induced photochemical process from the electrochemical process is that overcoming the threshold of the reaction involves several effects, photo excitation, the electrode potential and the interaction between molecules and adcluster of the metal surface, while in electrochemical process only the electrode potential controls the reaction threshold.

Resonant charge transfer is observed with the frequency dependence of the photolysis rate in Fig. 9. At a constant potential the photolysis rate reaches a maximum at a similar excitation frequency as the SERS intensity. From the potential dependence of the photolysis rate we can not see the resonance profile as seen in the SERS spectra since at around -0.5 V PNBA is electrochemically reduced. However, the increase in photolysis rate which occurs before the electrochemical reduction (-0.1 to -0.3 V) can be interpreted by a charge transfer mechanism. The change of the potential to the negative direction will

raise the Fermi level as a result of the decrease of the charge transfer threshold. Thus a higher photolysis rate will be observed at more negative potentials.

As a mater of fact, there are many other damping processes which will also be enhanced by the surface. The competition of the reduction process with other damping processes leads to a large difference in the reactivity for PNBA as compared with other molecules. The reason why o-nitrobenzoic acid or m-nitrobenzoic acid do not show photochemical reduction under the same conditions as in the case of PNBA, may be attributed to the competition of the following chemical step with other damping processes. We assume that the enhancement of the pumping of the electron is similar for these isomers, but adsorbed PNBA has its nitro group pointing out. Thus PNBA has a more favorable position to react with solvent than o-nitrobenzoic acid or m-nitrobenzoic acid.

In conclusion, the change of the SERS spectra of PNBA on Ag island films and Ag electrode surfaces is attributed to a surface induced photochemical reduction. Heating the sample does not cause the conversion of the spectra, indicating that the reaction is not thermally induced. The potential dependence and frequency dependence of the photolysis rate also indicates that the change of the spectra is not thermally induced. It is found that both the rough metal surface and the excitation with laser light is necessary for the surface induced photochemical reaction. The reduction takes place at much more positive elec-

trode potentials than a simple electrochemical reduction and under a much lower excitation energy (visible rangy) than a simple photochemical reduction (necessitates a UV excitation). It is more likely that the reduction product is PABA. However, based on the observation of the solvent dependence of the photolysis rate it is also possible that the main reduction products are azo compounds. A charge transfer mechanism can be used to explain the potential dependence and frequency dependence of the photolysis rate. But a more detailed study of the surface induced mechanism and the identification of the reduction product is left for further investigation.

REFERENCES

[1] S. Garoff, D. A. Weitz, T. J. Gramila and C. D. Hanson, Opt. Letters 6, (1981) 245

[2] A. M. Glass, P. F. Liao, J. G. Bergman and D. H. Olson, Opt. Letters 5, (1980) 368

[3] H. Gerischer, Disc. Faraday Soc. 58, (1974) 219

[4] G. M. Goncher and C. B. Harris, J. Chem. Phys. 77(7), (1982) 3767

[5] S. Garoff, D. A. Weitz and M. S. Alverez, Chem. Phys. Lett., 93 (3), (1982) 283

[6] K. A. Bunding, R. A. durst and M. I. Bell, J. Electroanal. Chem., 150 (1983) 437

[7] T. H. Lu, R. L. Brike and J. R. Lombardi, 2, (1986) 305

[8] Abraham Nitzan and L. E. Brus, J. Chem. Phys. 75, (1981) 2205

[9] Abraham Nitzan and L. E. Brus, L. Chem. Phys. 74 (9), (1981) 5321

[10] M. Kerker, J. Colloid Interface Sci. 105, (1985)

[11] P. F. Liao and M. B. Stern, Opt. Lett. 7(10), (1982) 483

[12] J. C. Tsang, Ph. Avouris and J. R. Kirley, Chem. Phys. Lett., 94(2), (1983) 172

[13] J. C. Tsang, J. R. Kirtley, T. N. Theis and S. S. Jha, Phys. Rev. B25 (8), (1982) 5070

[14] C. A. Murray, D. L. Allara and M. Rhinewine, Phys. Rev. Lett., 46 (1), (1981) 57

[15] R. Dornhaus, R. E. Benner, R. K. Chang and I. Chabay, Surface Science 101, (1980) 367

[16] J. C. Tsang, Ph. Avouris and J. R. Kirtley, J. Chem. Phys. 79 (1), (1983) 493

[17] J. P. Heritage and D.L.Allara, Chem. Phys. Lett. 74 (1980) 507

[18] P. G. Roth, R. S. Venkatachaiam and F. J. Boerio, J. Chem. Phys. 85(2) (1986) 1150

[19] S. L. McCarthy, J. Vac. Sci. Technol. 13, (1976) 135

[20] S. Garoff, R. B. Stephens, C. D. Hanson and G. K. Sorenson, Optics Commun. 41, (1982) 257

[21] C. C. Yang, J. Y. Josefowicz and L. Alexandrov, Thin Solid Film 74, (1980) 117

[22] S. C. Sun, I. Bernard, R. L. Birke and J. R. Lombardi, L. Electro-anal. Chem. 196, (1985) 359

[23] J. T. Hall and P. K. Hansma, Surface Science 6, (1978) 61

[24] T. F. Heinz, H. W. K. Tom and Y. R. Shen, Phys. Rev. 28(3), (1983) 1883

[25] F. Kimura, J. Umemura and T. Tamenara, Langmuir 2, (1986) 96

[26] J. S. Suh, D. P. DiLella and M. Moskovits, J. Phys. Chem. 87, (1983) 1540

[27] D. P. DiLella and M. Moskovits, J. Phys. Chem. 85, (1981) 2042

[28] G. L. McIntire, D. M. Chiappardi, R. L. Casselberry and H. N. Blount, J. Phys. Chem. 86, (1982) 2632

[29] K. D. Asmus, A. Wiggerand A. Henglein, Ber. Bunsenges Phys. Chem. 70, (1966) 862

[30] D. A. Weitz, S. Garoff, J. I. Gersten and A. Nizan, J. Chem. Phys. 78 (9), (1983) 5325

[31] K. Brand, Die Elektrochemische Reduktion Organischer Nitrokorper, Stuttgart, 1908

[32] I. A. Titova, I. M. Levinson, V. G. Mairanovskii and A. B. Ershler, Elektrokhimiya, 9, (1973) 424

[33] E. Kariv, H. A. Terni and E. Gileadi, Electrochim. Acta, 18, (1973) 433

[34] N. V. Sidgwick 'The organic chemistry of nitrogen' ed. Oxford at the Clarendon press, 1937

[35] H. Shindo and C. Nishihara, Surface Science 158, (1985) 393

[36] C. Nishihara and H. Shindo, J. Electroanal. Chem. 202, (1986) 231

[37] C. Nishihara, H. Shindo and J. Hiraishi, J. Electroanal. Chem. 191 (1985) 425

[38] J. A. Barltrop and N. J. Bunce, J. Chem. Soc. (C) (1968) 1467

[39] J. R. Lombardi, R. L. Birke, L. A. Sanchez, I. Bernard and S. C. Sun, Chem. Phys. Lett. 86, (1983) 3166